



HAL
open science

Shared Control and Authority Distribution for Robotic Teleoperation

Rahaf Rahal

► **To cite this version:**

Rahaf Rahal. Shared Control and Authority Distribution for Robotic Teleoperation. Robotics [cs.RO]. Univ. Rennes 1, 2020. English. NNT : . tel-03284125v1

HAL Id: tel-03284125

<https://theses.hal.science/tel-03284125v1>

Submitted on 29 Dec 2020 (v1), last revised 12 Jul 2021 (v2)

HAL is a multi-disciplinary open access archive for the deposit and dissemination of scientific research documents, whether they are published or not. The documents may come from teaching and research institutions in France or abroad, or from public or private research centers.

L'archive ouverte pluridisciplinaire **HAL**, est destinée au dépôt et à la diffusion de documents scientifiques de niveau recherche, publiés ou non, émanant des établissements d'enseignement et de recherche français ou étrangers, des laboratoires publics ou privés.

UNIVERSITE

BRETAGNE

LOIRE / MATHSTIC

UNIVERSITÉ DE
RENNES 1

THESE DE DOCTORAT DE

L'UNIVERSITE DE RENNES 1

ECOLE DOCTORALE N° 601

*Mathématiques et Sciences et Technologies
de l'Information et de la Communication*

Spécialité : Automatique, Productique et Robotique

Par

« **Rahaf RAHAL** »

« **Shared Control and Authority Distribution for Robotic Teleoperation** »

Thèse présentée et soutenue à « Rennes », le « 17/12/2020 »

Unité de recherche : Institut de Recherche en Informatique et Systèmes Aléatoires (IRISA-UMR6074)

Thèse N° :

Rapporteurs avant soutenance :

Stéphane Régnier Professeur, Université Pierre et Marie Curie, France
Paolo Rocco Full Professor, Politecnico di Milano, Italy

Composition du Jury :

Président : Mehdi Ammi Professeur, Université Paris 8, France

Examineurs : Stéphane Régnier Professeur, Université Pierre et Marie Curie, France
Paolo Rocco Full Professor, Politecnico di Milano, Italy
Dongheui Lee Associate Professor, Technical University of Munich, Germany
Mehdi Ammi Professeur, Université Paris 8, France
Claudio Pacchierotti CRCN, CNRS, IRISA/Inria Rennes, France

Dir. de thèse : Paolo Robuffo Giordano

DR2, CNRS, IRISA/Inria Rennes, France

To my family

Acknowledgments

As my PhD journey comes to an end, I would like to take this chance to thank every person who helped me reach this point, in a way or another. Coming to France for my PhD was a big step full of uncertainty for me, and I am lucky to have been surrounded by wonderful people who made my experience more enjoyable and helped me get through the highs and the lows of the past three years.

I would like to start by expressing my deepest gratitude to my advisors, Paolo and Claudio, who are the main reason for the successful completion of my PhD thesis. When I was looking for a PhD opportunity during my master's degree, I was told that the choice of advisors would have a big influence on my thesis experience, and I honestly believe that I couldn't have made a better choice. I am truly grateful to have had the opportunity to work with you, learn from you, and interact with you on a daily basis. I have progressed a lot on the academic level, but also on the personal level as I have discovered my own capabilities by constantly challenging myself and aiming for better results. I also enjoyed our regular meetings and interactions, they were always pleasant and they motivated me to keep moving forward with my work. Thank you for all the opportunities that you gave me, for making me a better researcher, and most importantly, for always being available whenever I needed your help.

I would like to thank as well the members of my PhD jury, Dr. Stéphane Régnier, Dr. Paolo Rocco, Dr. Dongheui Lee and Dr. Mehdi Ammi. Thank you for accepting to attend my thesis defense and for your valuable comments on my thesis. I would like to extend my gratitude to the members of my PhD supervisory committee, Dr. Anatole Lécuyer and Dr. Domenico Prattichizzo.

Another big thank you to Fabien Spindler for his help with the robots. He was always here to help, both with hardware and software. I would also like to thank Firas who helped me get acquainted with the topic at the beginning of my PhD, I really enjoyed working with you.

During my last year as a PhD student, I got the chance to visit the Human-centered Assistive Robotics lab at TUM in Munich. I would like to thank Prof. Dongheui Lee for hosting me during this short visit in her lab. Even though my stay was shortened due to the Covid outbreak, I really enjoyed my time in

Germany. I would like to thank Youssef, Katrin, Alejandro, Dan, Thomas, Shile and Karna for making me feel welcome in their lab at TUM, and for all the interesting discussions and the lunches we had together. A special thank you to Youssef and Gabriel for helping me discover the city, and for the nice discussions about quite everything.

I would also like to thank the members of the Rainbow team for all the coffee breaks, the movie lunches, the basketball games and the events that we had together. There was always a nice atmosphere in the team which made me happy to go to the lab everyday. Thanks to Claudio, Firas, Fabien, Julien, Florian, Hadrien, Giulia, Adèle, Joudy, Noura, Wouter, Fabrice, H el ene, Marco A., Alexander, and many more people with whom I interacted every day and who made my time in the lab much more enjoyable. I'm sorry for not mentioning everyone by name as the list is long and it would be hard to not forget anyone. I would like to thank Giulia for being a great student and friend, I had the pleasure to work with you. I would also like to thank the office mates that I had over the years. A special thank you to Hadrien for the great discussions, the support, and for adding a positive atmosphere to the office. Thanks to Ad ele with whom I did not only share the office but also some of the most interesting conversations in the past year.

Of course, the PhD experience would not have been the same without my group of friends in Rennes and all over the world. Thanks to my group of girls, Routa, Farah, Tania and Nisrine for the great trips, the food, the laughs, and the daily support. Thanks to Fabien, Julien, Florian, Hadrien, Giulia, Coralie, Rebecca, Pol and Ad ele for the wonderful times we had together, in bars, restaurants, at the beach or around a camping fire. Thanks to my lockdown buddies, Firas, Hiba and Julien. You have made this period a lot easier for me. Thanks to Ali for being a great friend and neighbour. Thanks to Fatima, Samer, Dana, Eliana, and all of my friends from Lebanon who are now in different parts of the world.

I would like to also thank my family in France, Hicham, Sophie, Yola, Mona and Samy with whom I spent amazing moments. Thank you for making me feel at home.

Finally, I would like to thank my family for being my greatest support over the years. To my parents Houssein and Mona, thank you for all your sacrifices, for your love and your kind words that kept me going even in the hardest times. Thank you for encouraging me to pursue my dreams, you are the reason why I am here today. To my sister Rouba and my brother Rawad, thank you for being the greatest siblings anyone could ask for, and for always being by my side despite the distance. Thank you for the wonderful times that we have spent together, and the great memories which gave me the strength to keep moving forward.

Résumé en français

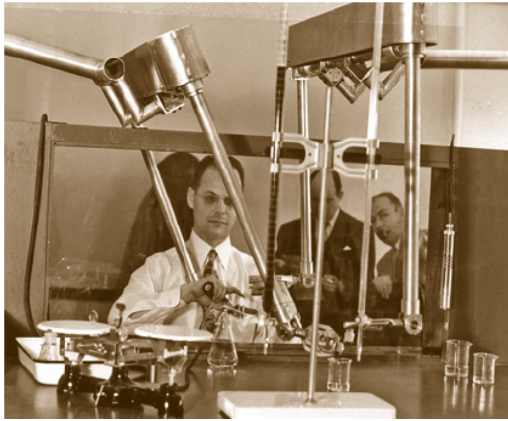
Introduction

La robotique est un domaine en pleine expansion qui intègre de plus en plus les multiples facettes de notre société moderne. Du monde industriel à l'exploration spatiale, en passant par les domaines de la santé et de l'interaction sociale, les robots deviennent des éléments essentiels de notre vie quotidienne.

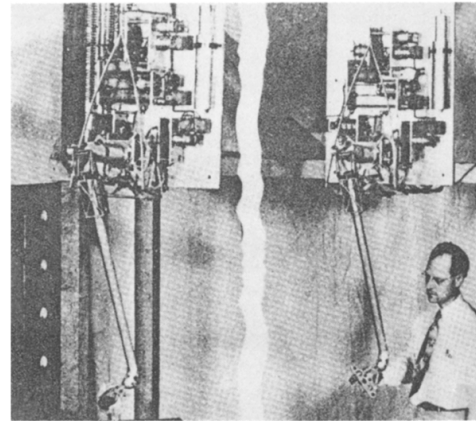
Bien que les humains aient cherché à créer des machines intelligentes et des artefacts à leur image depuis les toutes premières civilisations, la robotique au sens moderne du terme a commencé à se développer dans les années 1950. La première manifestation a été motivée par les besoins de l'industrie nucléaire [1]. Elle était constituée d'une paire de manipulateurs reliés mécaniquement permettant à l'homme de manipuler des matières radioactives. Cependant, comme les systèmes couplés mécaniquement ne peuvent fonctionner que sur une distance limitée, Goertz a plus tard saisi l'intérêt des manipulateurs couplés électriquement et a ainsi fondé les bases du domaine moderne de la télérobotique [2]. Les deux systèmes sont présentés sur la Figure 1. De nombreux autres systèmes de téléopération ont suivi, avec des manipulateurs également contrôlés manuellement par des opérateurs humains en l'absence de tout contrôle par ordinateur.

Les systèmes de téléopération comprennent deux parties : la partie maître, qui est commandée par l'homme, et le robot à distance chargé d'exécuter la tâche et d'interagir avec l'environnement. Les deux côtés sont reliés par un canal de communication, et interagissent par l'intermédiaire d'un ensemble de capteurs qui permettent la transmission de données sur les mouvements et les forces qui s'exercent entre eux.

Ces dernières années, l'automatisation a connu un énorme développement, rendu possible par les progrès technologiques et les hautes capacités des ordinateurs et des capteurs modernes. Les systèmes de contrôle autonomes ont évolué rapidement compte tenu des progrès récents des architectures de hardware et de software, notamment avec l'essor de l'apprentissage machine et de l'intelligence



(a) Premier système de téléopération mécanique



(b) Premier système de téléopération électrique

Figure 1 – (a) Le premier système maître-robot à liaisons mécaniques conçu par Goertz dans les années 1950 [3], et (b) le premier système électrique (1954) construit par Goertz au Laboratoire National d'Argonne [4].

artificielle. Et évidemment, les systèmes contrôlés par ordinateur ont conduit à de nombreuses applications robotiques dans la société humaine moderne.

Cependant, bien que l'autonomie robotique ait été perfectionnée dans des environnements structurés et prévisibles, l'apport humain (et la télérobotique) est encore nécessaire dans de nombreux cas, en particulier dans des environnements variables. Par exemple, dans les contextes nucléaires, de recherche et de sauvetage, et d'opérations sous-marines ou spatiales, l'homme ne peut pas être physiquement présent sur site pour effectuer la tâche désirée vu les risques encourus dans ce type d'environnement dangereux. En parallèle, malgré les développements de l'automatisation ces dernières années, les systèmes autonomes sont toujours incapables de faire face à des événements inconnus ou imprévisibles et ne disposent toujours pas de la logique et des capacités humaines de résolution des problèmes. Dans d'autres domaines comme la microchirurgie, l'homme peut être capable d'effectuer la tâche par lui-même, mais la précision et la capacité d'adaptation d'échelle du robot sont souvent souhaitées pour faciliter cette opération. La robotique médicale étant un secteur très conservateur car en contact direct avec des patients humains, elle ne fait toujours pas confiance au robot, dans son état actuel d'avancement, pour effectuer les opérations chirurgicales de manière autonome. La téléopération permet donc de coordonner les compétences robotique et humaine pour effectuer des tâches délicates dans de nombreux environnements. En revanche, la téléopération directe est souvent trop pénible et fatigante pour l'homme. Ceci a mené au développement de nouvelles approches où le contrôle du système est *partagé* entre l'opérateur et le robot, appelées architectures de contrôle partagé.

Aperçu de la Thèse et Contributions

L'objectif de cette thèse est de concevoir de nouvelles architectures de contrôle partagé pour une téléopération robotique sûre et intuitive, avec différents types d'interaction et différents niveaux d'automatisation. Nous nous concentrons dans ce travail sur l'utilisation de l'haptique comme moyen d'interaction, que ce soit pour fournir des forces de contact en retour à l'utilisateur, ou comme moyen de guider l'utilisateur dans l'exécution de la tâche. Nous soulignons également le rôle de l'interaction haptique et de l'apport humain dans la conception d'algorithmes de saisie autonomes. Ainsi, nous présentons différentes méthodes d'interaction entre les composants humain et automatisé d'un système robotique afin d'exécuter avec succès la tâche en question.

Les travaux de cette thèse se concentrent sur deux applications principales, la saisie et la manipulation, et la découpe robotique. Les principales contributions sont les suivantes :

- La conception de nouvelles méthodes haptiques de contrôle partagé appliquées à la préhension et à la manipulation robotique, ciblant à la fois les phases pré- et post-préhension.
 - Nous élaborons une nouvelle architecture de contrôle partagé qui vise à minimiser la charge de travail humaine pendant la phase d'approche vers l'objet à saisir, ainsi que dans la tâche post-saisie exécutée par l'utilisateur dans ce cas.
 - Pour la phase post-saisie, nous nous concentrons également sur la minimisation de l'effort exercé sur les articulations du manipulateur pendant l'exécution d'une trajectoire autonome souhaitée après la saisie.
- La conception d'une nouvelle technique haptique de contrôle partagé pour la découpe robotisée imposant des contraintes non holonomes motivées par la tâche de découpe.
- L'utilisation de l'expérience humaine et des retours haptiques pour apprendre des politiques de saisie autonome pour les objets conformes.

Plusieurs des travaux présentés ont déjà été publiés et présentés dans des conférences internationales [5–8]. La section suivante décrit avec plus de détails les différentes parties et les contributions présentées dans ce manuscrit.

Structure de la Thèse

La thèse est divisée en quatre parties principales. La première partie présente les notions principales utiles pour la compréhension de la thèse, et résume les travaux les plus pertinents développés dans la littérature. Les deuxième et troisième parties présentent le contenu original et les contributions de la thèse. Nous concluons ensuite avec la quatrième partie en introduisant les remarques finales et les directions futures possibles, ainsi que les questions à résoudre dans le domaine.

Partie I

La première partie est un bilan de l'état de l'art en rapport avec la thèse. Le **Chapitre 2** est divisé en deux parties. La première est une synthèse sur la télérobotique - y compris les principaux avantages et défis des systèmes de téléopération et l'utilisation de retours haptiques. La télérobotique peut en effet être perçue comme un mode de commande manuel où l'utilisateur a le contrôle total du système à distance. La deuxième partie, d'autre part, présente les travaux relatifs à l'interaction homme-robot (HRI), l'autonomie partagée, et le rôle des retours haptiques par rapport au contrôle partagé. Ces deux sujets sont importants pour la suite de la thèse, qui présentera de nouvelles méthodes de contrôle partagé pour la téléopération avec des degrés d'autonomie variables.

Partie II

Cette partie présente deux méthodes de contrôle partagé pour la saisie robotique et la télémanipulation. Les architectures présentées visent à partager le contrôle du système entre le système autonome et l'opérateur humain, afin d'améliorer l'exécution des tâches en fonction d'un critère différent dans chaque cas. Le premier travail vise à optimiser une fonction-objectif liée à la tâche, qui dans ce cas inclut les couples exercés au niveau des articulations du robot distant pendant la phase post-préhension. Le second est par ailleurs orienté vers l'utilisateur, et vise à maximiser le confort de l'utilisateur pendant la téléopération. Dans les deux travaux, l'utilisateur est guidé, grâce à des retours haptiques et/ou des données visuelles, dans la direction de l'exécution de la tâche qui améliore l'objectif du système. Cependant, l'utilisateur reste l'acteur en charge de la décision finale, et peut choisir de suivre ou non les recommandations qui lui sont données. Par conséquent, les méthodes de cette partie sont considérées comme des méthodes avec *autorité humaine*.

Le **Chapitre 3** présente une nouvelle méthode de contrôle partagé pour minimiser les efforts articulaires du manipulateur lors d'une téléopération bilatérale. Ceci permet de réduire le coût de fonctionnement du système et élargit la gamme des objets qu'il peut manipuler. L'architecture que nous proposons génère, pendant la téléopération, un retour visuo-haptique de navigation pour aider l'opérateur à choisir une configuration de saisie locale, minimisant l'effort attendu dans la phase de post-préhension souhaitée. Nous démontrons également l'efficacité de l'approche proposée à travers une série d'expériences représentatives et une étude sur des sujets humains, où nous comparons les effets du guidage visuel et haptique sur les performances de l'utilisateur.

Le **Chapitre 4** présente une architecture de contrôle partagé visant à minimiser la charge de travail de l'utilisateur lors d'une tâche de télémanipulation. En effet, les méthodes de contrôle partagé sont généralement utilisées dans différentes applications - par exemple, pour suivre une trajectoire en minimisant l'effort du manipulateur (voir Chapitre 3) ou pour éviter des zones potentiellement dangereuses de l'espace de travail - mais peu de travaux ont porté sur leur utilisation pour tenir compte du confort de l'utilisateur. Nous avons réalisé des études sur des sujets humains pour démontrer l'efficacité de l'approche proposée, et nous en présentons les résultats à la fin du chapitre.

Partie III

Contrairement à la partie précédente où l'utilisateur était en plein contrôle, et pouvait toujours négliger l'aide qui lui est apportée par le système autonome, dans cette partie de la thèse nous présentons deux systèmes où l'interaction homme-robot est plus orientée vers l'autonomie du robot que vers le contrôle humain. L'utilisateur est bien sûr toujours dans la boucle, et l'interaction haptique est présente et utilisée pour aider à l'exécution de la tâche. Cependant, l'utilisateur intervient de manière moins directe. Dans le premier travail, nous ciblons une application de découpe robotique. Des contraintes faibles et fortes sont imposées à l'utilisateur qui prennent en compte la spécificité de la tâche et assurent l'application de la contrainte non holonome représentative d'une tâche de découpe. Le second travail est encore plus sur le côté autonomie du spectre HRI, et vise l'utilisation de données humaines et haptiques dans l'apprentissage d'un algorithme de saisie autonome pour les objets souples.

Au **Chapitre 5** nous présentons deux approches de contrôle partagé avec

retours haptiques pour la découpe robotisée, conçues pour aider l'opérateur humain en appliquant différentes contraintes non holonomes représentatives de la cinématique de découpe. Pour valider notre approche, nous avons réalisé une expérience avec des sujets humains dans un scénario de découpe réel, et nous avons comparé nos techniques de contrôle partagé entre elles et avec un schéma de téléopération haptique standard.

Au **Chapitre 6**, contrairement aux travaux précédents où les informations haptiques sont fournies pour refléter les forces de contact ou pour guider l'utilisateur dans une tâche de téléopération, les données de téléopération avec retour haptique sont utilisées comme moyen pour entraîner un algorithme de saisie autonome. En fait, la manipulation robotique d'objets fragiles et conformes, tels que des produits alimentaires, se heurte encore à de nombreux défis. Pour améliorer les algorithmes autonomes existants, nous proposons une politique d'apprentissage par la démonstration (LfD), centrée sur l'homme et basée sur l'haptique, qui permet une saisie autonome des objets à l'aide d'un système robotique anthropomorphe. Cette politique intègre des données provenant de la téléopération et de la manipulation humaine directe d'objets, incarnant l'intention humaine et les zones d'interaction importantes avec l'objet. Nous évaluons enfin la solution proposée par rapport à une politique de LfD récente ainsi que par rapport à deux méthodes classiques de contrôle d'impédance.

Partie IV

Cette dernière partie est composée d'un chapitre (**Chapitre 7**), présentant une conclusion et quelques remarques finales et points de discussion liés aux travaux présentés dans cette thèse. Elle propose également quelques orientations futures à prendre dans le domaine en général, et plus particulièrement en relation avec les contributions de la thèse.

Contents

Acknowledgments	i
Contents	ix
1 Introduction	1
1.1 Thesis Overview and Contributions	3
1.2 Thesis Outline	4
1.2.1 Part I	5
1.2.2 Part II	5
1.2.3 Part III	6
1.2.4 Part IV	6
1.3 Publications Related to this Thesis	7
I Preliminaries and State of the Art	9
2 State of the Art	11
2.1 Telerobotics	12
2.1.1 History of Telerobotics	12
2.1.2 Teleoperation Systems	14
2.1.3 Haptic Feedback in Teleoperation	15
2.2 Shared Autonomy	17
2.2.1 Human Robot Interaction	18
2.2.2 Shared Control	20
2.2.2.1 Virtual Fixtures	20
2.2.2.2 Haptic Shared Control	22
2.2.2.3 Semi-autonomous control	23
2.2.2.4 Mixed Initiative Control	24
2.2.3 Level of Authority	25

II Haptic Shared-Control Methods with Human Authority 27

3 Haptic Shared-Control System to Minimize Torque Effort during Robotic Telemanipulation	29
3.1 Related Works	33
3.2 Shared-Control Method	37
3.2.1 System details	39
3.2.2 Manipulator Dynamics Under Load	41
3.2.3 Task Oriented Torque Effort (TOTE) Cost Function	43
3.3 Navigation Information	43
3.3.1 Haptic Navigation Guidance	44
3.3.2 Visual Navigation Guidance	45
3.4 Pick-and-Place Experiment	46
3.4.1 Experimental Setup	46
3.4.2 Task and Methods	47
3.4.3 Results	50
3.5 Human-Subjects Study	51
3.5.1 Task and Feedback Conditions	51
3.5.2 Participants	52
3.5.3 Results	52
3.6 Discussion	56
4 Haptic Shared Control for Enhanced User Comfort in Robotic Telemanipulation	59
4.1 Related Works	61
4.2 System Details	62
4.2.1 System Model	62
4.2.2 Human Arm Model	63
4.2.3 User Workload Parametrization	63
4.2.4 Inverse Kinematics and Solving the Redundancy	64
4.3 Shared-Control Architecture	65
4.3.1 Human Workload Cost Function	65
4.3.2 Task-Related Cost Function	65
4.3.3 Haptic Feedback	66
4.4 Experimental Evaluation	68
4.4.1 Setup and Participants	68
4.4.2 Task and Conditions	68

4.4.3	Results	70
4.5	Discussion	72
III Haptic Shared-Control Methods with Partial Human Authority		75
5	Shared Control for Robotic Cutting	77
5.1	Related Works	79
5.2	Methods	81
5.2.1	Standard Haptic Teleoperation (Condition T)	82
5.2.2	Unicycle Approach (Condition U)	83
5.2.3	Car-like Approach (Condition C)	85
5.3	Experimental Evaluation	86
5.3.1	Setup	87
5.3.2	Task and Conditions	87
5.3.3	Participants	88
5.3.4	Results	88
5.4	Discussion	91
6	Human-Inspired Haptic Learning for Autonomous Grasping	93
6.1	Related Works	94
6.2	Contribution and Motivation	96
6.3	Grasping-Data Gathering	98
6.3.1	Direct Grasping by Hand	100
6.3.2	Teleoperated grasping by an expert operator	101
6.4	Machine Learning	104
6.4.1	Standard SVR	105
6.4.2	SVR with Time-Series	105
6.4.3	SVR with Heat-Map Weighting	106
6.5	Experimental Evaluation	107
6.5.1	Setup	107
6.5.2	Grasping Policies	107
6.5.3	Autonomous Grasping Task	109
6.5.4	Results and Discussion	110
IV Conclusions and Future Work		115
7	Concluding Remarks	117

7.1	Discussion and Conclusions	118
7.1.1	Part II	118
7.1.2	Part III	120
7.2	Additional Remarks and Future Directions	121
	Bibliography	127

CHAPTER

1

Introduction

Contents

1.1	Thesis Overview and Contributions	3
1.2	Thesis Outline	4
1.2.1	Part I	5
1.2.2	Part II	5
1.2.3	Part III	6
1.2.4	Part IV	6
1.3	Publications Related to this Thesis	7

Robotics is a fast-growing field that is integrating multiple facets of our modern society. From the industrial world, to space exploration, healthcare, and social interaction, robots are becoming essential components of our daily life.

The origin of the term “Robot” goes back to the 1920’s, when the concept was created. It originates from the Czechoslovakian word *robota* – meaning “work”– used for the first time in a play by Karel Chapek, *Rossum’s Universal Robots*. While this modern definition of the concept appeared in the first half of the 20th century, the notion of robot-like behaviour have existed for centuries in mythology, religion, philosophy and fiction. Since the early civilizations, humans have been trying to create intelligent machines and artifacts in their image. For example, the legend of Talus, the bronze slave forged by Hephaestus in Greek Mythology dates back to 3500 BC, and the Egyptians’ oracle statues hiding priests inside (2500 BC) were some of the earliest forms of our modern thinking machines. In the next centuries, human creativity led to the invention of many other devices such as the automaton theatre of Hero of Alexandria (100 AD), the water-raising and humanoid machines of Al-Jazari (1200), and Leonardo da Vinci’s multiple designs such as the mechanical man (1495). The development of automata also continued to flourish in the eighteen century as many complex mechanical systems have been perfected to entertain the public (e.g. Jaquet Droz’s automata) [9].

After that, early robot implementations were remotely operated devices with no or minimal autonomy. Examples are Nicola Tesla’s radio-controlled boat from 1898, which he described as incorporating “a borrowed mind”, and the Naval Research Laboratory’s “Electric Dog” robot from 1923. The first actual manifestation of robotics was then built in the 1950s, driven by the needs of the nuclear industry [1]. It consisted of a pair of mechanically linked manipulators for humans to handle radioactive material. Many other teleoperation systems followed, with more details on them in Sec. 2.1.1. However, all these manipulators were also manually controlled by human operators without an overlaying logic in the absence of any ‘computer-control’. The robots were insensitive to their environment and there was no feedback loop from the robot to the operator that could modify the control command.

It wasn’t until a decade later that the first ‘computer-controlled robot’ was introduced by Heinrich Ernst [10]. Ernst removed the human intermediary and gave the computer full command over the manipulator used, which was one of the early electromechanical manipulators designed by Goertz and equipped with tactile sensing. Using the sensors, the robot was able to autonomously search for a

box on a table, to search for cubes, grasp them, and then place them inside the box without any previous knowledge of their positions. In recent years, automation has seen a huge development, made possible by the technological advancement and the high capabilities of modern computers and sensors. Autonomous controllers have evolved rapidly given the recent advances in hardware and software architectures, namely with the rise of machine learning and AI. And of course, computer-controlled systems led to many robotic applications in the modern human society.

However, while robotic autonomy has been perfected in structured and predictable environments, the human input is still needed in many cases, especially in a variable setting. In addition, all robotic systems, including the most autonomous ones, are directly or indirectly related to the human since they were first and foremost created to fulfill a human need or accomplish a task desired by the operator. As such, the interaction between robots and humans is unavoidable, which brings us to the field of Human-Robot Interaction (HRI) under which this thesis falls. The field of HRI has gained a lot of interest in the recent years. To address the limited capabilities of autonomous robots in unpredictable settings, many approaches fusing human intelligence with the precision and efficiency of autonomous systems have been developed in the form of human-robot shared-control architectures [1, 11], which is the main type of HRI that we focus on in this thesis.

1.1 Thesis Overview and Contributions

The work presented in this thesis falls under the general HRI topic. More specifically, the thesis deals with remote interaction under the form of teleoperation. The aim of the thesis is to design novel shared-control architectures for safe and intuitive robotic teleoperation, with various types of interaction and different levels of automation. Shared-control algorithms have been investigated as one of the main tools for designing effective yet intuitive robotic teleoperation systems, helping operators in carrying out increasingly challenging tasks. This approach enables to *share* the command of the system between the operator and an autonomous controller.

We focus in this work on the use of haptics as a means of interaction, whether for providing contact forces as a feedback to the user, or as a means of guiding the user in the task execution. We also highlight the role of haptic interaction and human input in the design of autonomous grasping algorithms. As such, we present different ways the human and the automation components of a robotic

system can interact to successfully perform the task at hand. We finally note that, as the focus of this thesis is mostly on the design and evaluation of several haptic shared control algorithms, we do not explicitly address stability issues of the teleoperation systems presented in the next chapters. Indeed, in most cases one can resort to one of the many passification algorithms presented in the last years (e.g., tank-based approaches [12–16], PSPM [17], time-domain passivity [18–21]) for including an additional stabilisation layer on top of any bilateral teleoperation scheme. In the following we then assume that such a passification layer is always implemented and active in the presented schemes.

The work presented in this thesis focuses on two main applications, robotic cutting, and grasping and manipulation. The contributions of the thesis are in:

- Designing new haptic shared-control methods applied to robotic grasping and manipulation, targeting both the pre-grasp and the post-grasp phases.
 - For the post-grasp phase, we consider the manipulator dynamics and focus on minimizing the torque effort in following a desired autonomous trajectory after a grasp has been performed (Chapter 3).
 - We also design a novel shared-control architecture that aims to minimize the human workload during the approaching phase towards the object to be grasped, as well as in the post-grasp task executed by the user in this case. The system targets the human comfort as a goal, instead of only focusing on the task or the robot performance alone (Chapter 4).
- Designing a novel haptic shared-control technique for robotic cutting imposing nonholonomic constraints motivated by the task (Chapter 5).
- Using the human experience and haptic feedback to learn autonomous grasping policies for compliant objects (Chapter 6).

1.2 Thesis Outline

The thesis is divided into four main parts. The first part starts by presenting the main concepts used in the thesis, and summarizes the most relevant works developed in the literature. The second and third parts present the original content and contributions of the thesis. We then end with the fourth section introducing concluding remarks, possible future directions and open questions to be addressed in the field.

1.2.1 Part I

The first part is a review of the state of the art relevant for the thesis. **Chapter 2** is divided into two parts. We start with a review on telerobotics – including the main advantages and challenges of teleoperation systems and the use of haptic feedback. In some way, telerobotics can be seen as a manual control where the user is in full control of the remote system. We then introduce the works related to HRI in teleoperation, shared autonomy, and the role of haptic feedback in shared control. These two topics are important for the rest of the thesis, which will be presenting new shared-control methods for teleoperation with variable degrees of autonomy.

1.2.2 Part II

This part presents two haptic shared-control methods for robotic grasping and telemanipulation. The architectures presented aim to share the control of the system between the autonomy and the human operator, in order to improve the task execution based on a different metric in each case. The first one aims to optimize a task-related cost function, while the second one is oriented towards the user comfort. In both chapters, the user is guided, through haptic guidance and/or visual data, in the direction of task execution that improves these metrics of interest. However, the user is the final decision maker in the system, and can choose to follow or not the guidance that is given to him/her. As such, we refer to the methods in this part as methods with “human authority”.

In **Chapter 3**, we present a haptic shared-control method for minimizing the manipulator torque effort during bilateral teleoperation. Minimizing torque is important because it reduces the operating cost of the system and extends the range of objects it can manipulate. Our proposed architecture generates, during teleoperation, visuo-haptic navigation feedback to help the operator in choosing a grasping configuration locally minimizing the expected torque effort in the desired post-grasp manipulative phase. We also demonstrate the effectiveness of the proposed approach in a series of representative pick-and-place experiments as well as in a human subjects study, and compare the effects of visual and haptic guidance on the user performance.

In **Chapter 4** we present a haptic-enabled shared-control approach aimed at minimizing the user’s workload during a teleoperated manipulation task. In fact, while haptic shared-control methods are usually used for different purposes, such as navigating along paths minimizing the torques requested to the manipulator (e.g., **Chapter 3**) or avoiding possibly dangerous areas of the workspace, few works

have focused on using these ideas to account for the user’s comfort. We performed studies with human subjects to show the effectiveness of the proposed approach, and show the results in the end of this chapter.

1.2.3 Part III

Unlike in the previous part, where the user was in control and could still disregard the “help” from the autonomous system, Part III presents two systems where the human-robot authority is more shifted towards robot autonomy than human control. The user is of course still in the loop, and haptic interaction is present and used to help the task execution. However, the user intervenes in a less direct way.

In **Chapter 5** we present two haptic shared-control approaches for robotic cutting, which are designed to assist the human operator in the cutting task. Soft and hard constraints are imposed on the user that take into account the specificity of the task and ensure the nonholonomic constraint representative of a cutting task is applied. To validate our approach, we carried out a human-subject experiment in a real cutting scenario, and we compared our shared-control techniques with each other and with a standard haptic teleoperation scheme.

In **Chapter 6**, we shift towards autonomy even further. Unlike in previous chapters, where haptic information is provided to reflect contact forces or to guide the user in a teleoperation task, here we used teleoperation data with haptic feedback as a means to train an autonomous grasping algorithm. In fact, the robotic manipulation of fragile and compliant objects, such as food items, still faces many challenges. To improve existing autonomous algorithms, we propose a human-centered, haptic-based, Learning from Demonstration (LfD) policy that enables pre-trained autonomous grasping of food items using an anthropomorphic robotic system. The policy combines data from teleoperation and direct human manipulation of objects, embodying human intent and interaction areas of significance. We finally evaluate the proposed solution against a recent state-of-the-art LfD policy as well as against two standard impedance controller techniques.

1.2.4 Part IV

This last part is comprised of one chapter (**Chapter 7**), presenting concluding remarks and discussion points related to the contributions presented in this thesis. It also proposes some future directions to take in the field in general, and more particularly in relation to the thesis contributions.

1.3 Publications Related to this Thesis

- **R. Rahal**, G. Matarese, M. Gabiccini, A. Artoni, D. Prattichizzo, P. Robuffo Giordano, & C. Pacchierotti. “Caring about the Human Operator: Haptic Shared Control for Enhanced User Comfort in Robotic Telemanipulation.” *IEEE Transactions on Haptics*, vol. 13, no. 1, pp. 197-203, 1 Jan.-March 2020.

Video available at: <https://youtu.be/DodGI4wMRFA>.

- A. Lillienkiold, **R. Rahal**, P. Robuffo Giordano, C. Pacchierotti, & E. Misimi. “Human-Inspired Haptic Enabled Learning from Prehensile Move Demonstrations.” *IEEE Transactions on System, Man, and Cybernetics: Systems*, 2020. Accepted.

Video available at: <https://youtu.be/0LaDPbGwZlw>.

- **R. Rahal**, A. M. Ghalamzan-E., F. Abi-Farraj, C. Pacchierotti, & P. Robuffo Giordano. “Haptic Shared-Control System to Minimize Torque Effort during Robotic Telemanipulation.” Submitted to *IEEE Transactions on Robotics (TRO)*, 2020.

Video available at: <https://youtu.be/vqDop2YRCzA>.

- **R. Rahal**, F. Abi-Farraj, P. Robuffo Giordano, & C. Pacchierotti. “Haptic Shared-Control Methods for Robotic Cutting under Nonholonomic Constraints.” *IEEE/RSJ International Conference on Intelligent Robots and Systems (IROS)*, 2019.

Video available at: <https://youtu.be/DkW40cjgX9M>.

- **R. Rahal**, G. Matarese, M. Gabiccini, A. Artoni, D. Prattichizzo, P. Robuffo Giordano, & C. Pacchierotti. “Haptic Shared Control for Enhanced User Comfort in Robotic Telemanipulation.” *IEEE ICRA workshop on Shared Autonomy: Learning and Control*, 2020.

- **R. Rahal**, F. Abi-Farraj, P. Robuffo Giordano, & C. Pacchierotti. “Haptic Shared-Control Methods for Robotic Cutting under Nonholonomic Constraints.” *International Workshop on Human-Friendly Robotics*, 2019.

Part I

Preliminaries and State of the Art

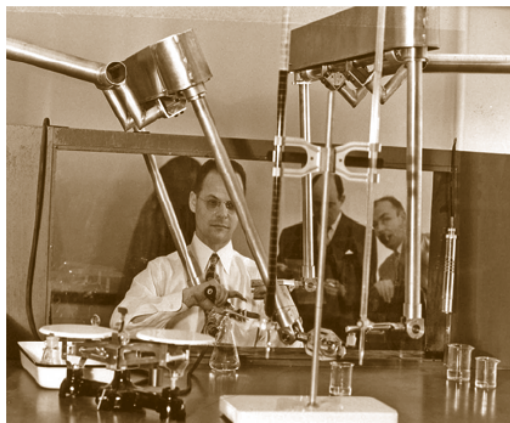
CHAPTER

2

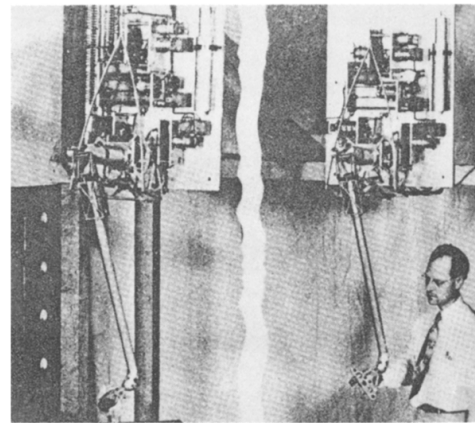
State of the Art

Contents

2.1	Telerobotics	12
2.1.1	History of Telerobotics	12
2.1.2	Teleoperation Systems	14
2.1.3	Haptic Feedback in Teleoperation	15
2.2	Shared Autonomy	17
2.2.1	Human Robot Interaction	18
2.2.2	Shared Control	20
2.2.2.1	Virtual Fixtures	20
2.2.2.2	Haptic Shared Control	22
2.2.2.3	Semi-autonomous control	23
2.2.2.4	Mixed Initiative Control	24
2.2.3	Level of Authority	25



(a) First mechanical teleoperation system



(b) First electrical teleoperation system

Figure 2.1 – (a) The first mechanically linked teleoperation system designed by Goertz in the 1950s, photo courtesy of [3], and (b) the first (1954) electric one built by Goertz at Argonne National Laboratory, photo taken from [4].

In this thesis, we are mainly interested in designing haptic based control algorithms for robotic teleoperation, with variable degrees of autonomy. We start in this chapter by a brief summary and related works on telerobotics, a specific branch of human robot interaction which allows the user to command a robot at a distance. We then explore shared autonomy and the different ways humans and robots can interact to improve the task execution and make it more intuitive for the user.

2.1 Telerobotics

2.1.1 History of Telerobotics

The term *telerobotics* - or alternatively *teleoperation* or *telemanipulation* - comes in fact from the Greek “tele” which literally translates to “distant” [3]. Teleoperation was first introduced by Raymond C. Goertz in the late 1940s to answer to the needs of the nuclear research, allowing the human operator to handle radioactive material from a safe place. Starting from an electrical system to control the robot from behind a shielded wall, which proved to be slow and not easy to operate, Goertz built the first mechanically linked teleoperation system, shown in Fig. 2.1. This new system allowed the user to transmit motion more naturally, and provided haptic feedback from the remote environment [22]. However, mechanically connected systems can only work within a limited distance, which led to Goertz recognizing the value of electrically coupled manipulators and laying the foundations of the modern telerobotics field [2].

In the next decades, many systems were developed, such as the bilateral servo-manipulators for teleoperation developed by the french Commissariat à l'énergie atomique (CEA) by Vertut and his team [23, 24], also inspired by nuclear applications. Another early example is the Central Research Laboratory model M2 (1982) which was the first telerobotic system to realize force feedback with separate master and remote robot electronics and was used for different demonstration tasks in military, space and nuclear applications [3].

In the 1980s and 1990s, the nuclear-related activities declined, and interest shifted to other areas such as space, medical and underwater robotics, which was also facilitated by the increased availability of computer power and the development of haptic devices such as the PHANToM device [25]. Similarly to the case of nuclear application, the use of telerobotics in other fields was motivated in scenarios where the human operator cannot be physically present in the remote environment, whether for safety purposes or because of the high cost incurred. For example, telerobotics has been used in space and underwater applications. In 2001, the first transatlantic telesurgery was performed with the patient in Strasbourg, France and the surgeon in New York, USA, relying on visual feedback only [26]. This successful experiment showcased many benefits of remote surgery, from the removal of geographical constraints in access to healthcare – with patients in less advantaged communities or in an emergency situation having access to surgeries by experienced surgeon – to surgical education, with surgeons teaching the performance of an advanced or new technique with the possibility of real-time intervention.

Beyond the constraint of the user's presence in the remote environment, the use of telerobotics is also motivated by the limited capabilities that the human and the robots each have separately. For example, the human can benefit from the robot precision and scaling of motion to accomplish micro or nano-level maneuvers like in micro-surgeries. On the other hand, robots can also benefit from the human capacities and high-level decision-making. In fact, while autonomous robots have recently gained a lot of new capabilities, they are still far from the reliability and safety required by many applications, such as medical robotics [27] or hazardous waste management [28]. In these industries, robotic teleoperation is an effective tool to combine the experience and cognitive capabilities of a human operator with the precision, strength, and repeatability of a robotic system. Examples are in nuclear waste decommissioning [29], minimally-invasive surgery [30], demolition [31], tissue palpation [32, 33], and needle insertion [32].

2.1.2 Teleoperation Systems

Teleoperation systems consist of two sides: the master side, which is commanded by the human, and the slave or remote side, in charge of executing the task and interacting with the environment, also referred to as *teleoperator*. The two sides are connected through a communication channel, and they interact through a set of sensors that allows the transmission of motion and force information between them. Fig. 2.2 illustrates an example of a teleoperation system. The user, present at the master level, commands the remote robot by actuating the master interface. Sensors are present to measure this input and transmit it as a command to the robot which performs the desired task. Actuators and sensors are also present at the remote side, and feedback information (such as haptic and visual feedback) is given back to the user to increase transparency.

In recent years, many systems with a virtual remote environment were implemented. The virtual environment simulates the real setting in terms of interaction with the operator, and could be used for training or testing a control scheme before implementation on the real hardware. This could be useful for example for medical training [34, 35], or in space exploration settings, where training can be performed in a flexible and safe environment which would lead to reduced costs and time, and an increased success rate for future missions [36]. Virtual teleoperation is also an active field in microscale applications where it can be used for education, training and system evaluation [37].

In the design of teleoperation systems, achieving telepresence is a very important goal. *Telepresence* is the ideal situation where the user feels in a natural way the interaction that happens with the environment, as if he/she is physically present at the remote site [38, 39]. To allow this, the system should have enough transparency, which could be defined as a correspondence between the master and remote robot positions and forces, or a match between the impedance perceived by the user and that of the environment [40]. However, transparency and stability are usually conflicting conditions [41], and thus a trade-off needs to be done in such a way that transparency is reduced to guarantee stable operation in the wide range of environment impedance values [41, 42].

This brings us to another important condition in the design of control architectures for teleoperation, which is guaranteeing system stability. To ensure that this condition is satisfied, many control methods have been presented in the literature, especially to deal with time delay and its effect on stability. These methods are summarized in [43]. Among these methods, passivity-based controllers are particularly popular. Simply put, a system is passive if and only if the system does not

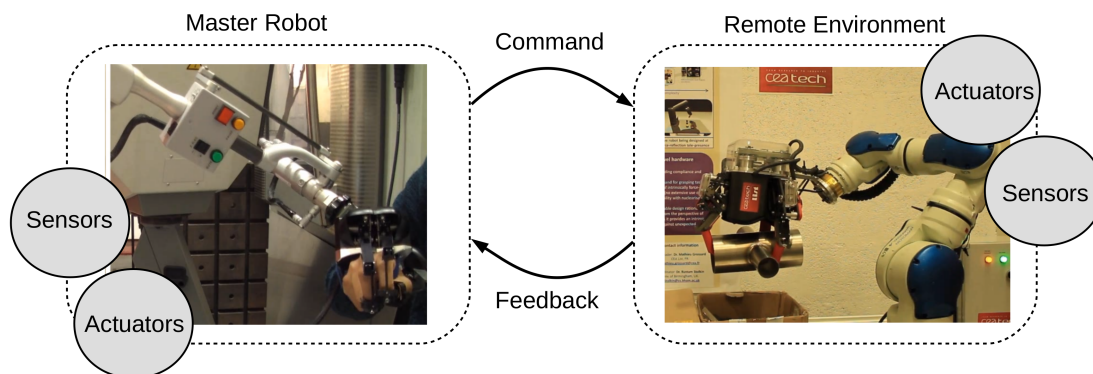


Figure 2.2 – General architecture of a teleoperation system.

generate energy, i.e. the energy output is bounded by the initial and accumulated energy in the system. If the individual blocks of a system are passive, the entire system is passive, and the human operator and the environment are usually considered as passive subsystems [3]. However, while passive systems are guaranteed to be stable, they are usually overly conservative which often reduces the transparency of the system and leads to a degraded performance. New methods, such as energy tanks, have been implemented in the literature to achieve high system performance while keeping a passive behavior (e.g. [12–16]). Other examples of stability-imposing algorithms are Passive-Set-Position-Modulation (PSPM) [17], and time-domain passivity algorithms [18–21]. Of course, the stability of the system also depends on the technological development and the state of the hardware. The time delay and jitter in the network, the robot capabilities and its sensor precision, as well as the haptic device characteristics all play a role in rendering the system stable. An important factor is also the stiffness of the remote environment. Since haptic feedback is an important element of telepresence but could also be a source of instability in the system, more and more research is being done on the topic of safely providing haptic information in teleoperation.

2.1.3 Haptic Feedback in Teleoperation

This thesis focuses on haptics and its use in robotic teleoperation. As such, in this section, we briefly introduce the advances in the field, the different types of haptic stimuli used in the literature, the challenges and limitations. The concentration here is mainly on the use of haptics as feedback information from the environment (e.g., contact forces). A later section (Sec. 2.2.2) will deal with the use of haptic stimuli for shared control and user guidance.

The broad definition of *haptics* refers to the sense of touch of the human being. Using both kinesthetic (force/position) and cutaneous (tactile) receptors,

humans are capable of perceiving, interacting with, and manipulating objects around them. Simple examples from everyday life demonstrate the importance of this sense, for example, in writing, trying to reach an object in the dark, or buttoning a shirt. Nonetheless, even more basic tasks would not be possible to complete without haptic information. For instance, humans would not be able to walk, move their limbs or grasp objects – even in broad daylight – without the cutaneous sensations under their feet or in their fingertips. In the robotics and virtual reality literature, haptics is defined as the various combinations of real and simulated touch interactions between robots, humans, and real, remote, or simulated environments. These interactions are made possible through haptic interfaces, that allow human operators to experience the sense of touch in remote (teleoperated) or simulated (virtual) environments [44].

As explained in Sec. 2.1.2, achieving telepresence relies on the transmission of different types of information from the remote environment to the user executing the task. This is achieved through different types of feedback, such as visual and haptic feedback. Traditionally, teleoperation systems relied primarily on visual feedback to the operator, which is implemented until now in many commercially available systems, such as the da Vinci Surgical System, by Intuitive Surgical, USA. However, relying on visual feedback alone results in a high cognitive load on the operator [45], or could result in performance degradation in case of partial occlusion of the view. Therefore, interest in haptic feedback started increasing and led to the development of different types of haptic interfaces providing kinesthetic feedback (such as the Omega developed by Force Dimension, Switzerland, the Phantom by 3D Systems, USA, or the Virtuose 6D by Haption, France), and cutaneous feedback. Kinesthetic feedback gives the human operator information about the position and velocity of the neighboring objects, as well as applied forces and torques through receptors in the skin, muscles and joints. Devices that provide this type of feedback are usually called *grounded* haptic devices [46]. On the other hand, cutaneous feedback provides information on the local properties of objects by applying shear, vibratory, or indentation forces on the user’s skin to induce local deformations, which are sensed by the mechanoreceptors in the skin. While grounded haptic interfaces also provide cutaneous sensations, wearable (or *ungrounded*) devices are usually used for this purpose, e.g. [47,48]. In teleoperation scenarios, fingertips cutaneous devices are the most popular [33,49,50] as this part of the body is usually the most involved in haptic interactions with objects. More recently, there has been a growing interest in non-contact haptic devices that can convey haptic information without hindering the user motion [51], such as mid-air haptic devices that provide cutaneous feedback remotely through focused

ultrasound phased arrays [52, 53].

Previous works have shown the role of haptic feedback in improving different parameters like completion time [54, 55], accuracy [54], and force applied by the user [56]. In recent years, haptic feedback has gained considerable attention especially in the medical field, and it showed reduction in errors and decrease in operation time and damage to the environment [45]. The combination of visual and haptic feedback has also shown to improve the performance of the operator. For example, in [57], the authors use a 3D virtual representation of the scene and haptic information to help the user perform a microscale manipulation task between Paris, France and Oldenburg, Germany.

Despite the proven benefits of adding haptic feedback in the loop, the actual implementation of such feedback, especially through grounded haptic interfaces, is still limited given the potential instability it could lead to, especially when going into contact with a stiff material, or in the case of communication delays. In addition, other cons of using grounded haptic feedback is the high cost and the encumbrance of the user motion. The use of ungrounded haptic devices has been developed to tackle these issues, and as a means to decrease the instability by decoupling the sensing and actuation on the master side. Designing the right control algorithm could of course ensure stability as explained in Sec. 2.1.2, however, they lead to a reduced transparency of the system. In this respect, teleoperation systems still present multiple challenges to marry stability and telepresence. In [58], the authors propose to combine kinesthetic and cutaneous force feedback by mixing the cutaneous-only approach of sensory subtraction with a time-domain passivity control algorithm. This allows to preserve the performance by providing a suitable amount of cutaneous force when kinesthetic feedback needs to be modulated.

2.2 Shared Autonomy

As we have explained in the first part of this chapter, telerobotics is still a relevant and necessary field for many areas of application. In nuclear environments, search and rescue missions, and deep sea or space operations, the human cannot be physically present to perform the task given the hazardous type of the environment and the risks incurred. At the same time, despite the developments in automation in recent years, autonomous systems are still incapable of dealing with unseen or unpredictable events and still lack the logic and problem solving capabilities of humans. In other cases like micro-surgery, the human might be capable of performing the task on his/her own, but the robot precision and scaling ability

is often desired. Given that medical robotics is a very conservative field in direct contact with human patients, the robot, in its current state of advancement, is still not trusted to perform operations on its own. As such, teleoperation allows to combine both competences of humans and robots to perform delicate tasks in multiple settings. Having said that, direct teleoperation is often too challenging and tiring for the human. This led to new approaches where the control of the system is *shared* between the operator and the robot, referred to as shared-control architectures. Early forms of HRI experiments, such as supervisory control, were reported in [59]. They were followed by many contributions ranging from advanced control theoretical methods to teleoperation-oriented software languages, visual enhancements and hybrid representations [43, 60–62]. The field slowly evolved over the years, and was established as an independent multi-disciplinary field in the 1990s [11]. In the next part, we present a more in depth literature review on shared autonomy, its position in the HRI spectrum, and the role of haptics in shared-control architectures.

2.2.1 Human Robot Interaction

Although many of the early robotics works can be considered to be part of HRI, this multi-disciplinary field gained its independence starting the mid 1990s and early 2000s. HRI drew the attention of researchers from many disciplines: robotics, psychology, cognitive science, human factors, natural language and human–computer interaction. They all helped in driving forward the advancements in the area. As defined in [11], HRI is a field of study that is “dedicated to understanding, designing, and evaluating robotic systems for use by or with humans”. As we have explained, every robotic system, even the most autonomous one, is operated by humans or used to fulfill a certain human need. Therefore, a minimal interaction between the human and the robot is necessary. However, HRI is mainly related to a more direct and continuous interaction that could be remote (as in teleoperation) or proximate (as in service robots).

Autonomy is thus for HRI a means rather than a goal in itself. Therefore, the *level of autonomy (LOA)* describes the degree with which the robot can act by itself, and varies depending on the application. While different representations of these levels have been presented in the literature, the scale that was presented by Sheridan [63] is still the most widely used to represent the different levels of autonomy:

1. Computer offers no assistance; human does it all.

-
2. Computer offers a complete set of action alternatives.
 3. Computer narrows the selection down to a few choices.
 4. Computer suggests a single action.
 5. Computer executes that action if human approves.
 6. Computer allows the human limited time to veto before automatic execution.
 7. Computer executes automatically then necessarily informs the human.
 8. Computer informs human after automatic execution only if human asks.
 9. Computer informs human after automatic execution only if it decides to.
 10. Computer decides everything and acts autonomously, ignoring the human.

The scale displays a continuum between direct manual command (or direct teleoperation, which we have presented in the previous chapter), and complete robot autonomy. Many other scales were also exposed in the literature (e.g. [64]), and some authors noted that the scale should not be applied to the entire domain but rather to each subtask of the problem alone [65].

In the context of telerobotics, control architectures have been classically divided into three categories based on the level of automation: *direct control*, *shared control*, and *supervisory control* [3]. *Direct control* involves no autonomy, and it is represented by simple teleoperation systems that have been developed and presented in Sec. 2.1.2. *Supervisory control*, on the other hand, relies on a strong local robot autonomy. The user commands high level goals for the system, while the robot takes care of the low level execution details. For example, in the case of a grasping scenario, the user could be in charge of choosing the final grasping pose, but the path to arrive there could be automatically planned by the robot. The human in this case is not in control of particular degrees of freedom of the system, but chooses from a set of pre-defined subtasks that the system executes autonomously. This type of control is useful for routines tasks such as handling parts on manufacturing assembly lines or delivering packages, mail, or medicine in warehouses, offices, and hospitals [1]. It is also common in remote environments where direct control is not possible due to long time delays [66–68]. For example, the Mars Rovers are controlled in supervisory control mode because of the large time delay between the Earth and Mars preventing any instantaneous communication [69]. Teleprogramming [67, 70] is an extension to earlier supervisory methods that deals with communication delays by automatically issuing

a sequence of elementary motion commands, based on the operator’s action in a simulated environment, to the remote robot [71]. In between the two endpoints, *shared control* allows the human operator to be in full or partial control of the system, while being assisted by the autonomy in the task execution. A good example to illustrate shared control is the case of a dual-arm robotic system where one of the robots is teleoperated by a human, while the other robot autonomously executes a task in the same workspace. The human and the automation components work together to perform the task at hand. For instance, the autonomous robot could be in charge of keeping the object in the field of view using a camera [72–74], while the human is in full (or partial) control of the other one, to perform the grasping of the object.

In this thesis, we are interested in this latter type of HRI in particular. In the next section, we describe in more details the types of assisted control that exist, and focus on the role that haptic information can play in the design of such systems.

2.2.2 Shared Control

Shared control is a type of assisted control where the human and the autonomy interact while performing the task to decrease the cognitive load on the user, and improve the performance and the task execution. In assisted control, different types of autonomous assistance can be provided to the user, such as visual, haptic or auditory feedback, as well as assistance in control [75]. While the focus of this thesis is on shared control for the teleoperation of robotic manipulators, shared-control systems have been used for a wide range of applications, from teleoperating serial manipulators [76–81] to controlling wheelchairs [82–84], surgical tools [85, 86], vehicle guidance [87–89], Unmanned Aerial Vehicles (UAVs) [90–93], and mobile robots [94, 95].

Different types of shared-control methods have been treated in the literature, and the fact is that nomenclature is not always clear, and in many cases these methods are correlated to each other so it is hard to draw the line between them.

2.2.2.1 Virtual Fixtures

Virtual fixtures (VFs) are widely used in shared-control systems. They were introduced in [79], and were metaphorically defined to act “Like a ruler guiding a pencil in the real world”. In practice, VFs restrict the system state to a specific space, adding constraints to the manipulability of the robot. VFs have been used in many applications, e.g. [96–100], and previous works have proven that they sig-

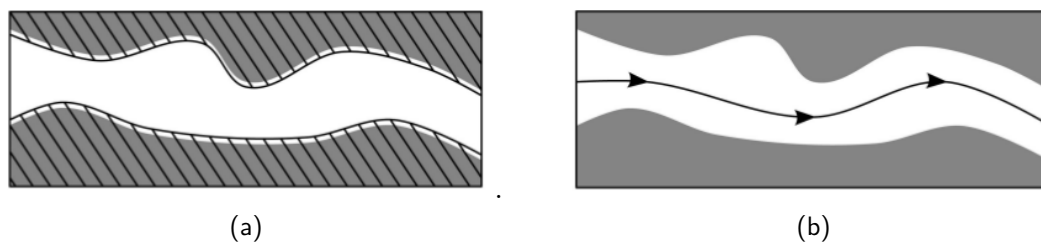


Figure 2.3 – (a) Forbidden region virtual fixtures and (b) Guidance virtual fixtures. Obstacles are represented in gray and the constraints are shown in black. Photo courtesy of [103]

nificantly improve the task performance [79,101] and reduce the mental workload experienced by the user [102].

VFs (also called active constraints) are characterized by the type of geometry-related constraint, and the constraint enforcement method. The geometry constraint can be of any dimension, such as points, lines, curves, surfaces or volumes. The enforcement method can also vary between *Guidance Virtual Fixtures*, where the user is encouraged to move the robot along a specific pathway or towards a specific target, and *Forbidden-Regions Virtual Fixtures (FRVF)* that limit the robot to specific regions within its task or joint space [103]. These two types of VFs are illustrated in Fig. 2.3. Depending on the type of constraint to apply, we can also distinguish *soft* and *hard* VFs. In [104], the authors present a controller for bilateral teleoperation that relies on hierarchical optimization to obtain kinematic correspondence between the master robot and the remote manipulator, while allowing the simultaneous definition of hard and soft virtual fixtures.

A main limitation of VFs relates to the fact that they are highly task-dependent and usually cannot adapt to changes in the environment. For example, in [105], the authors compare several FRVF constraints, on four different control architectures using three different metrics: tracking, safety and submittance. Results have shown that different FRVRs performed best for each of the three metrics, and thus the choice of the best fixture is related to the application and task at hand.

Another limitation is the level of assistance that the virtual fixture should provide the user with, or in other words, the right magnitude of the virtual spring force. This choice depends on many factors, including the task, the capabilities of the human operator (cognitive or neuromuscular), the quality of the automation system etc.. And in fact it is not an easy choice to make. If the spring is too stiff, the performance of the user improves, but the system is harder to overrule [106]. Some of the existing works on the choice of the level of assistance are discussed in more details in Sec. 2.2.3.

VFs can be defined either on the master or on the remote robot side. In

fact, these may consist of force cues, additional motion commands applied to the manipulator itself, a restriction of the motion of the manipulator, or even a graphical representation in the form of visual cues [97]. For example, in [79], FRVFs were implemented as impedance surfaces on the master side for guiding the user in a peg-in-hole task. In [96], FRVFs were implemented on the remote robot by rejecting master commands into the forbidden region. In [97], virtual fixtures were implemented on both the master and remote manipulators to guide the remote manipulator to perform a predetermined task. In [105], the authors present different control architectures for providing the user with efficient FRVFs and compare whether implementing virtual fixtures on the master or the remote side (or both) leads to the most desirable system behavior. Soft and hard virtual fixtures are implemented and tested in a comprehensive user study.

When implemented on the master side, VFs can either be rendered using information from the master or from the remote robot, and these two approaches have been used in the literature, even though this choice is not always justified. For instance, some works rendered the constraints on the master, e.g. [71, 107, 108], while others rendered them based on the robot information, such as in [109–113]. The advantage of rendering the VFs on the master side is that the resulting system is more stable, however, if the robot is not exactly following the master motion, this could lead to the wrong application of the VFs on the remote robot side. Therefore, VFs rendered on the remote side are more suitable for applications requiring a precise robot motion.

2.2.2.2 Haptic Shared Control

The name *Haptic Shared Control* (HSC) was proposed by Abbink et al. in [114]. The work reviewed several implementations of haptic shared control, arguing that it can be useful to meet common design guidelines for the interaction between humans and autonomous controllers. According to the authors, virtual fixtures are the first instances of HSC developed in the literature. Subsequently, many HSC methods were developed for multiple applications such as car-following problems [114, 115] and teleoperation [101, 116–118].

Haptic shared control is defined as a method of human-automation interaction that “...allows both the human and the [automation] to exert forces on a control interface, of which its output (its position) remains the direct input to the controlled system.” As a result, in HSC, the human retains the final authority in deciding on the command. The system can provide the user with haptic guidance to inform them on the automation preference, but the operator can override this

information.

HSC has been successfully used in a variety of applications. For example, it has been employed to guide the human operator towards a reference position or along a given path [119–122], avoid certain areas of the environment [123] or dangerous configuration of the remote robot [124], learn a manual task [125], and ease the grasp of irregularly-shaped objects [110]. Other applications of HSC include surgical suturing [30], industrial pick-and-place [126], mobile robotics [127], and industrial robotics [73].

More recently, Hong and Rozenblit [128] presented a haptic shared-control approach for surgical training. The trainee is guided away from dangerous areas of the environment using active constraints whose magnitudes change according to the trainee’s proficiency level. Similarly, Ghalamzan et al. [129] presented a haptic shared control for teleoperated grasping. The operators are in full control of the robotic manipulator and capable of choosing any grasping pose they like. At the same time, an active constraint guides them toward the direction that optimizes the end-effector manipulability over the post-grasp trajectory.

Recently, machine learning techniques and intention estimation methods have gained popularity, and they have allowed to develop new shared-control methods. For instance, Learning from Demonstration (LfD) was used to learn the task model and to provide the user with the needed assistance in a structured manner [130–132]. It has also been used to determine the desired level of autonomy based on the confidence of the human and automation components [133, 134]. In [135], the authors present an LfD approach specifically designed to handle inconsistent demonstrations from teleoperation, with large spatial and temporal variations, which was tested with two shared-control architectures. Incremental learning was also introduced to allow the user to modify the learnt model if a change in the environment occurs. For instance, in [136], the learned distributions are autonomously refined through interactive task execution. In [137], the authors propose an online incremental learning method which allows the operator to partially modify a learned model through teleoperation, during the task execution. The system implements a shared-control method with dynamic authority distribution and kinesthetic coupling between the user and the automation.

2.2.2.3 Semi-autonomous control

Depending on the partition of the control space between the human operator and autonomy, assisted control methods can be divided into two groups:

- **Partitioned space**

The control of the state variables is divided between the user and the automation system. An example is a task where the position and the orientation of the robot end-effector are shared between the two. For instance, the user controls the position manually while the assistive system controls the orientation.

This type of control is known as *Semi-Autonomous Control*.

- **Shared space**

The state variables are jointly controlled by the operator and the automation. As such, the degrees of freedom (DoF) of the system receive commands from the two actors, and the command of each side can be modified or overridden by the other. The weighting between the two inputs determines the level of automation, which we will explain in more details in the next section.

Depending on their application, VFs can be either seen as a type of shared control or semi-autonomous control [133].

2.2.2.4 Mixed Initiative Control

In addition to the categorization presented above that is based on the control space partition, shared-control methods can also be divided depending on the level at which the human and the automation intentions are mixed. As explained in Sec. 2.2.2.2, HSC methods (and the majority of VFs which also fall under this category) are designed such that the automation information is translated through haptic interaction at the master side. The intentions are then mixed at the operator level (e.g. [79, 96, 138, 139]). The advantage of such a method is that the user is fully aware of the system behaviour, and of the information the automation system is trying to provide. [133].

Alternatively, the user commands and the automation information could be mixed directly at the robot level. This type of control is referred to as Mixed Initiative Control [140] or State Shared Control, since the intentions of the human and the automation are mixed at the state level. It was also given other names in the literature, such as input-mixing shared control [141], input blending control [142] or policy blending [143]. The two inputs to the robot are usually mixed using a weighted combination, which allows to control the level of authority of the automation component. More on this will be explained in the Sec. 2.2.3.

2.2.3 Level of Authority

A main issue in the design of shared-control methods is the level of authority to give to each of the human and the automation side. Authority allocation in shared control is a challenging topic that has been extensively discussed in the literature. The optimal degree of automation versus human input in a robotic system is in fact not easy to determine. Traditionally, the level of automation was constant in shared-control scenarios, then sliding autonomy, adjustable autonomy, and sliding scale autonomy were introduced, where the robot shifts between pre-defined discrete levels of autonomy. More recently, continuous change in autonomy was introduced in a new definition of sliding scale autonomy [143]. Most works on the topic are in the context of mixed initiative control, but authority allocation has also been investigated in haptic shared-control scenarios.

In [114], Abbink et al. argue that haptic shared control is a promising approach in human-automation interaction, especially in the automotive applications. In the design guidelines proposed, they introduce the level of automation (LoA) as an important factor to be properly chosen. They distinguish *adaptive automation* which is an automation-initiated change in LoA, and *adaptable automation* where the user has control on this switch in automation level. The advantage of haptic shared-control methods is that they allow to design shifts in control authority through physical interaction: the guiding force could be tuned to be high, low or even absent (full automation) for the same error (between current and target angle for example). So the human is always the one in control, in contrast to mixed initiative shared control, as we have previously explained. The authors of [114] then mention some implementations of haptic shared-control systems with fixed (usually chosen by trial and error) and variable authority, introducing the level of haptic authority (LoHA) metric [144].

Shifting between automation levels could be either through discrete levels (ex: [120]), or in a continuous manner. In [120], the issue of distributing control among human and assistant in a haptic shared-control scenario is raised by varying the amount of haptic support provided to the operator. While previously designed assistance functions do not deal with unexpected events since assistance is not updated using environmental information, what they propose is to tune the assistance online to optimize task performance and human effort simultaneously. The assistance level should increase in known environment where human and haptic assistance work together, but decrease in case unexpected events occur so that the user can freely react and not be hindered by the assistant (causing more human effort). To do this, [120] considers a 2D maze application and dis-

tinguishes between the 2 scenarios above using a measure of interactive forces. The optimal weight for the haptic assistance force is then chosen for each scenario (from discrete values already fixed).

On the other hand, some works switch the variable assistance in a more continuous fashion. The autonomous controller is typically the party in charge of switching between the levels of assistance, depending on the user performances [145], potentially dangerous situations [115] or the robot confidence in the prediction of the user motions and the difficulty of the task [146], [143].

In [143], a policy blending is introduced as an interpretation of shared control: a formalism for the robot assistance as an arbitration of two policies, namely, the user input and the robot prediction of the user intent. At any instant, the robot combines the input and the prediction using a state-dependent arbitration function. In terms of prediction the problem is formulated based on an inverse reinforcement learning. Instead of using autonomy as a factor, this paper uses aggressiveness; arbitration should be moderated by the robot confidence in the prediction.

The paper [147] summarizes many of the previous works on the topic. In addition, there are multiple recent works have presented methods with variable authority allocation [133, 148–151]. For instance, Zeestraten et al. [133] present a method to determine the level of automation online, by combining the confidence of automation and that of the user. They implement their approach in haptic shared control and in a mixed initiative control by using Programming by Demonstration. However, determining the right authority level is still not easy to answer, and remains one of the open questions in the shared control field. In fact, an interesting question was raised by the authors of this paper when discussing the confidence of the user input estimation: “... *who has the final say in control authority, the user or the assistive system?*”.

Part II

Haptic Shared-Control Methods with Human Authority

CHAPTER

3

Haptic Shared-Control System to Minimize Torque Effort during Robotic Telemanipulation

Contents

3.1	Related Works	33
3.2	Shared-Control Method	37
3.2.1	System details	39
3.2.2	Manipulator Dynamics Under Load	41
3.2.3	Task Oriented Torque Effort (TOTE) Cost Function	43
3.3	Navigation Information	43
3.3.1	Haptic Navigation Guidance	44
3.3.2	Visual Navigation Guidance	45
3.4	Pick-and-Place Experiment	46
3.4.1	Experimental Setup	46
3.4.2	Task and Methods	47
3.4.3	Results	50
3.5	Human-Subjects Study	51
3.5.1	Task and Feedback Conditions	51
3.5.2	Participants	52

3.5.3 Results	52
3.6 Discussion	56

As explained in Chapter 2, teleoperating dexterous robotic manipulators can be rather complicated and cognitively demanding for the human operator. Therefore, shared-control methods have been designed and used in multiple applications where teleoperation systems are still popular, such as in the remote handling of hazardous material. In this part of the thesis, we are interested in designing new haptic shared-control methods (see Sec. 2.2.2.2) for robotic grasping and manipulation, where we provide the user with haptic information to help him/her performing the task. The haptic information is provided on the master interface level, informing the operator of the desirable action to take in terms of minimizing some task-related (Chapter 3) or human-related metric (Chapter 4). The human is given the final authority despite this guidance information, as will be explained in more details in the next two chapters.

In the context of this Part II, the task can be divided into three stages: the **pre-grasping** phase, where the user teleoperates the robot in the direction of the object to grasp, the **grasping** phase, and the **post-grasping** phase involving lifting and manipulative movements related to the object grasped.

In this chapter, we are interested in the post-grasp phase of the task. Haptic shared control in robotic teleoperation has been employed to, e.g., guide the human operator towards a reference position or along a given path, to avoid certain areas of the robot workspace, to teach the operator a manual task, and to ease the grasp of irregularly-shaped objects. However, shared control has rarely been used to optimize a relevant metric over the future consequences of a local operator's action, such as maximizing the robot workspace in a certain direction after releasing an object, positioning the robot body so as to optimize the user's viewpoint on a future action, or choosing the best grasp pose to minimize the torque exerted by the robot over a post-grasp trajectory. Targeting the future trajectory in the design of the shared-control algorithm for the pre-grasp phase is important in many applications. As an example, we can consider a nuclear decommissioning site where the user should command the remote robot to grasp different objects and move them to another location. The grasping action, in many cases, cannot be automated. In fact, the human's cognitive abilities are still needed in the cases of cluttered environment, or even simply to judge the best grasping pose of an object based on its physical properties. The grasping can thus be semi-automated, with the system suggesting possible grasp poses automatically, and allowing the user to make the final decision. On the other hand, the post-grasp trajectory of the object is well-defined and can be computed based on the initial and final desired pose using any modern trajectory planner. As such, it can be autonomously executed by the robot. However, while the object trajectory is fixed, the grasping

pose chosen by the operator decides on the trajectory performed by the robot in the post-grasp phase. Since the user usually does not have an intuition about the robot performance in the future trajectory based on the grasping pose, shared control can be used to help the user in the choice of the grasp that would optimize a future metric over the post-grasp task. This interesting problem was tackled in a preliminary study by Ghalamzan et al. [126], where the authors proposed a shared-control algorithm able to guide the human operator towards a grasping pose that minimizes the proximity to robot singularities during the execution of the object future trajectory. Although the preliminary results of [126] were quite promising, it was noticed that directly providing the haptic cues may sometimes result confusing for the human operator since the cues (that follow the gradient of the chosen cost function w.r.t. the current pose) may end up guiding the operator towards unfeasible grasping poses.

Therefore, this chapter improves on the previous work, and presents a haptic shared-control method for minimizing the manipulator torque effort during the post-grasp phase. Minimizing torque is important because it reduces the system operating cost and extends the range of objects it can manipulate. In fact, the robot has a limited control authority, e.g., in terms of maximum joint torques, and carrying the object from the wrong grasping pose might lead to reaching the joint torques limit in the future trajectory, thus leading to an unnecessary failure of the manipulation task. In addition, unlike [126], our algorithm makes sure that the cues will always guide towards a feasible grasping pose.

First, we use a geometric grasping algorithm to find all the feasible grasp poses on the designated object. Then, for each feasible grasp pose, we evaluate the (integral) torque the remote robot would exert to pick up the object and move it along a desired pre-planned trajectory. We propose to convey this torque-related information using haptic guidance, visual guidance, or a combination of the two. We demonstrate the feasibility and effectiveness of the proposed approach in a set of representative pick-and-place tasks as well as in a human subjects study, where we compare the performance of the above three feedback modalities. The contributions that we present in this chapter can be summarized as follows:

- present a shared-control technique selecting the best local grasping pose to minimize the robot torque over a future post-grasp trajectory;
- devise three feedback techniques to guide the operator towards the best local grasp pose: haptic-only, visual-only, and combined visuo-haptic guidance;
- carry out real-world trials using three representative objects having different shape, dimension, and weight;

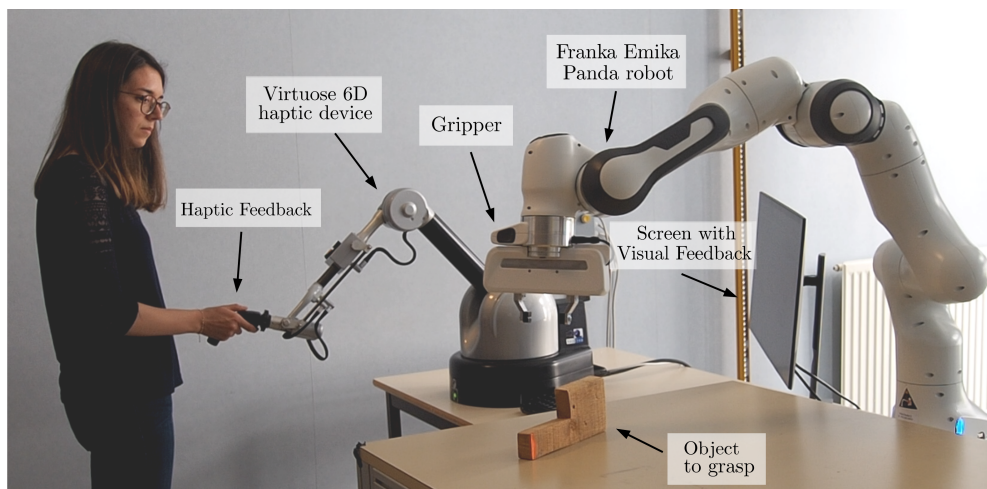


Figure 3.1 – Teleoperation setup. The human operator uses a Virtuose 6D grounded haptic interface (Haption, France) to control a 7-DoF Panda robotic manipulator (Franka Emika, Germany), used as a 6-DoF manipulator. The user receives haptic feedback through the haptic interface and visual feedback from an LCD screen.

- carry out a human subjects evaluation with 15 subjects, using statistical tools to compare the considered feedback conditions over six metrics.

The proposed framework is compatible with any dexterous robotic teleoperation system and it only requires the 3-dimensional model and inertia matrix of the target object(s). As a proof of concept, we consider a teleoperation system (Fig. 3.1) composed of a 6-DoF grounded haptic interface and a 7-DoF robotic manipulator equipped with a parallel jaw gripper, reduced to a 6-DoF manipulator by fixing one of its joints.

This chapter includes work that was done in collaboration with the University of Lincoln, UK, and submitted to IEEE Transactions on Robotics (TRO). A video summarizing the chapter is available at <https://youtu.be/vqDop2YRCzA>.

3.1 Related Works

Robotic grasping and manipulative movements are key elements to build a reliable robotic solution. Simple robotic manipulation task can be classified in two categories: (i) synthesizing grasp poses, and (ii) performing manipulative movements. There is a bulk of research on synthesising grasp poses from given single/multiple point clouds, *e.g.*, by sim-to-real learning [152], deep learning via domain randomization [153], deep learning that learns hand-eye coordination for grasping unknown objects [154] and probabilistic generative models of grasping configurations [155]. Other works, *e.g.* [156], reported improved performance in

synthesising grasping configuration for unknown objects by shape completion, *e.g.*, via primitive shape fitting to point cloud [157]. Nonetheless, autonomous grasping approaches lack reliable robustness for conservative industries, such as nuclear waste decommissioning. For instance, Kopicki et al. [158] propose an approach to improve some of these shortcomings reported in [155] such that the approach can partially generalize across different working conditions, unknown objects and unknown environments. Although the improved performance reported in [158] (i.e. < 25% improvement in the success w.r.t. the result reported in [155]) is significant, the obtained success rate is still far away from 100% which is demanded by conservative industries [29].

The works above are only concerned with (i) reach-to-grasp, (ii) forming grasping configuration on an object surface and (iii) lifting the object [159]. Nonetheless, the robot may need to deliver complex manipulative movements after making a stable grasp. Other lines of research studied the planning and control of manipulative movements [28, 160, 161] to deliver complex (e.g. post-grasp) actions. For instance, a robot may need to grasp an air paint spray gun and follow a specific trajectory to deliver the quality painting. There is a range of different manipulative movements, *e.g.*, they can be a simple pick-and-place task [162], suturing with a non-invasive surgical robot [30], robotic painting or robotic cutting [28]. The optimization based manipulation planning algorithm [161, 163, 164] can encode the environmental constraints into a cost function where it can be used to find the optimum trajectory in a given environment. While the robot can optimally perform a task using trajectories computed by optimization based approaches, they are usually computationally very expensive [163] and may not be suitable if the robot needs to quickly adapt to the changes in its environment. Robot learning from demonstrations (LfD) [165] was proposed to overcome this shortcoming and quickly generalize demonstrated trajectories to different static and dynamic environments [160].

These two lines of research, namely grasp synthesising and manipulative movements planning, have been studied mostly in isolation. However, synthesized grasping configurations may impose some constraints on feasible post-grasp manipulative movements. For example, a certain grasping configuration could lead to reaching singularities or joint limits in the post-grasp task. Moreover, the desired manipulative movements may limit the choice of suitable grasping configuration, *e.g.*, the screwing task determines a robot must form a stable grasp on the handle of a screwdriver. In this regard, Detry et al. [166] select the grasping pose with the maximum corresponding affordance utility value.

There are a few numbers of studies on jointly considering the problem of

grasping an object, and delivering desired post-grasp manipulative movements. For instance, [159, 162] studied how the choice of a grasp pose can be used to avoid singularities and collision during manipulative movements. Two-phase optimizations were used in [167] to generate the contact necessary for making a stable grasp on an object and to find the optimal object path that can be followed, given the optimal grasping configuration. In contrast, [168, 169] studied the optimal grasps resulting in a maximum manipulability at initial grasping configuration. Similarly, Mavrakis et al. [170, 171] studied the selection of the grasping configuration yielding the best safety value and torque efforts during the post-grasp manipulative movements. These works, however, assume a reliable planner can generate several precise/stable grasp poses where there does not yet exist a reliable autonomous system fully trusted by conservative industries for different scenarios, *e.g.*, for an arbitrary object in a variety of lighting conditions, makes this an open research challenge [172].

We propose to allow the human operator to be in charge of the grasping part of the task through haptic-based teleoperation, and the autonomous system to perform the post-grasp manipulative actions. Several assisted teleoperation frameworks have been proposed to tackle the problem of grasping or manipulation. For example, Achibet et al. [173] introduced a paradigm for visual-haptic manipulation of objects and [174] discussed the impact of different force-feedback-based control strategies on the operator’s performance during grasping. Similar studies for different manipulation tasks are presented in [175, 176]. In these works, the haptic feedback provided to the operator aims at transmitting the forces, which are sensed through tactile and/or force sensors of the robotic arm, to the operator. In contrast, Mason et al. [177] proposed an approach in which the operator is informed about the feasibility of modifying an intended trajectory. However, these assisted teleoperation approaches are used only for solving either reach-to-grasp (RtG) or post-grasp manipulative movements (PGMM). Neither of those facilitates planning jointly for both RtG and PGMM. Hence, a selected grasp by a human may not be optimal for post-grasp motions. In other words, the human operators are not informed about the consequences of their actions in a receding time horizon, *i.e.* about the quality of their preferred grasp pose in terms of control effort or singularity over the post-grasp motions.

Haptic-guided shared control has recently caught the attention of the researchers to improve the telemanipulation experience which helps joint solution of RtG and PGMM. For instance, [30] computes the optimal grasping configuration in a manifold of grasping configuration around a needle where the robot does not face any singularities or joint limits.

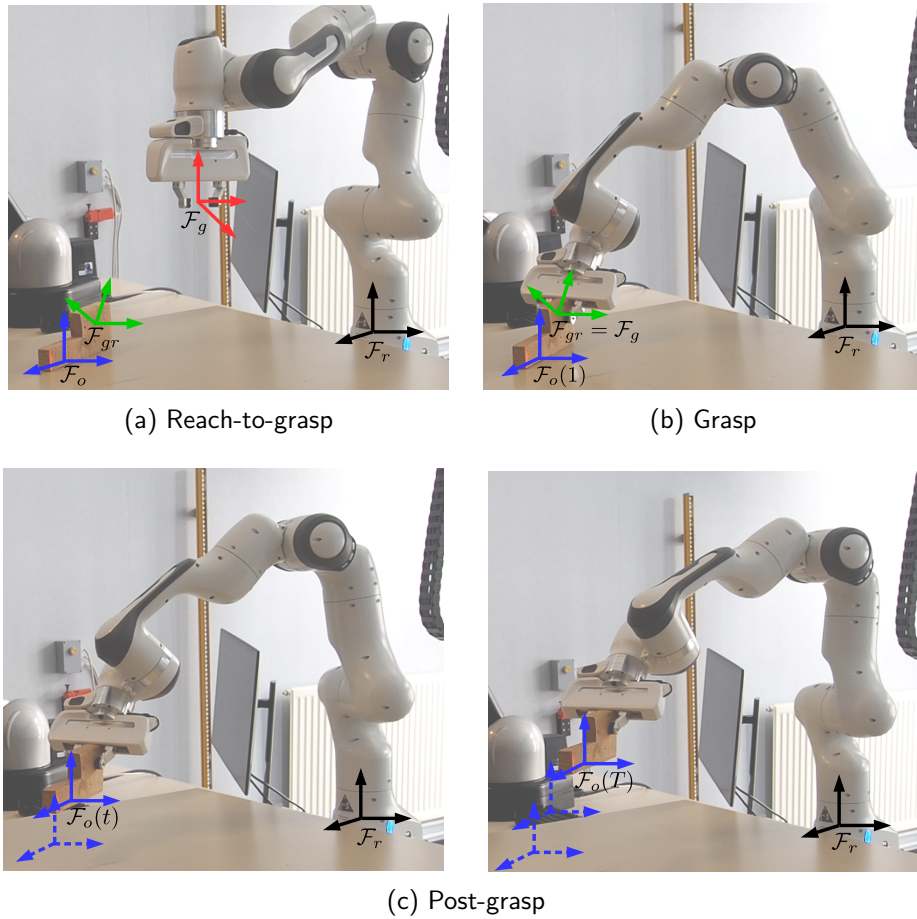


Figure 3.2 – Three phases of grasping an object: (a) *reach-to-grasp*—moving the robotic arm towards the object to be grasped; local coordinate frames are attached to the end-effector (red), centre of mass (CoM) of the object (blue) and the selected grasp pose (green); (b) grasping the target object, and (c) performing the required post-grasp manipulation; the past local frames attached to the CoM are shown with blue dashed lines. In this chapter, the first two phases are carried out via teleoperation, while the last one is performed autonomously. During the teleoperation, we provide visual-haptic feedback about the grasp poses minimizing the robot torque during the future autonomous manipulation phase.

However, the previous works do not consider the joint effort of the manipulator during manipulative movements. Ghalamzan et al. [126] studied how the user can benefit from the predictive singularity cost computation– based on a Task-Oriented Velocity manipulability (TOV) cost function– and select a grasping configuration so that the robot avoids singularities during manipulative movements. However, this optimization was performed without accounting for whether the resulting optimized end-effector pose was compatible with the main task of grasping the object as the force cues based on TOV cost can disagree with the movements toward the object to grasp. Moreover, neither of the works (i) use a combination visual-haptic guidance, nor (ii) use a discretized grasping manifold to provide a space of possible grasp poses. This chapter presents a shared-control system to address the above shortcomings and inform the operator about the grasp choice corresponding with the minimum torque effort – Task Oriented Torque Effort (TOTE) – the robot will exert during the manipulative movements. A grasp pose yielding the minimum joint effort is a very important factor as minimum joint effort correlates with the minimum robots running cost. It may also yield a safe distance to min/max joint effort limits imposed by the electrical motors at each joint. This can also result in an extended lifetime of the joint motors.

3.2 Shared-Control Method

Whenever an operator grasps an object using a teleoperated robotic manipulator, the grasping actions can be divided into three phases (see Fig. 3.2): (a) *reach-to-grasp*, when the remote robot moves towards the object to be grasped; (b) *grasp*, when the robot securely grasps the object with its end-effector; and (c) *post-grasp movements*, when the manipulator carries out the desired manipulation (e.g., moving the object towards a desired location).

As explained in Sec. 3.1, in this chapter, we decide to leave the human operators free to approach and grasp the target object according to their preferences and to then switch to the robot autonomy as soon as the object is grasped. In this way, the operator participates to the part of the task which is most demanding in terms of cognition while leaving more dull/easy parts to the robot autonomy. While the operator approaches the object, we provide feedback information about the torque necessary for the robot during delivering the object in the post-grasp autonomous movement phase. In fact, as shown in Fig. 3.3, for the same autonomous post-grasp manipulation defined for the object, two different grasp poses lead to different robot configurations, resulting, in turn, to different torques required by the motors.

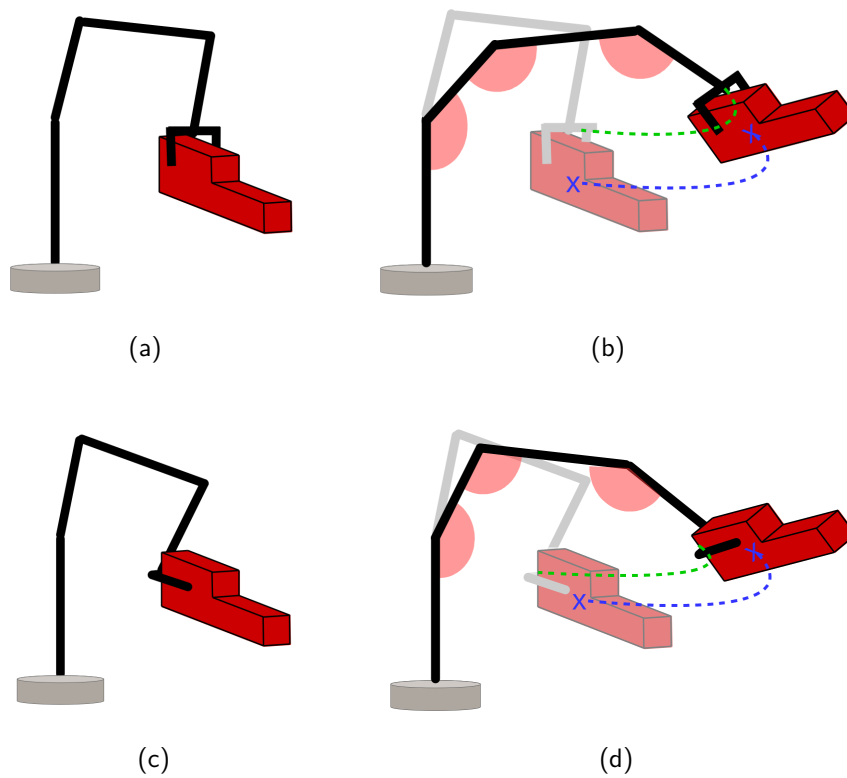


Figure 3.3 – Two choices of grasp pose shown in (a) and (c). The choice of grasp pose and the corresponding robotic arm configuration determines the following joint space trajectory of the robotic arm for the very same object trajectory. (b) and (d) show two shots of the robotic arm (corresponding to the grasping choices shown in (a) and (c), respectively) for moving the object to the predefined pose. The joint configurations during motion are different in the two cases, as well as the torques exerted by the robot for moving the object (due to different gravity, Coriolis and acceleration terms).

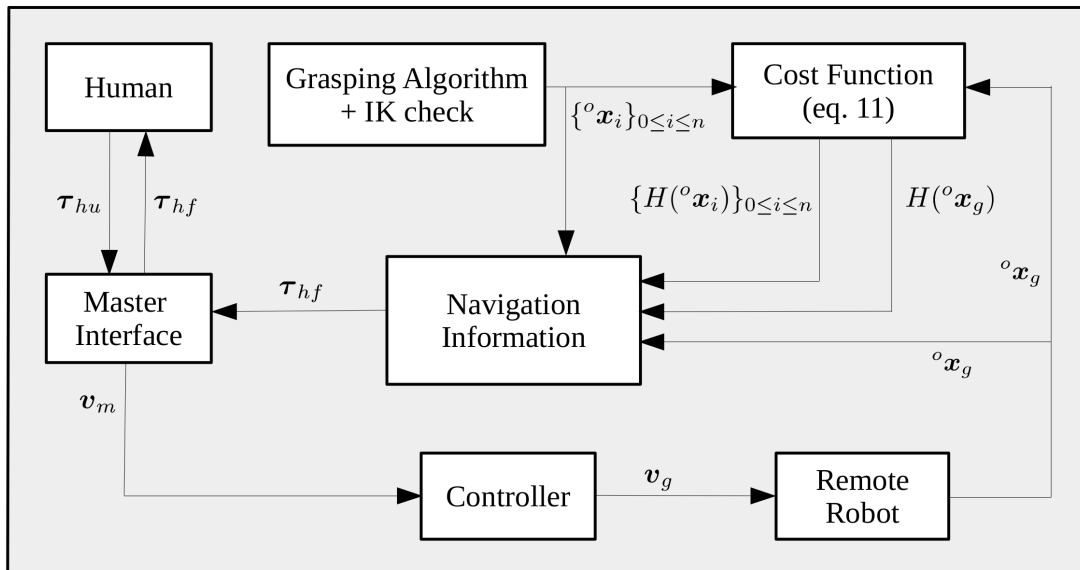


Figure 3.4 – Block diagram summarizing the shared-control framework. A set of feasible grasps $\{{}^o\mathbf{x}_i\}$ is generated by a grasping algorithm. Then, we calculate the torque cost function $H({}^o\mathbf{x}_i)$ at each of these poses to design the visuo-haptic feedback $\boldsymbol{\tau}_{hf}$ to guide the human user. Finally, the operator controls the robot in velocity using the grounded haptic interface.

We summarize the architecture of the control system in Fig. 3.4 and describe it in details in the following sections. A grasping algorithm generates a dense distribution of feasible grasp poses using the 3-dimensional model of the object. Any data-driven grasping approaches, *e.g.* [158], can be employed for this purpose, and we used GraspIt! [178] in our system. The torque-related metric is then calculated for each grasp pose considering the object inertia matrix and the planned post-grasp trajectory. Finally, this information is used at runtime to guide the user towards the grasp poses locally minimizing the torque metric. Combining this information with their own experience and perception of the environment, the human operators can make the choice on how to grasp the object informed about the future expected cost.

3.2.1 System details

In our teleoperation setup, we consider a 7-DoF manipulator–remote arm–and a 6-DoF haptic device–master arm–(see Fig. 3.5). We fix joint-3 of the Panda robot to reduce it to 6-DoF, as this allows us to avoid complexities of the inverse kinematics of redundant robots in Sec. 3.2.2. As such, the robot acts and is referred to as a 6-DoF serial manipulator.

Let us define three reference frames (see Fig. 3.5): $\mathcal{F}_g \in SE(3)$, attached to the robot end-effector, $\mathcal{F}_o \in SE(3)$, attached to the object centre of mass, and

the robot base frame $\mathcal{F}_r \in SE(3)$. These frames are also shown in Fig. 3.2, along with \mathcal{F}_{gr} representing the robot end-effector frame at the chosen grasping configuration. $\mathcal{F}_m \in SE(3)$ is the base frame of the master device, without loss of generality taken parallel to the robot base frame $\mathcal{F}_r \in SE(3)$, and $\mathcal{F}_w \in SE(3)$ is the world frame.

The configuration of the haptic interface and its Cartesian velocity are defined in \mathcal{F}_w by $\mathbf{x}_m \in \mathbb{R}^6$ and $\mathbf{v}_m \in \mathbb{R}^6$, respectively. The device is modelled as a gravity pre-compensated generic mechanical system,

$$\mathbf{M}(\mathbf{x}_m)\dot{\mathbf{v}}_m + \mathbf{C}(\mathbf{x}_m, \mathbf{v}_m)\mathbf{v}_m = \boldsymbol{\tau}_{hf} + \boldsymbol{\tau}_{hu} - \mathbf{B}\mathbf{v}_m, \quad (3.1)$$

where $\mathbf{M}(\mathbf{x}_m) \in \mathbb{R}^{6 \times 6}$ is the positive-definite symmetric inertia matrix, $\mathbf{C}(\mathbf{x}_m, \mathbf{v}_m) \in \mathbb{R}^{6 \times 6}$ are the Coriolis/centrifugal terms, $\boldsymbol{\tau}_{hf}, \boldsymbol{\tau}_{hu} \in \mathbb{R}^6$ are the haptic feedback and the human operator's forces, respectively; $\mathbf{B} \in \mathbb{R}^{6 \times 6}$ is a damping matrix for stabilizing the system.

The velocity of the robot is defined as $\mathbf{v}_g \in \mathbb{R}^6$, and a velocity-to-velocity coupling between the master and the remote robot is implemented by setting $\mathbf{v}_g = \mathbf{v}_m$.

We let ${}^o\mathbf{x}_g = \{{}^o\mathbf{t}_g, {}^o\mathbf{R}_g\} \in SE(3)$ represent the grasp pose, which is defined as the relative pose between the gripper and the object to grasp.

As we have already mentioned, we consider the post-grasp trajectory to be assigned and carried out autonomously after the user grasps the object. For instance, considering a pick-and-place task, we generate this trajectory based on the initial position of the object and a given target location. It is defined in the world frame as ${}^w\mathbf{x}_o(t) = \{{}^w\mathbf{t}_o(t), {}^w\mathbf{R}_o(t)\} \in SE(3)$, $0 \leq t \leq 1$, with t being a time parametrization such that $t = 0$ is the starting point and $t = 1$ is the endpoint of the trajectory. From the planned post-grasp trajectory, we calculate the corresponding trajectory for the robot end-effector w.r.t. \mathcal{F}_w ,

$$\begin{aligned} {}^w\mathbf{R}_g(t) &= {}^w\mathbf{R}_o(t){}^o\mathbf{R}_g \\ {}^w\mathbf{t}_g(t) &= {}^w\mathbf{t}_o(t) + {}^w\mathbf{R}_o(t){}^o\mathbf{t}_g \end{aligned} \quad (3.2)$$

Using the inverse kinematics (IK) solver we then obtain the joint space trajectory $\boldsymbol{\theta}(t, {}^o\mathbf{x}_g) \in \mathbb{R}^6$, which is function of the object trajectory over time ${}^w\mathbf{x}_o(t)$ and the grasp pose ${}^o\mathbf{x}_g$. We want to inform the human operator about the quality of a candidate grasp pose ${}^o\mathbf{x}_g$ w.r.t. the torque that the robot would exert when moving the object after the grasp. We call this metric Task-Oriented Torque Effort (TOTE), and it is function of the previously calculated desired joint trajectory. Our shared-control system provides the operators with feedback information

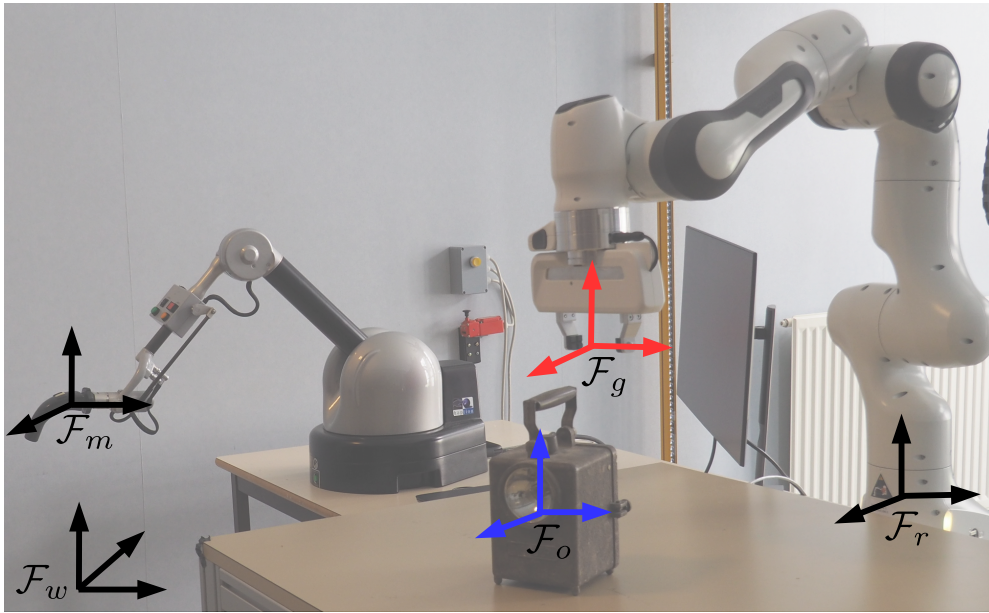


Figure 3.5 – We consider several coordinate frames including (i) the world reference frame, and coordinate frames attached to (ii) the handle of master-arm, (iii) the end-effector of the remote-arm, base of the remote-arm, and (iv) the object.

guiding them towards poses that minimize the TOTE index *and* are also feasible grasp poses.

3.2.2 Manipulator Dynamics Under Load

To evaluate Task Oriented Torque Effort (TOTE) for a given grasp pose, we need to calculate an augmented equation of motion which accounts for the grasped object as well as the dynamics of the manipulator.

We present our approach for a non redundant manipulator. The extension to redundant manipulators provides us with one extra degree of freedom which can be, *e.g.*, used to further optimize a secondary objective [179]. Following [180], the joint space dynamic model of a 6-DoF manipulator is defined as

$$\mathbf{M}(\boldsymbol{\theta})\ddot{\boldsymbol{\theta}} + \mathbf{C}(\dot{\boldsymbol{\theta}}, \boldsymbol{\theta})\dot{\boldsymbol{\theta}} + \mathbf{N}(\boldsymbol{\theta}) = \boldsymbol{\tau}, \quad (3.3)$$

where $\boldsymbol{\theta} \in \mathbb{R}^6$ and $\boldsymbol{\tau} \in \mathbb{R}^6$ are the vectors of joint positions and torques, respectively, and $\mathbf{M}(\boldsymbol{\theta})$ is the manipulator inertia matrix. On the other hand, the Coriolis and centrifugal force terms are defined by

$$\mathbf{C}_{ij}(\dot{\boldsymbol{\theta}}, \boldsymbol{\theta}) = \frac{1}{2} \sum_{k=1}^n \left(\frac{\partial \mathbf{M}_{ij}}{\partial \boldsymbol{\theta}_k} + \frac{\partial \mathbf{M}_{ik}}{\partial \boldsymbol{\theta}_j} - \frac{\partial \mathbf{M}_{kj}}{\partial \boldsymbol{\theta}_i} \right) \dot{\boldsymbol{\theta}}_k, \quad (3.4)$$

while

$$\mathbf{N}(\boldsymbol{\theta}, \dot{\boldsymbol{\theta}}) = \frac{\partial V}{\partial \boldsymbol{\theta}} \quad (3.5)$$

defines a gravitational force term where $V(\boldsymbol{\theta})$ is the gravitational potential energy of the system.

We are interested in determining the joint space dynamic equations of motion while also incorporating the dynamics of the grasped object. Let \mathbf{M}_{obj} denote the generalized inertia matrix of the object to be grasped, which we treat as a single rigid body,

$$\mathbf{M}_{obj} = \begin{pmatrix} m\mathbf{I}_{3 \times 3} & 0 \\ 0 & \mathbf{I}_{CoM} \end{pmatrix},$$

where $m \in \mathbb{R}$ and $\mathbf{I}_{CoM} \in \mathbb{R}^{3 \times 3}$ indicate the object mass and inertia tensor w.r.t. the object Centre of Mass (CoM), respectively. Assuming a secure and steady grasp, the inertia tensor can then be expressed in a frame attached to the robot end-effector, as follows:

$$\mathbf{M}_o({}^o\mathbf{x}_g) = \mathbf{E}^{-T}({}^o\mathbf{x}_g)\mathbf{M}_{obj}\mathbf{E}^{-1}({}^o\mathbf{x}_g), \quad (3.6)$$

where $\mathbf{E}({}^o\mathbf{x}_g) \in \mathbb{R}^{6 \times 6}$ is the matrix transforming the linear and angular velocities of the object CoM to generalized velocities in the frame \mathcal{F}_g attached to the end-effector. We can then compute the grasped object inertia matrix and, hence, the governing equation of motion of the augmented robot and grasped object in the joint space is:

$$\mathbf{M}_o({}^o\mathbf{x}_g, \boldsymbol{\theta}) = \left[J^T(\boldsymbol{\theta})\mathbf{M}_o({}^o\mathbf{x}_g)J(\boldsymbol{\theta}) \right], \quad (3.7)$$

where $J(\boldsymbol{\theta}) \in \mathbb{R}^{6 \times 6}$ is the the robot Jacobian. Next, we compute the effect of the object on the Coriolis and gravitational term of the robot dynamic equation of motion in eq. (3.3). From eq. (3.4), (3.6), and (3.7), the following holds

$$\mathbf{C}_o({}^o\mathbf{x}_g, \boldsymbol{\theta}, \dot{\boldsymbol{\theta}}) = \frac{1}{2} \sum_{k=1}^n \left(\frac{\partial M_{o,ij}}{\partial \boldsymbol{\theta}_k} + \frac{\partial M_{o,ik}}{\partial \boldsymbol{\theta}_j} - \frac{\partial M_{o,kj}}{\partial \boldsymbol{\theta}_i} \right) \dot{\boldsymbol{\theta}}. \quad (3.8)$$

Finally, the gravitational term of the dynamics of the grasped object in the robot joint space can be defined using eq. (3.5),

$$\mathbf{N}_o({}^o\mathbf{x}_g, \boldsymbol{\theta}) = \frac{\partial V_o({}^o\mathbf{x}_g, \boldsymbol{\theta})}{\partial \boldsymbol{\theta}}, \quad (3.9)$$

where $V_o({}^o\mathbf{x}_g, \boldsymbol{\theta}) = mgh_o({}^o\mathbf{x}_g, \boldsymbol{\theta})$ and $h_o({}^o\mathbf{x}_g, \boldsymbol{\theta})$ can be computed using the forward kinematics of the robot. The resulting equation of motion accounting for the dynamics of the system can then be written as

$$\bar{\mathbf{M}}({}^o\mathbf{x}_g, \boldsymbol{\theta})\ddot{\boldsymbol{\theta}} + \bar{\mathbf{C}}({}^o\mathbf{x}_g, \dot{\boldsymbol{\theta}}, \boldsymbol{\theta}) + \bar{\mathbf{N}}({}^o\mathbf{x}_g, \boldsymbol{\theta}) = \bar{\boldsymbol{\tau}}({}^o\mathbf{x}_g, \boldsymbol{\theta}, \dot{\boldsymbol{\theta}}, \ddot{\boldsymbol{\theta}}), \quad (3.10)$$

where $\bar{\boldsymbol{\tau}}({}^o\mathbf{x}_g, \boldsymbol{\theta}, \dot{\boldsymbol{\theta}}, \ddot{\boldsymbol{\theta}}) \in \mathbb{R}^6$ represents the joint torques needed to perform the target manipulative action while

$$\begin{aligned}\bar{\mathbf{M}}({}^o\mathbf{x}_g, \boldsymbol{\theta}) &= \mathbf{M}_o({}^o\mathbf{x}_g, \boldsymbol{\theta}) + \mathbf{M}(\boldsymbol{\theta}), \\ \bar{\mathbf{C}}({}^o\mathbf{x}_g, \boldsymbol{\theta}, \dot{\boldsymbol{\theta}}) &= \mathbf{C}_o({}^o\mathbf{x}_g, \boldsymbol{\theta}, \dot{\boldsymbol{\theta}}) + \mathbf{C}(\boldsymbol{\theta}, \dot{\boldsymbol{\theta}}),\end{aligned}$$

and

$$\bar{\mathbf{N}}({}^o\mathbf{x}_g, \boldsymbol{\theta}, \dot{\boldsymbol{\theta}}) = \mathbf{N}_o({}^o\mathbf{x}_g, \boldsymbol{\theta}, \dot{\boldsymbol{\theta}}) + \mathbf{N}(\boldsymbol{\theta}, \dot{\boldsymbol{\theta}}).$$

3.2.3 Task Oriented Torque Effort (TOTE) Cost Function

The grasp pose ${}^o\mathbf{x}_g$ specifies the joint space trajectory of the robot needed to perform the post-grasp manipulation (see eq. (3.2)) and affects the dynamics of the post-grasp manipulative motions, which includes the robot and the grasped object. As a consequence, the grasp pose ultimately affects the robot joint torques, $\bar{\boldsymbol{\tau}}({}^o\mathbf{x}_g, \boldsymbol{\theta}, \dot{\boldsymbol{\theta}}, \ddot{\boldsymbol{\theta}})$ (hereafter referred to by $\bar{\boldsymbol{\tau}}({}^o\mathbf{x}_g)$ for simplicity), needed to move the robot (and the object) over the desired trajectory. Torques $\bar{\boldsymbol{\tau}}(t, {}^o\mathbf{x}_g)$ expected at each time t of the trajectory are defined following (3.10) as

$$\begin{aligned}\bar{\boldsymbol{\tau}}(t, {}^o\mathbf{x}_g) &= \bar{\mathbf{M}}\left({}^o\mathbf{x}_g, \boldsymbol{\theta}(t, {}^o\mathbf{x}_g), \ddot{\boldsymbol{\theta}}(t, {}^o\mathbf{x}_g)\right) \\ &+ \bar{\mathbf{C}}\left({}^o\mathbf{x}_g, \dot{\boldsymbol{\theta}}(t, {}^o\mathbf{x}_g), \boldsymbol{\theta}(t, {}^o\mathbf{x}_g)\right) + \bar{\mathbf{N}}\left({}^o\mathbf{x}_g, \boldsymbol{\theta}(t, {}^o\mathbf{x}_g)\right).\end{aligned}\tag{3.11}$$

Let $H({}^o\mathbf{x}_g)$ be a cost function defining the torque effort the robot exerts to perform the post-grasp manipulation, i.e., moving the object along a pre-defined trajectory in our case. Of course, this cost function can be defined for any other type of post-grasp manipulation, depending on the task at hand. Given an object and a desired trajectory to follow ${}^w\mathbf{x}_o(t)$, we can finally define task oriented torque effort (TOTE) cost function $H({}^o\mathbf{x}_g)$ as

$$H({}^o\mathbf{x}_g) = \int_0^1 \|\bar{\boldsymbol{\tau}}(t, {}^o\mathbf{x}_g)\| dt,\tag{3.12}$$

where $\|\bar{\boldsymbol{\tau}}(t, {}^o\mathbf{x}_g)\|$ is the L2 norm of the joint torques over the post-grasp trajectory.

3.3 Navigation Information

During reach-to-grasp, we would like to guide the operator towards grasp poses locally minimizing the TOTE index (which corresponds with the minimum torque effort during post-grasp manipulative motions), using a combination of haptic and visual navigation feedback.

3.3.1 Haptic Navigation Guidance

The objective of our haptic navigation cues $\boldsymbol{\tau}_{hf}$ is to guide the user towards the direction minimizing the TOTE metric $H({}^o\boldsymbol{x}_g)$. A first approach to achieve this objective would be to provide force cues along the negative gradient of $H({}^o\boldsymbol{x}_g)$ w.r.t. optimization variable ${}^o\boldsymbol{x}_g$, as in [126]. However, this method might lead to undesired behaviours, as it does not consider where the feasible grasp poses are, e.g., it could lead to a pose having a low value for $H({}^o\boldsymbol{x}_g)$ but from which it is impossible to grasp the object. In our system, we combine this gradient descent approach with knowledge regarding the feasible grasp poses. From the 3-dimensional model of the object, we use GraspIt! to retrieve a dense set of grasp poses. Then, for each pose, we calculate the corresponding end-effector and joint post-grasp trajectories, excluding those for which no feasible inverse kinematic solution exists. This step leaves us with a set of n feasible grasp poses ${}^o\boldsymbol{x}_i$ where $0 \leq i \leq n$. Finally, we compute the TOTE for each feasible grasp pose ${}^o\boldsymbol{x}_i$, called $H_i({}^o\boldsymbol{x}_i)$. This information is used to inform the user about the direction to follow so as to minimize the robot effort during the post-grasp action.

The most straightforward way to provide the user with a meaningful feedback may be to drive her/him towards the grasp pose corresponding with the minimum cost. However, the operator may still consider that the grasping pose corresponding to the minimum value of TOTE is not the best choice because of other constraints important to task completions (or her/his own judgment). In general, robotic grasping/manipulation may involve different application specific objectives, e.g., the manipulation may be subject to a suitable affordance of the object or collision-free movements. The goal is then to provide the users with a local, continuous and informative guidance such that they get informed on how to move in the vicinity of their current gripper pose so as to minimize the torques needed for the post-grasp action. To achieve this, we do not rely on the cost function value alone in the design of the haptic cues, but also take into consideration the distance of each proposed grasp pose to the current gripper pose.

To this end, we define the roto-translational distance between any grasp candidate ${}^o\boldsymbol{x}_i$ and the current gripper pose ${}^o\boldsymbol{x}_g$, similarly to [110], as

$$|{}^o\boldsymbol{x}_i - {}^o\boldsymbol{x}_g| = \|{}^o\boldsymbol{p}_i - {}^o\boldsymbol{p}_g\| + \mu |{}^g\theta_i|, \quad (3.13)$$

where ${}^g\theta_i \in [-180, +180]$ is the angular part of the angle-axis representation of ${}^g\boldsymbol{R}_i = {}^g\boldsymbol{R}_o {}^o\boldsymbol{R}_i$, and $\mu > 0$ is used to properly scale the angular component of the distance with respect to the linear one ($\mu = \pi/180$ in our experiments). This measure allows us to compute the distance between the current grasping pose

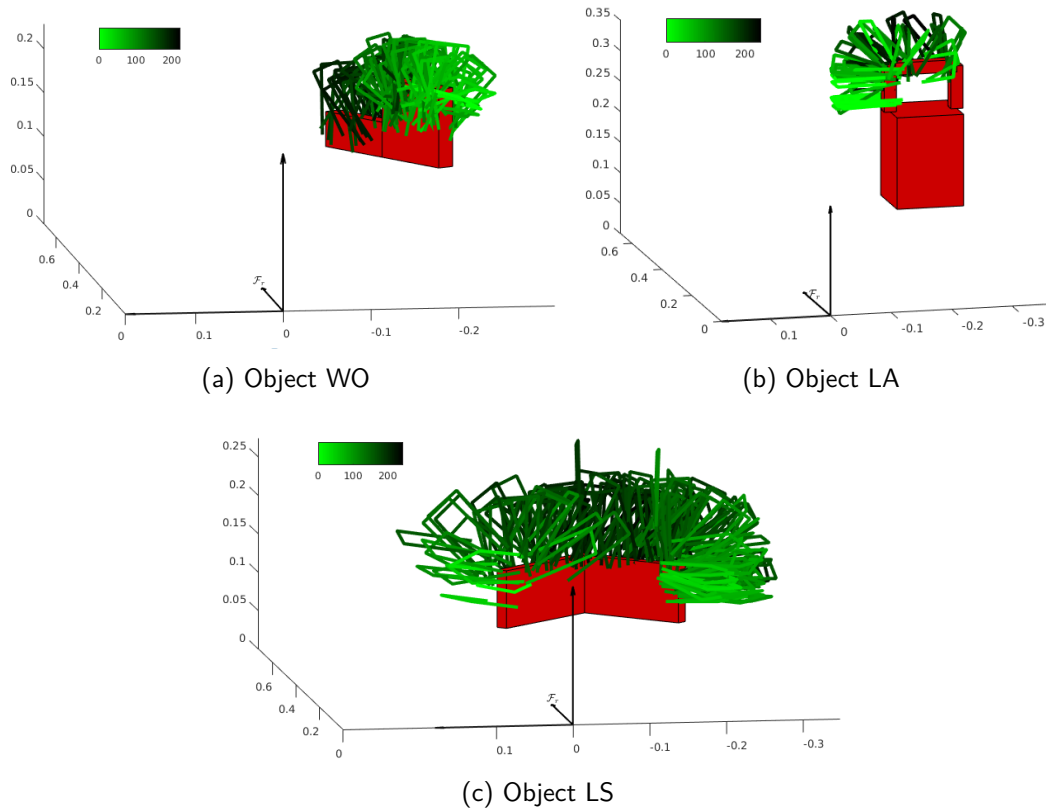


Figure 3.6 – Feasible grasps and TOTE cost $H({}^o\mathbf{x}_g)$ for the three objects used in our experiments. The grasping candidates are colour-coded according to the corresponding cost value. Lighter green corresponds to a lower cost function.

and any candidate grasping pose, accounting for both translation and rotation components.

Finally, the force cues are calculated as the weighted average of multiple force vectors guiding the user towards nearby grasp poses having a low cost. The lower $H_i({}^o\mathbf{x}_i)$, the stronger the force guidance; moreover, each force vector is weighted inversely to the distance between its grasp pose ${}^o\mathbf{x}_i$ and the current gripper pose ${}^o\mathbf{x}_g$, i.e.,

$$\boldsymbol{\tau}_{hf} = \frac{1}{n} \sum_{i=1}^n \frac{H({}^o\mathbf{x}_g) - H_i({}^o\mathbf{x}_i)}{1 + k|{}^o\mathbf{x}_i - {}^o\mathbf{x}_g|^m} \begin{bmatrix} {}^o\mathbf{p}_i - {}^o\mathbf{p}_g \\ \frac{\|{}^o\mathbf{p}_i - {}^o\mathbf{p}_g\|}{g\Delta_i} \end{bmatrix} \quad (3.14)$$

if $H({}^o\mathbf{x}_g) > H_i({}^o\mathbf{x}_i)$

where $g\Delta_i$ is the axis part of the angle-axis representation of ${}^g\mathbf{R}_i = {}^g\mathbf{R}_o {}^o\mathbf{R}_i$, and k and m are positive control gains ($k = 6$ and $m = 8$ in our experiments).

3.3.2 Visual Navigation Guidance

In addition to the haptic feedback described above, we provide the user with a visual representation of the different possible grasping poses to give them a pre-

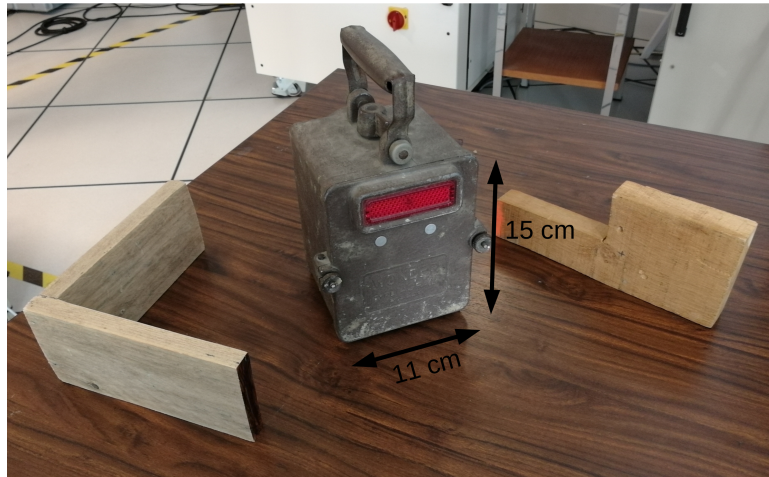


Figure 3.7 – Objects used in our grasping experiments. From left to right, an L-shaped wooden object (LS), a lamp (LA), and a b-shaped wooden object (WO). These objects have been chosen following a discussion within the European H2020 project “Robotic Manipulation for Nuclear Sort and Segregation” (RoMaNS), which considered them as good representatives for the sort and segregation of nuclear waste.

liminary idea of how “good” the different grasps are, and allow them to plan ahead their grasping pose in a way to make the post-grasping manipulation more efficient for the robot. This is achieved by color coding the grasping configurations, as shown in Fig. 3.6, where grasps are represented with different shades of green depending on their TOTE cost values. In Sec. 3.5, we study the impact of haptic, visual and visuo-haptic feedback on the human performance in an comprehensive human subject tests, and the effect of combining them together on the user performance.

3.4 Pick-and-Place Experiment

To test the effectiveness of our proposed shared-control approach, we carried out a first pick-and-placement experiment on three different objects.

3.4.1 Experimental Setup

The experimental setup is shown in Fig. 3.1. The master side is composed of a 6-DoF grounded haptic interface (Virtuose 6D, Haption, France); while the remote side is composed of a 7-DoF robotic manipulator (Panda manufactured by Franka Emika) with one joint fixed, and therefore used as a 6-DoF manipulator. An LCD screen is placed in front of the human operator (i.e. subjects). The master interface is placed next to the remote robotic manipulator to provide the subjects with a direct view on the remote workspace. This simplifies our study

as we avoid any complexities caused by the choice of camera views and screens showing the remote workspace.

The environment is composed of three different objects placed on a table in front of the robot:

WO: a wooden object made of $10 \times 2.6 \times 4$ cm and $11 \times 2.6 \times 9$ cm rectangles, 275 g (right of Fig. 3.7).

LA: a $11 \times 11 \times 15$ cm rectangular lamp of 1958 g with an handle (center of Fig. 3.7);

LS: an L-shaped object made of two $14 \times 1.2 \times 6.5$ cm rectangles, with a mass of 228 g (left in Fig. 3.7);

They were chosen for their similarity with common objects used in nuclear decommissioning scenarios [110].

3.4.2 Task and Methods

One expert operator carried out the pick-and-place task. The operator was asked to control the robotic manipulator with the grounded haptic interface to grasp the considered objects. We visualize the post-grasp trajectory before the start of the experiment and describe it the subjects that the aim of the experiments is to choose a grasping pose minimizing the overall torque exerted by the robot during autonomous post-grasp motions. Once the object was grasped, the autonomous system moves the remote robot to pick the object up and deliver it at the planned pose, following a pre-planned autonomous trajectory.

We employed the shared-control method described in Sec. 3.2. We used velocity-to-velocity mapping for commanding the master-remote robot system. Since the workspace of the master device is smaller than that of the remote robot, we used a clutch button on the master interface to decouple the motion of the master and remote systems, allowing the user to reposition the haptic device in a comfortable position before controlling again the robot [110]. We considered two navigation feedback modalities: (T) standard human-in-the-loop teleoperation, where the operator receives no guidance about suitable grasp poses; (H) our haptic shared-control teleoperation approach, where the subject receives haptic guidance toward grasps minimizing $H({}^o\mathbf{x}_g)$, as described in Sec. 3.3.1. The post-grasp trajectory was designed to include both a translational and rotational component and is different for each of the 3 objects, as shown in the video available at <https://youtu.be/vqDop2YRCzA>.

Table 3.1 – Average error between the measured joint torques $\boldsymbol{\tau}_g$ and the calculated ones using eq. 3.11 (with and without the effect of velocity and acceleration) for a sample task for our experiments.

Calculated (eq. 3.11)	Calculated (no acceleration)	Calculated (no acceleration or velocity)
0.479 N.m	0.475 N.m	0.480 N.m

The haptic feedback is computed according to the TOTE cost value calculated as per eq. 3.11. We observe that at low velocities, the torques on the robot joints $\bar{\boldsymbol{\tau}}(t, {}^o\boldsymbol{x}_g)$ could be approximated solely using the gravity vector, $\bar{\mathbf{N}}({}^o\boldsymbol{x}_g, \boldsymbol{\theta}(t, {}^o\boldsymbol{x}_g))$, as the other two components were negligible. To test this observation, we move an object of 1 Kg, grasped by the gripper of the Panda robot, along a sample predefined trajectory with low velocity similar to the ones we used in our experiments. We compare the measured torques over the post-grasp trajectory to the calculated torques using eq. 3.11, with and without the effect of the velocity and acceleration components. The results are summarized in Table 3.1, and show that the effect of adding these terms is negligible. We thus used this approximation to simplify the calculation of the TOTE. Higher velocity tasks should of course include the dynamics components in the calculations.

The human operators started by grasping “WO”. As described in Sec. 3.2, the system generated the set of feasible grasp poses, calculating for each of them the TOTE cost $H({}^o\boldsymbol{x}_g)$ over the post-grasp trajectory. Then, haptic feedback guides the user towards the pose locally minimizing the cost, in case of H. Fig. 3.6a shows $H({}^o\boldsymbol{x}_g)$ for the feasible grasps on the object used in our experiments. The feasible grasping candidates are colour coded where the darker the green colour of the grasping candidate, the higher the corresponding cost value. The user, then, grasps object LA, receiving the same type of guiding feedback. This object represented a particular challenge for the system, as it is quite heavy and, if not handled correctly, might require torques too high for the robot to exert during the post-grasp trajectory. Again, Fig. 3.6b illustrates $H({}^o\boldsymbol{x}_g)$ for the feasible grasps on this object using different shades of green. Finally, the user grasped object LS and Fig. 3.6c shows $H({}^o\boldsymbol{x}_g)$ for the feasible grasps on this object.

It is important to highlight that the navigation feedback guides the operator towards the pose *locally* minimizing $H({}^o\boldsymbol{x}_g)$. This behaviour still enables the human operator to decide from where to approach the object, combining the knowledge of the system about $H({}^o\boldsymbol{x}_g)$ with the experience and additional environmental information brought by the operator. For example, from Fig. 3.6c, we can see that $H({}^o\boldsymbol{x}_g)$ is equally low if grasping the object from its right or left hand

side. The user might prefer one or the other considering information unavailable to the system, e.g., one part looks damaged/corroded or it is too close to other objects.

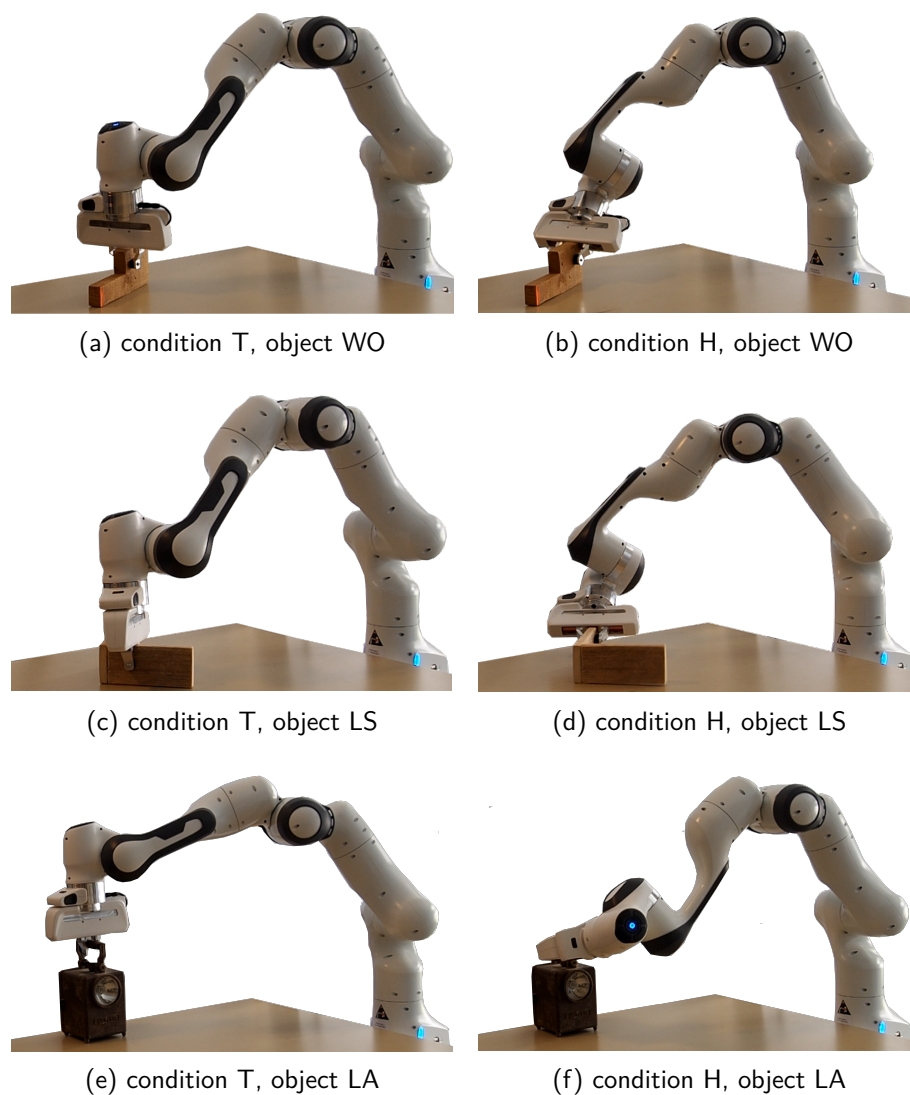


Figure 3.8 – Grasp poses teleoperated in T (fully teleoperated) and H (haptic-guided shared-control teleoperated) modes of the control system: (a), (c) and (e) are grasp poses for WO, LS, and LA chosen by the user in T control mode; (b), (d) and (f) are grasp poses for WO, LS, and LA chosen by the user in H control mode;

3.4.3 Results

We registered the grasp pose chosen by the operator and the torques exerted by the robot over the post-grasp trajectory in the two different control modalities (T vs. H—full teleoperation and the haptic shared control) for the three considered objects (WO vs. LA vs. LS).

As expected, the grasp pose chosen by the user differed between the T and H modalities. In condition T, the operator chose the most intuitive grasp poses, shown in Figs. 3.8a, 3.8c, 3.8e, which are usually along top edge/surface line of the object.

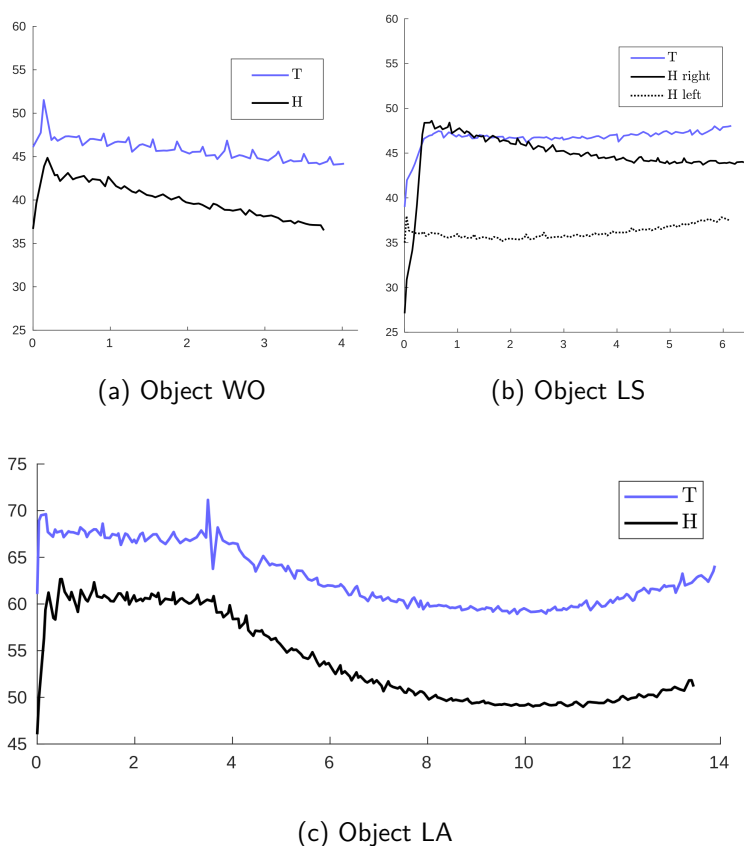


Figure 3.9 – Norm of the joint torques τ_g [Nm] vs. time [s] during the post-grasp trajectory for T and H control mode and three objects: (a) WO (corresponding with Figs. 3.8a and 3.8b), (b) LS (corresponding with Figs. 3.8c and 3.8d), and (c) LA (corresponding with Figs. 3.8e and 3.8f)

However, the robot may require a large amount of torque effort to deliver desired manipulative movements during the corresponding post-grasp manipulative movements and those grasps are not the ones with the corresponding minimum $H(\mathbf{x}_g)$. In condition H, the shared-control algorithm guides the user to grasp poses shown in Figs. 3.8b, 3.8d, 3.8f, which are less intuitive but more efficient in

terms of $H({}^o\mathbf{x}_g)$.

After forming successful grasps, the operators stop teleoperating the remote robot and an autonomous controller picks up the object and moves it along a planned trajectory. Fig. 3.9 shows the evolution of the L2 norm of the joint torques $\|\boldsymbol{\tau}_g\|$ over time during the post-grasp trajectory, for the three objects in case of H and T control mode. As expected, torques are minimized when the user is guided towards grasps with low $H({}^o\mathbf{x}_g)$.

It is interesting to see that our haptic-guided shared control allow the operator to freely choose different local optimal solution– it is shown in Fig. 3.9b that the operator can chose left and right hand side grasp pose, shown with H left and H right, which have $H({}^o\mathbf{x}_g)$ value lower than the intuitively selected grasp pose, shown with T.

3.5 Human-Subjects Study

The experiments above showcase the features of our proposed haptic-guided shared control. To further illustrate the efficiency of our approach, we present a series of human subject tests showing the effectiveness of our approach to minimize the TOTE cost in comparison with the basic teleoperation setup. We consider again the robotic system described in Secs. 3.2, 3.4.1 and shown in Fig. 3.1.

In this section, we only consider object WO (right hand side of Fig. 3.7) because it does not present any handling risk for novice users–the lamp mass, e.g., may be dropped by novice and damaging the experimental setup– and also provide a larger area of grasp choices for the user. This provides a good example to compare the use of basic teleoperation and our proposed haptic-guided shared-control teleoperation setups.

3.5.1 Task and Feedback Conditions

Similar to the experiments in Sec. 3.4, participants were asked to control the motion of the robotic manipulator to grasp the object, following the guidance information provided by the system. We describe the experiments and the task for the user, i.e. the users need to teleoperate reach-to-grasp and form a stable grasp where the post-grasp movements are performed autonomously. They were also informed that we would ideally like to have the minimum joint torque efforts during the entire experiments including post-grasp movements. The task started when the manipulator moved for the very first time, and it was considered successful completion when the robot completed the planned post-grasp trajectory.

We consider four different ways of enabling the user to control the system for completing the grasping task,

T: basic teleoperation, where the subject receives no haptic guidance about suitable grasp poses.

H: our proposed haptic shared-control approach, where the subject receives haptic guidance toward grasp poses locally minimizing $H({}^o\mathbf{x}_g)$, i.e., the torque the robot needs to exert along the post-grasp trajectory.

V: visual guidance, where the subject is shown a graphical representation of the scene indicating the value of $H({}^o\mathbf{x}_g)$ for each grasp pose using a colour scale (see Fig. 3.6a). In this case, the users were informed about the relationship between the color of the grasps and their corresponding cost function value. They were also given time to explore the figure, rotate it, and decide before starting the experiment on the best grasping configuration. The figure was also kept available to support the user throughout the grasping task.

HV: a combination of H and V, where the subject receives haptic guidance toward grasp poses minimizing $H({}^o\mathbf{x}_g)$ and is shown a graphical representation of the scene indicating the value of $H({}^o\mathbf{x}_g)$ for each grasp pose using a colour scale.

Conditions T and H are the same already employed in Sec. 3.4. In all conditions, the user controls all the DoF of the robotic manipulator through the haptic interface, as described in Secs. 3.2 and 3.4.1.

A video showing trials in all experimental conditions is available at <https://youtu.be/vqDop2YRCzA>.

3.5.2 Participants

Fifteen right-handed subjects (average age 27.6, 12 males, 3 females) participated in the study. Seven of them had previous experience with haptic interfaces. The experimenter explained the procedures and spent about two minutes adjusting the setup to be comfortable before the subject began the experiment. Each subject then spent about three minutes practising the control of the system before starting the experiment.

3.5.3 Results

To evaluate the effectiveness of our telemanipulation system and the usefulness of the proposed shared-control approach, we recorded (*i*) the completion time,

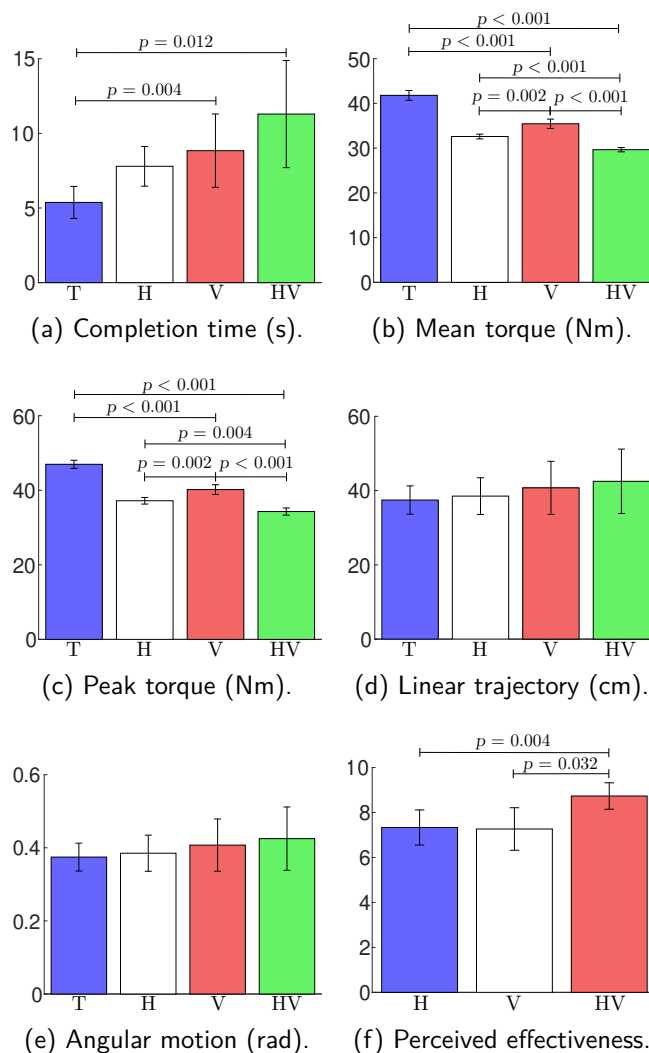


Figure 3.10 – Human subjects experiments: Mean and 95% confidence interval of (a) completion time, (b) mean torque and (c) peak torque over the post-grasp trajectory, (d) linear trajectory and (e) angular motion of the end effector for the four conditions (T, H, V, HV).

(*ii*) the mean torque exerted by the manipulator joints during the post-grasp phase, (*iii*) the peak torque exerted by the manipulator joints during the post-grasp phase, (*iv*) the linear trajectory followed by the robotic end-effector, and (*v*) the angular motion of the robotic end-effector. Moreover, immediately after the experiment, subjects were also asked to report (*vi*) the effectiveness of each feedback condition in completing the given task using bipolar Likert-type eleven-point scales.

To compare the different metrics, we ran one-way repeated-measures ANOVA tests (first five metrics) and Friedman tests (last metric) on the data. Four control modalities (standard teleoperation vs. our haptic shared control vs. visual guidance vs. visuo-haptic shared control—T vs. H vs. V vs. HV) were considered.

Data from the first five metrics (i) – (v) passed the Shapiro-Wilk normality test. Table 3.2 summarizes this experiment.

Fig. 3.10a shows the average task completion time. One user took significantly more time than any other to grasp in the H condition (41.96 s, five times the average of the other users). We did not consider this outlier in calculating the mean and 95% confidence interval showed in the figure. However, we considered it in the following statistical analysis. Mauchly’s Test of Sphericity indicated that the assumption of sphericity had been violated ($\chi^2(5) = 16.255$, $p = 0.006$). The one-way ANOVA test with a Greenhouse-Geisser revealed a statistically significant change in the task completion time across the conditions ($F(1.868, 26.148) = 3.572$, $p = 0.045$, $a = 0.05$). Post hoc analysis with Bonferroni adjustments revealed a statistically significant difference between conditions T vs. V ($p = 0.004$) and T vs. HV ($p = 0.012$). The Bonferroni correction is used to reduce the chances of obtaining false-positive results when multiple pair-wise tests are performed on a single set of data.

Fig. 3.10b shows the mean torque applied by the manipulators’ joints along the post-grasp trajectory. Data passed the Mauchly’s Test of Sphericity. The one-way ANOVA test revealed a statistically significant change in the task mean torque across the conditions ($F(3, 42) = 160.778$, $p < 0.001$, $a = 0.05$). Post hoc analysis with Bonferroni adjustments revealed a statistically significant difference between all conditions, as summarized in table 3.2.

Fig. 3.10c shows the peak torque applied by the manipulators’ joints along the post-grasp trajectory. Data passed the Mauchly’s Test of Sphericity. The one-way ANOVA test revealed a statistically significant change in the task peak torque across the conditions ($F(3, 42) = 108.291$, $p < 0.001$, $a = 0.05$). Post hoc analysis with Bonferroni adjustments also revealed a statistically significant difference between all conditions.

Fig. 3.10d shows the linear trajectory described by the robot end-effector during the task. Mauchly’s Test of Sphericity indicated that the assumption of sphericity had been violated ($\chi^2(5) = 11.728$, $p = 0.039$). The one-way ANOVA test with a Greenhouse-Geisser correction revealed no statistically significant change in the task linear trajectory across the conditions ($F(2.085, 29.187) = 0.677$, $p > 0.05$, $a = 0.05$).

Fig. 3.10e shows the summed angular motion described by the robot end-effector during the task. Data passed the Mauchly’s Test of Sphericity, and the one-way ANOVA test also revealed no statistically significant change in the angular trajectory across the conditions ($F(3,42) = 2.203$, $p > 0.05$, $a = 0.05$).

At the end of the experiment, we asked the participants to rate the perceived

Table 3.2 – Summary of the experiment

Task	Control the haptic teleoperation system to grasp and lift an object.
Participants	15 subjects (12 males, 3 females)
Conditions	T (standard teleoperation), H (haptic shared control), V (visual guidance), HV (haptic shared control and visual guidance)

Statistical analysis (one-way rm ANOVA or Friedman test)Completion time

T vs. V	$p = 0.004$	T vs. HV	$p = 0.012$
---------	-------------	----------	-------------

Mean torque

T vs. H	$p < 0.001$	T vs. V	$p < 0.001$
---------	-------------	---------	-------------

T vs. HV	$p < 0.001$	H vs. V	$p = 0.002$
----------	-------------	---------	-------------

H vs. HV	$p < 0.001$	V vs. HV	$p < 0.001$
----------	-------------	----------	-------------

Peak torque

T vs. H	$p < 0.001$	T vs. V	$p < 0.001$
---------	-------------	---------	-------------

T vs. HV	$p < 0.001$	H vs. V	$p = 0.002$
----------	-------------	---------	-------------

H vs. HV	$p = 0.004$	V vs. HV	$p < 0.001$
----------	-------------	----------	-------------

Linear trajectory

No statistically significant difference between conditions.

Angular motion

No statistically significant difference between conditions.

Perceived effectiveness

H vs. HV	$p = 0.004$	V vs. HV	$p = 0.032$
----------	-------------	----------	-------------

Most effective condition (chosen by subjects)

Thirteen subjects out of fifteen chose HV, two chose V.

effectiveness of the three conditions in guiding them (H vs. V vs. HV). The responses were given using bipolar Likert-type scales that ranged from 0 to 10, where a score of 0 meant “very low” and a score of 10 meant “very high” [181, 182]. Fig. 3.10f shows the perceived effectiveness of the four experimental conditions. A Friedman test showed a statistically significant difference between the means of the three feedback conditions ($\chi^2(2) = 13.192$, $p = 0.001$). The Friedman test is the non-parametric equivalent of the more popular repeated-measures ANOVA. The latter is not appropriate here since the dependent variable was measured at the ordinal level. Post hoc analysis with Bonferroni adjustments revealed a statistically significant difference between H vs. HV ($p = 0.004$) and V vs. HV ($p = 0.032$).

Finally, thirteen subjects out of fifteen found condition HV to be the most effective at completing the grasping task. Two subjects preferred condition V. Quite surprisingly, no subject indicated H as their preferred condition.

3.6 Discussion

Shared control is becoming a popular technique to improve the performance and intuitiveness of robotic telemanipulation systems. This chapter aims at improving the human operator’s awareness of some future manipulation related metrics, which might be non-intuitive or difficult to predict at the master side during teleoperation. As a proof of concept, we evaluated the torques exerted by the robot over a future trajectory set to be autonomously executed after the object is grasped via teleoperation. This scenario is relevant, e.g., in the sort and segregation of dangerous waste, where it is important to leave operators free to choose which object and how to grasp while providing them as much information as possible on the constraints and objectives relevant to the remote system and environment. Minimizing the torque expenditure is not only relevant because it reduces the energy used by the robot—hence reduces the operation cost— but also because it extends the range of objects the system can manipulate. Indeed, as the robotic system can only provide limited torque, knowing where and how to grasp enables the manipulator to handle, e.g., heavier objects. It might be argued that expert operators know well the system dynamics and therefore can already estimate how the robot torques will evolve over a given post-grasp trajectory. However, especially when handling dangerous waste, operators do not have a direct and clear view of the environment and it might be rather difficult to estimate such a complex metric just from looking at the system from a distant window. Even if the operator has a good view of the environment, as in our experimental setup, receiving

intuitive haptic cues can significantly reduce the cognitive load and speed up the process, which is already an important result. For example, the Sellafield (UK) nuclear site stores 140 tonnes of civil plutonium and 90,000 tonnes of radioactive graphite [183]. The robotic systems in use provide teleoperation capabilities through primitive master consoles (e.g., passive joystick or teach pendants), making the process too slow for processing the material in a reasonable time, hence the need for faster-teleoperation solutions. Finally, increasing the intuitiveness of these robotic systems is expected to flatten the learning curve, enabling more operators to become proficient in a shorter time (subjects in Sec. 3.5 were all novices).

Of course, our framework can be adapted to consider different metrics of predicted costs, e.g., relevant for the post-grasp phase, such as cost of maximising the robot workspace in a certain direction at the end of the manipulation or positioning the robot body to optimize the user’s viewpoint on future actions. As long as the set of feasible grasp poses can be assigned with relevant cost values, our approach can be adapted with very little efforts.

First, we evaluated our shared-control technique in a preliminary pick-and-place experiment on three different objects. We asked experienced users to grasp each object using classic teleoperation (T) in which they received no guidance about suitable grasp poses, and our haptic shared control (H) in which they received haptic feedback towards poses locally minimizing $H({}^o\mathbf{x}_g)$. Shared control H takes into account all the feasible grasp poses evaluated by the grasping algorithm, weighted by their distance to the current pose of the robot. In this way, the feedback is never abrupt and is gently updated as the robot moves around the object. This characteristic enables the user to always know where the best local grasp is, while still being able to move away if needed, which is paramount for many applications. We want to leave operators free to ultimately choose where to grasp because they might pick up on some information unknown to the system. Results of this first experiment show that robot torques during the autonomous part of the task are lower when using the haptic shared-control approach.

After this preliminary experiment, we carried out a human subject study enrolling fifteen human subjects. We tested the performance of four experimental conditions: classic teleoperation (T), haptic shared control (H), visual guidance (V), where each grasp pose is color-coded to indicate its $H({}^o\mathbf{x}_g)$ value, and combined visuo-haptic guidance (HV), which provides both haptic and visual feedback as in H and V. As a measure of performance, we evaluated the time-to-completion for each experiment, robot mean and peak torque, end-effector trajectory length and angular motion, as well as users’ perceived effectiveness. Results showed

that, in all the considered metrics but three (time-to-completion, linear and angular motion), the proposed visuo-haptic guidance HV outperformed more classic teleoperation T. Moreover, the great majority of subjects preferred HV over the other approaches. Results also show that in the two most relevant metrics, mean and peak torque, both haptic approaches (H and HV) perform significantly better than any other, proving the effectiveness of haptic guidance in optimizing the robot torque during telemanipulation. However, as expected, providing users with this type of guidance led to a longer time-to-completion, which, of course, needs to be taken into consideration. In this respect, it is interesting to notice that condition H requires 12% and 31% less time than V and HV, respectively. At the same time, it requires 8% less torque than V and only 9% more torque than HV. In some scenarios, such an improvement in time-to-completion might be worth a small increase in torque demands. Finally, the role of visual guidance merits special attention. While it clearly makes the task longer to complete (both V and HV), it is very well appreciated by users, who chose HV and V as the most preferred conditions. This preference is not unexpected, as humans are generally rather used to follow visual navigation feedback (e.g., turn-by-turn car navigation systems based on road signs), while they are not used to follow haptic navigation cues at all. For this reason, we expect more training to significantly improve the performance of the haptic modality in all the considered metrics.

We also want to highlight that our approach is independent from the grasping algorithm. Although here we used *GraspIt!* to generate the grasp poses, our framework is capable to work on top of any other similar approach. For the same reason, as long as the algorithm can generate feasible grasp poses, our framework is expected to work on objects of any shape which are, *e.g.*, sensed by rgb-d sensors.

Limitations of our approach include the need for the 3-dimensional model of the object and inertia matrix, which might not always be easily available. The former can be acquired at runtime using depth cameras mounted on the robot end-effector, as was done in [110], while the latter could be estimated using robot pushing actions [184], vision-based (e.g., recognising the material) or force-based (e.g., palpating the object) techniques. Finally, as in our target application most waste consists of single rigid bodies, the proposed framework currently does not support the handling of deformable objects. This feature could be added by considering the uncertainty on the relative pose of the robot hand w.r.t. the object surface.

CHAPTER

4

Haptic Shared Control for Enhanced User Comfort in Robotic Telemanipulation

Contents

4.1	Related Works	61
4.2	System Details	62
4.2.1	System Model	62
4.2.2	Human Arm Model	63
4.2.3	User Workload Parametrization	63
4.2.4	Inverse Kinematics and Solving the Redundancy	64
4.3	Shared-Control Architecture	65
4.3.1	Human Workload Cost Function	65
4.3.2	Task-Related Cost Function	65
4.3.3	Haptic Feedback	66
4.4	Experimental Evaluation	68
4.4.1	Setup and Participants	68
4.4.2	Task and Conditions	68
4.4.3	Results	70
4.5	Discussion	72

In the previous chapter, we presented a haptic shared-control architecture that aimed to minimize the torques on the robot joints over the post-grasp trajectory. The haptic and visual information guided the user, during the pre-grasping phase, to perform the grasping task, with the goal to optimize the joint torques over the post-grasping manipulative phase, completely autonomous in that case.

In this chapter, we target a grasping and manipulation application where the task is to be solely performed by the user, from pre-grasp to post-grasp. The main difference with the previous chapter is in the metric to optimize, as we shift our attention from the task to the user himself/herself. In fact, in this contribution, we use haptic shared control to account for the user's comfort in addition to minimizing a robot-related metric. The method presented aims at minimizing the user's workload during a teleoperated manipulation task, while accomplishing the task at hand.

This chapter introduces a haptic shared-control technique minimizing the user's workload during robotic teleoperation. Using an inverse kinematic model of the human arm and an online implementation of the Rapid Upper Limb Assessment (RULA) tool [185], the proposed approach starts by estimating the current user's discomfort at runtime. Then, this metric is combined with some knowledge of the target task and system (e.g., direction to follow, target position to reach, effort demanded to the robot) to generate dynamic active constraints guiding the user towards a successful completion of the task along directions that require a reduced workload. The user is nevertheless always in control of the robot motion through the master interface and can deviate from the proposed path if needed, similarly to [126]. As such, the human has the final authority, same as in the previous chapter. This approach is compatible with any robotic teleoperation framework and can be combined with as many additional pieces of information on the task and system as needed. As a proof of concept in this thesis, we use a similar setup as the one used in the previous chapter, shown in Fig. 4.1, however without reducing the robot to 6-DoF. To demonstrate the validity of the proposed approach, we carried out a bilateral telemanipulation experiment with 15 participants, evaluating the effect of our approach in the task performance and in the workload perceived by the users.

This chapter includes work that was accepted and presented in two international venues [6, 7]. A video is also available at <https://youtu.be/DodGI4wMRFA>.

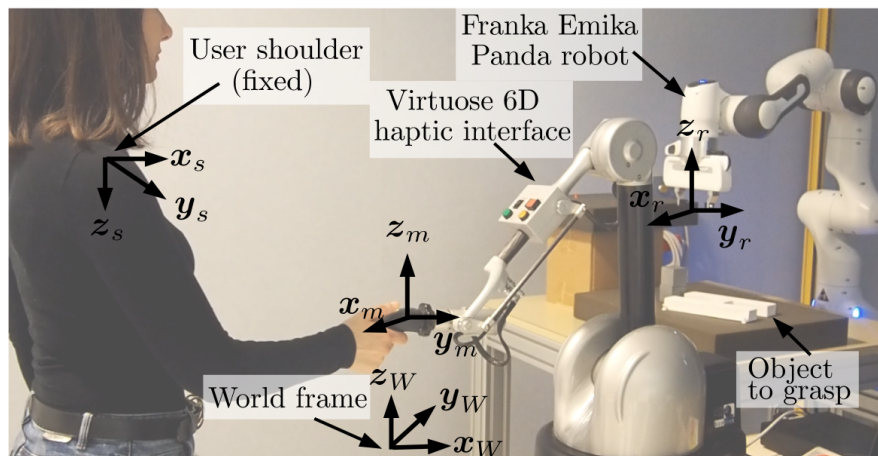


Figure 4.1 – The experimental setup for the pick and place task. On the master side, a Haption Virtuose 6-DoF haptic device, on the remote side a 7-DoF Franka Emika Panda robot. The user shoulder is assumed to be fixed.

4.1 Related Works

Haptic shared control has been successfully used to perform different tasks, e.g., to guide the operator toward a reference position [103, 119–122], to avoid certain areas of the environment [33, 103, 123, 186], and for learning manual tasks [125, 187]. However, researchers have rarely focused on the user’s comfort during robotic telemanipulation, and never – to the best of our knowledge – has haptic shared control been designed for this specific purpose. Nonetheless, this is a very important issue, as operators in many high-impact scenarios use the robotic teleoperation system for long uninterrupted time periods (e.g., a robotic prostatectomy generally takes 2-4 hours). To our knowledge, a few examples are available in the field of human-robot direct interaction. For example, Busch et al. [188] used a simplified human model to calculate the user’s body configuration in human-robot collaboration. They derived a continuous cost function based on the Rapid Entire Body Assessment score (REBA) and used it to choose the robot position optimizing the human joint angles (and thus the ergonomic comfort). Marin et al. [189] optimized the ergonomics of an HRI task where subjects are asked to drill on a board carried by the robot. They relied on musculoskeletal simulations to train a Contextual Ergonomics Model through a probabilistic supervised learning Gaussian process. Chen et al. [190] modeled the human arm as a 7-degrees-of-freedom (7-DoF) robotic manipulator, and its muscular effort was derived based on the estimated value of the joint torques. Similarly, Peternel et al. [191] estimated muscular effort from torques during co-manipulation tasks.

In this chapter, we were inspired from these human-robot collaboration ap-

plications to design a haptic shared-control method for teleoperation scenarios taking the human comfort into account. The method proposed will be explained in more details in the next section.

4.2 System Details

4.2.1 System Model

The master side is composed of the 6-DoF haptic interface, while the remote side consists of the Franka Panda 7-DoF manipulator equipped with a gripper. Fig. 4.2 gives an overview of the entire system architecture.

We consider four reference frames in our system (see Fig. 4.1): \mathcal{F}_r : $\{\mathcal{O}_r, \mathbf{x}_r, \mathbf{y}_r, \mathbf{z}_r\}$ is the robot frame attached to the gripper; \mathcal{F}_m : $\{\mathcal{O}_m, \mathbf{x}_m, \mathbf{y}_m, \mathbf{z}_m\}$ is the frame attached to the end-effector of the master interface; \mathcal{F}_s : $\{\mathcal{O}_s, \mathbf{x}_s, \mathbf{y}_s, \mathbf{z}_s\}$ is the frame attached to the shoulder of the user, which is assumed to be fixed; and \mathcal{F}_W : $\{\mathcal{O}_W, \mathbf{x}_W, \mathbf{y}_W, \mathbf{z}_W\}$ is the world frame. Let $\mathbf{x}_m = (\mathbf{p}_m, \mathbf{R}_m) \in \mathbb{R}^3 \times \mathcal{SO}(3)$ be the pose of the master interface end-effector, $\mathbf{x}_r = (\mathbf{p}_r, \mathbf{R}_r) \in \mathbb{R}^3 \times \mathcal{SO}(3)$ the pose of the robot end-effector, and $\mathbf{x}_s = (\mathbf{p}_s, \mathbf{R}_s) \in \mathbb{R}^3 \times \mathcal{SO}(3)$ the pose of the user's shoulder, all expressed in the common world frame \mathcal{F}_W . The linear/angular velocities of the master and robot in \mathcal{F}_W are denoted by $\mathbf{v}_m = (\dot{\mathbf{p}}_m^T, \boldsymbol{\omega}_m^T)^T \in \mathbb{R}^6$ and $\mathbf{v}_r = (\dot{\mathbf{p}}_r^T, \boldsymbol{\omega}_r^T)^T \in \mathbb{R}^6$, respectively.

The master device is modeled as a generic, gravity pre-compensated, mechanical system

$$\mathbf{M}_m(\mathbf{x}_m)\dot{\mathbf{v}}_m + \mathbf{C}_m(\mathbf{x}_m, \mathbf{v}_m)\mathbf{v}_m = \mathbf{f}_m + \mathbf{f}_h, \quad (4.1)$$

where $\mathbf{M}(\mathbf{x}_m) \in \mathbb{R}^{6 \times 6}$ is the positive-definite and symmetric inertia matrix, $\mathbf{C}(\mathbf{x}_m, \mathbf{v}_m) \in \mathbb{R}^{6 \times 6}$ represents the Coriolis/centrifugal terms, $\mathbf{f}_h \in \mathbb{R}^6$ is the spatial force applied by the human operator to the master interface, and $\mathbf{f}_m \in \mathbb{R}^6$ the feedback forces provided to the operator. On the other hand, the remote robot is controlled in velocity,

$$\mathbf{v}_r = \mathbf{v}_m + \lambda \begin{bmatrix} \mathbf{p}_{r,d} - \mathbf{p}_r \\ \mathbf{R}_r^{-1}(\boldsymbol{\theta}\mathbf{u})_{r,d} \end{bmatrix}, \quad (4.2)$$

where λ is a gain parameter, $\mathbf{p}_{r,d} = (\mathbf{p}_m - \mathbf{p}_{m0}) + \mathbf{p}_{r0}$ is the desired robot position calculated from the current master position \mathbf{p}_m , and \mathbf{p}_{m0} and \mathbf{p}_{r0} are the initial poses of the master and the remote robot. For the angular velocity term, we rely instead on ${}^r(\boldsymbol{\theta}\mathbf{u})_{r,d}$, the angle-axis representation of the relative rotation between the desired and the current robot orientations [192].

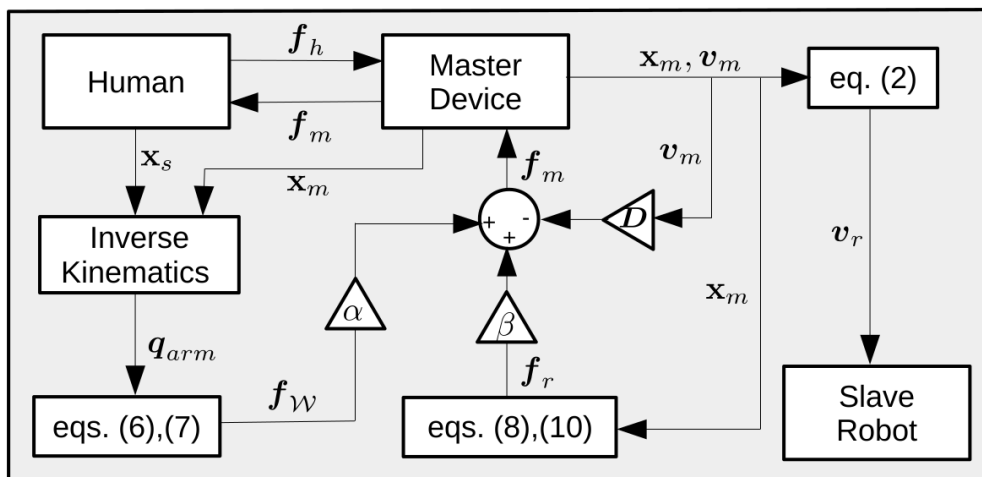


Figure 4.2 – Block diagram summarizing the system architecture and the shared-control algorithm presented in Secs. 4.2 and 4.3.

4.2.2 Human Arm Model

To estimate the user’s discomfort due to arm posture in real-time, we need an estimate of the configuration of his/her arm throughout the teleoperation task. In fact, we decided to rely on a non-invasive technique for estimating the ergonomic comfort, using only the joint angles of the arm. We will consider other approaches in the future (see Sec. 4.5).

For this purpose, the human arm is modeled as a 7-DoF robotic arm, similarly to the work of Shimizu et al. [193]. A spherical joint is used for representing the shoulder and the wrist, while the elbow is represented by a revolute joint (Fig. 4.3a). We use an XYZ Euler convention to represent the spherical joints, to be consistent with the RULA metric which will be introduced in Sec. 4.2.3. Given that the operator is asked to keep the shoulder at a fixed position throughout the task, we can estimate the joint values of the user’s arm $\mathbf{q}_{arm} = [q_1, \dots, q_7]^T$ using solely the position of the master end-effector, which coincides with the user’s palm, using inverse kinematics (details in Sec. 4.2.4).

4.2.3 User Workload Parametrization

Human posture is often used to estimate and prevent work-related musculoskeletal risks, as posture is indeed one of the risk factors for workers. In this respect, the Rapid Upper Limb Assessment (RULA) method [185] is a discrete metric in which a score is given for each upper limb configuration. Depending on the range of each angle in the human arm, a score can be extracted from the RULA table, and the sum of these scores represents the overall workload experienced by the user. The

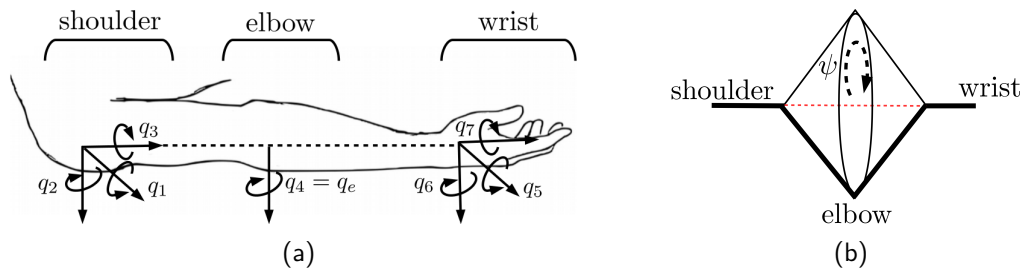


Figure 4.3 – (a) The joints for the human arm. (b) Definition of the arm angle ψ .

RULA table includes other parameters besides the arm angles, however we focus in our system on the arm and wrist as they are the most involved in the teleoperation task.

In our system, the load or discomfort estimate needs to be continuously updated as a function of the user arm configuration throughout the teleoperation task. To do so, we derive a RULA-inspired continuous metric, which increases as the deviation from the resting and most comfortable position of each joint angle in the arm increases. We calculate, at each time step, $\mathbf{q}_s = [q_1, q_2, q_3]^T$ the shoulder angles, $q_e = q_4$ the elbow angle, and $\mathbf{q}_w = [q_5, q_6, q_7]^T$ the wrist angles. As such, $\mathbf{q}_{\text{arm}} = [\mathbf{q}_s^T, q_e, \mathbf{q}_w^T]^T$ (see Fig. 4.3a). The workload \mathcal{W} is then defined as the sum of the squared differences between the angles and their rest positions ($\pi/2$ for the elbow angle, and 0 for the others),

$$\mathcal{W} = \mathbf{q}_s^T \mathbf{q}_s + (q_e - \pi/2)^2 + \mathbf{q}_w^T \mathbf{q}_w. \quad (4.3)$$

This workload calculation behaves similarly to the RULA metric. \mathcal{W} is low when the arm angles are close to their resting position, and increases when the user moves to a less comfortable position. Of course, the RULA-inspired ergonomic metric is just one example of methods to calculate the human workload during teleoperation. Other methods exist, e.g. EMG data, but as we have mentioned in Sec. 4.2.2, we chose a non-invasive method that does not require any additional sensors on the user's arm.

4.2.4 Inverse Kinematics and Solving the Redundancy

Calculating the workload \mathcal{W} assumes that the joint angles \mathbf{q}_{arm} of the user arm are known at each time step. However, given that the arm is represented with a 7-DoF kinematic model, the inverse kinematics is not straightforward. Similarly to [194], we define an arm angle $\psi \in [0, \pi]$, which represents the swivel angle of the arm around a virtual line connecting the shoulder to the wrist, as shown in Fig. 4.3b. If ψ is known, the redundancy is resolved, since the shoulder and wrist

angles can be parametrized using it, and the elbow angle q_e can be computed solely based on geometry.

At each time step, we calculate the inverse kinematics result \mathbf{q}_{arm} from the user hand position, using all possible values of ψ (discrete values with increments of 0.01 in the $[0, \pi]$ range). Then, we compute the corresponding \mathcal{W} value assuming that the user naturally chooses the most comfortable configuration *of the elbow* when presented with a set of options. To do so, we choose the inverse kinematics solution corresponding to the ψ value leading to the least discomfort between the possible solutions (lowest \mathcal{W}), similarly to what was done in [190]. This assumption only affects the swivel angle of the elbow and no other joint angle. Additional techniques that we will use in the future to improve this pose estimation are mentioned in Sec. 4.5. Finally, a condition is added to ensure that the resulting angles are close to the previous configuration of the arm, so that no abrupt changes occur.

4.3 Shared-Control Architecture

This section describes the shared-control algorithm used to guide the human operator during the teleoperation task. The main goal of this architecture is not only to account for task-related requirements, but to also target the maximization of the user’s comfort during the task. We thus divide our haptic feedback force into two components: a human-related component, $\mathbf{f}_{\mathcal{W}}$, and a robot/task-related one, \mathbf{f}_r .

4.3.1 Human Workload Cost Function

We want to minimize the muscular discomfort experienced during the task execution. This is obtained by minimizing the cost function $\mathcal{H}_{\mathcal{W}} = \mathcal{W}$, i.e., the workload. A comfortable arm configuration is thus defined as one with a small value for the workload cost \mathcal{W} .

4.3.2 Task-Related Cost Function

The second component of the haptic feedback is related to the task itself, as in more traditional shared-control architectures. A second cost function \mathcal{H}_r is thus introduced to represent this task-related metric to be optimized. The cost \mathcal{H}_r can be related to maximizing, e.g., the distance from joint limits, singularities, or obstacles. It could also be related to the distance from a target, or to the robot

joint velocities or torques (like in the previous chapter), in which case it should be minimized. While this cost function is general, we choose for our application to minimize the Euclidean distance to the target object pose, similarly to [195], by defining

$$\mathcal{H}_r = \begin{bmatrix} \mathbf{p}_{r,g} - \mathbf{p}_r \\ {}^r(\theta\mathbf{u})_{r,g} \end{bmatrix}^T \begin{bmatrix} \mathbf{p}_{r,g} - \mathbf{p}_r \\ {}^r(\theta\mathbf{u})_{r,g} \end{bmatrix}, \quad (4.4)$$

where \mathbf{p}_r and $\mathbf{p}_{r,g}$ are the current and goal positions of the robot end-effector, and ${}^r(\theta\mathbf{u})_{r,g}$ is the angle-axis representation of the relative rotation between the current and target robot poses. The same approach can be easily extended to any similar task-related metric.

4.3.3 Haptic Feedback

We design the haptic feedback to guide the user during teleoperation, such that both task- and human-comfort-inspired cost functions are minimized. To achieve this goal, the forces applied at the master end-effector are defined as

$$\mathbf{f}_m = \alpha \mathbf{f}_W + \beta \mathbf{f}_r - \mathbf{D}\mathbf{v}_m, \quad (4.5)$$

where \mathbf{f}_W is the force vector instantaneously guiding the user towards the position with the highest comfort, and vector \mathbf{f}_r is the force minimizing the task cost function, which in our case is related to the distance from the target release position. α and β are weights to be tuned depending on the importance to be given to each cost function ($\alpha + \beta = 1$). Finally, \mathbf{D} is a diagonal damping matrix to improve the bilateral stability of the system [5, 110]. We chose a damping value of 2 Ns/m in translation and 0.07 Nms/rad in rotation.

The feedback component related to \mathcal{H}_W is designed to be proportional to a desired velocity of the master device in a direction that minimizes the cost function,

$$\mathbf{f}_W = K_W \mathbf{v}_{m,d_W}, \quad (4.6)$$

where K_W is a proportional constant, and \mathbf{v}_{m,d_W} is the desired velocity of the master device end-effector, based on the metric maximizing the comfort. It is calculated from the desired joint velocities of the human arm, $\dot{\mathbf{q}}_{\text{arm},d}$, as follows: $\mathbf{v}_{m,d_W} = \mathbf{T}\mathbf{J}\dot{\mathbf{q}}_{\text{arm},d}$, where \mathbf{T} is a transformation matrix to take the desired velocity calculated from the shoulder frame \mathcal{F}_s to \mathcal{F}_m , and \mathbf{J} is the Jacobian of the human arm. The velocity $\dot{\mathbf{q}}_{\text{arm},d}$ is chosen for ensuring that \mathcal{H}_W is minimized, or, in other words, $\dot{\mathcal{H}}_W(\mathbf{q}_{\text{arm}}) = (\partial\mathcal{H}_W/\partial\mathbf{q}_{\text{arm}})\dot{\mathbf{q}}_{\text{arm}} \leq 0$. We thus choose the desired angular velocity of the arm angles to be in the negative direction of the gradient of the

human-related cost function,

$$\dot{\mathbf{q}}_{\text{arm},d} = -\frac{\partial \mathcal{H}_{\mathcal{W}}}{\partial \mathbf{q}_{\text{arm}}}. \quad (4.7)$$

Null values for $\mathbf{f}_{\mathcal{W}}$ in eq. (4.6), caused by the algorithm being stuck in a singular configuration $\bar{\mathbf{q}}$ (where $\mathbf{N}(\mathbf{J}(\bar{\mathbf{q}})) \neq 0$) different from the target one associated with the minimum RULA and where $\dot{\mathbf{q}}_{\text{arm},d} \in \mathbf{N}(\mathbf{J}(\bar{\mathbf{q}}))$, are very unlikely due to the quite limited range of motion of the user's arm.

The feedback component related to \mathcal{H}_r is designed similarly,

$$\mathbf{f}_r = K_r \mathbf{v}_{m,d_r}. \quad (4.8)$$

Since our haptic feedback is applied at the master side, and assuming no significant delays or communication issues occur between the master and the remote system, we start by defining a new cost function, \mathcal{H}_m , which encodes the difference between the master device pose and its target pose, computed from the target robot pose using a transformation matrix:

$$\mathcal{H}_m = \begin{bmatrix} \mathbf{p}_{m,g} - \mathbf{p}_m \\ {}^m(\theta\mathbf{u})_{m,g} \end{bmatrix}^T \begin{bmatrix} \mathbf{p}_{m,g} - \mathbf{p}_m \\ {}^m(\theta\mathbf{u})_{m,g} \end{bmatrix}, \quad (4.9)$$

where \mathbf{p}_m and $\mathbf{p}_{m,g}$ are the current and target positions of the haptic device end-effector. ${}^m(\theta\mathbf{u})_{m,g}$ is the angle-axis representation of the relative rotation between the current and the target master poses. The desired velocity of the haptic device is finally chosen such that it minimizes the distance to the target

$$\mathbf{v}_{m,d_r} = \begin{bmatrix} \dot{\mathbf{p}}_{m,d_r} \\ \boldsymbol{\omega}_{m,d_r} \end{bmatrix} = \begin{bmatrix} \mathbf{p}_{m,g} - \mathbf{p}_m \\ {}^m(\theta\mathbf{u})_{m,g} \end{bmatrix}, \quad (4.10)$$

as also done in, e.g., [192].

To avoid having one of the two components of the force (\mathbf{f}_r and $\mathbf{f}_{\mathcal{W}}$) masking the other one due to their difference in scale, we scale each of the forces to the same range before adding them in eq. (4.5). The linear and torque components of each spatial force vector are scaled to a norm of 2.5 N and 0.25 N.m, respectively. A similar technique was used in [196] to scale the 19 components of a biomimetic sensor so as to be able to combine and compare them. This choice allowed us to make sure the user receives the two types of feedback all the time, but along the direction decided by the weights as in eq. 4.5. The resulting force guides the users towards the pose minimizing the composite metrics, but it is always gentle enough to enable them to deviate from the suggested path, if needed. Additional feedback techniques for providing this guidance information will be discussed in

Chapter 7. Finally, once the user is within a threshold distance from the target position, we scale the two force components proportionally to the distance to the goal. Decreasing the human-related component is important to allow the user to reach the final goal, while decreasing the force feedback related to the task parameter avoids strong forces and oscillations as the user gets closer to the goal, similarly to [110].

4.4 Experimental Evaluation

4.4.1 Setup and Participants

The experimental setup is shown in Fig. 4.1 and described in Sec. 4.2. The remote environment is composed of three different sets of objects to grasp, pick up, and place on a target location, as detailed in the next section. To enable the operator to see the environment, the master interface was placed next to the robot manipulator.

Fifteen subjects participated in the study (10 males, 5 females). Each subject spent about two minutes practicing the control of the telemanipulation system before starting the experiment. At this moment, the pose of the user’s shoulder was measured and kept fixed throughout the experiment. This latter point is important because our workload parametrization and inverse kinematics assume a fixed position of the shoulder (see Secs. 4.2.3 and 4.2.4).

4.4.2 Task and Conditions

Participants used the master interface to control the manipulator. The task consisted in grasping the objects (first part of the task) and moving them to a target

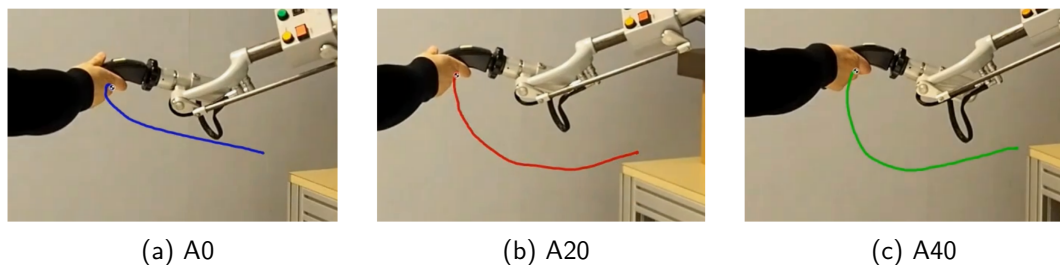


Figure 4.4 – User trajectory for a reaching movement for the three weightings A0 (blue), A20 (red), and A40 (green). In A0, only \mathcal{H}_r is considered, and the user trajectory is therefore almost horizontal. As the contribution of \mathcal{H}_W to the haptic feedback increases, the trajectory tries to minimize the user discomfort by moving the arm to a downward (more comfortable) position.

put-down location marked on the table (second part of the task). Participants were asked to complete the task as precisely and fast as possible. The task started when the manipulator moved for the first time, and it was considered completed when the object was released on the target.

As explained in Sec. 4.3, we combine different cost functions to take into account human-related metrics as well as robot- and task-related ones. In this experiment, we consider the estimated human workload as our human-related cost \mathcal{H}_W , and the distance from the target location (i.e., the grasping pose in the first part of the task and the put-down location in the second part) as our task-related cost \mathcal{H}_r . These two functions are then properly weighted and combined to generate the guiding feedback, as described in eq. (4.5). Of course, the proposed approach can be used for any other set of cost functions.

We consider three different weighting schemes for the contribution of \mathcal{H}_W and \mathcal{H}_r to the haptic guidance \mathbf{f}_m :

- (A0) $\alpha = 0, \beta = 1$ (the human-centered metric is disregarded and the operator is simply guided toward the target);
- (A20) $\alpha = 0.2, \beta = 0.8$ (weak human-centered guidance);
- (A40) $\alpha = 0.4, \beta = 0.6$ (strong human-centered guidance).

We only consider conditions with $\beta > 0.5$ to ensure that the guidance feedback always brings the user towards the completion of the task. In fact, a hypothetical human-centered-only condition with $\alpha = 1.0, \beta = 0$ would simply guide the user towards a comfortable arm position, with no information and guidance regarding the task.

For each weighting condition A0, A20, A40, participants were asked to pick and place three different sets of objects:

- (B) an empty cardboard box of dimensions $14 \times 4 \times 4$ cm;
- (C) two cubes, each of dimensions $4.2 \times 4.2 \times 4.2$ cm;
- (L) the wooden letter “H” with outer dimensions $21 \times 13 \times 2.5$ cm.

Each subject carried out eighteen randomized repetitions of the pick-and-place task, two for each weighting condition and set of objects. These two repetitions differed in the pick-up and put-down locations. A video is available at <https://youtu.be/DodGI4wMRFA>. Fig. 4.4 shows the effect of the weighting schemes in a simple reaching movement between two fixed points. Our scenario involved a pick and place task, in which the starting and target positions are placed on two

Table 4.1 – Statistical analysis (two-way repeated-measure ANOVA)

<u>Completion time</u>			
Main effect of weighting			
A0 vs. A20	$p = 0.020$	A0 vs. A40	$p < 0.001$
Main effect of object			
B vs. L	$p < 0.001$	L vs. C	$p < 0.001$
B vs. C	$p < 0.001$		
<u>Placing error</u>			
Main effect of object			
B vs. C	$p < 0.001$	L vs. C	$p = 0.003$
<u>Average $\mathcal{H}_{\mathcal{W}}$</u>			
Main effect of weighting			
A0 vs. A20	$p = 0.048$	A0 vs. A40	$p < 0.001$
A20 vs. A40	$p = 0.028$		
Main effect of object			
B vs. L	$p < 0.001$	L vs. C	$p < 0.001$
<u>Maximum $\mathcal{H}_{\mathcal{W}}$</u>			
Main effect of weighting			
A0 vs. A20	$p = 0.049$	A0 vs. A40	$p < 0.001$
A20 vs. A40	$p = 0.025$		
Main effect of object			
B vs. L	$p < 0.001$	L vs. C	$p = 0.002$
B vs. C	$p = 0.012$		
<u>NASA TLX workload index</u>			
Main effect of weighting			
A0 vs. A20	$p = 0.035$	A0 vs. A40	$p = 0.001$
A20 vs. A40	$p = 0.050$		

supports having different height. To avoid colliding with any of the supports and make our approach viable for any trajectory, we designed our task-related feedback by introducing an intermediate target point, $\mathbf{x}_{r,i} = (\mathbf{p}_{r,i}, \mathbf{R}_{r,i})$, higher than both supports. The user is first guided to this intermediate point. Then, once the robot reaches its neighborhood, the guiding force smoothly switches toward a new target pose, $\mathbf{x}_{r,g} = (\mathbf{p}_{r,g}, \mathbf{R}_{r,g})$, which is the final release position for our object. This approach can be easily used with any arbitrarily complex trajectory.

4.4.3 Results

To evaluate the effectiveness of the proposed human-centered shared-control approach, we recorded (*i*) the completion time, (*ii*) the error in placing the objects

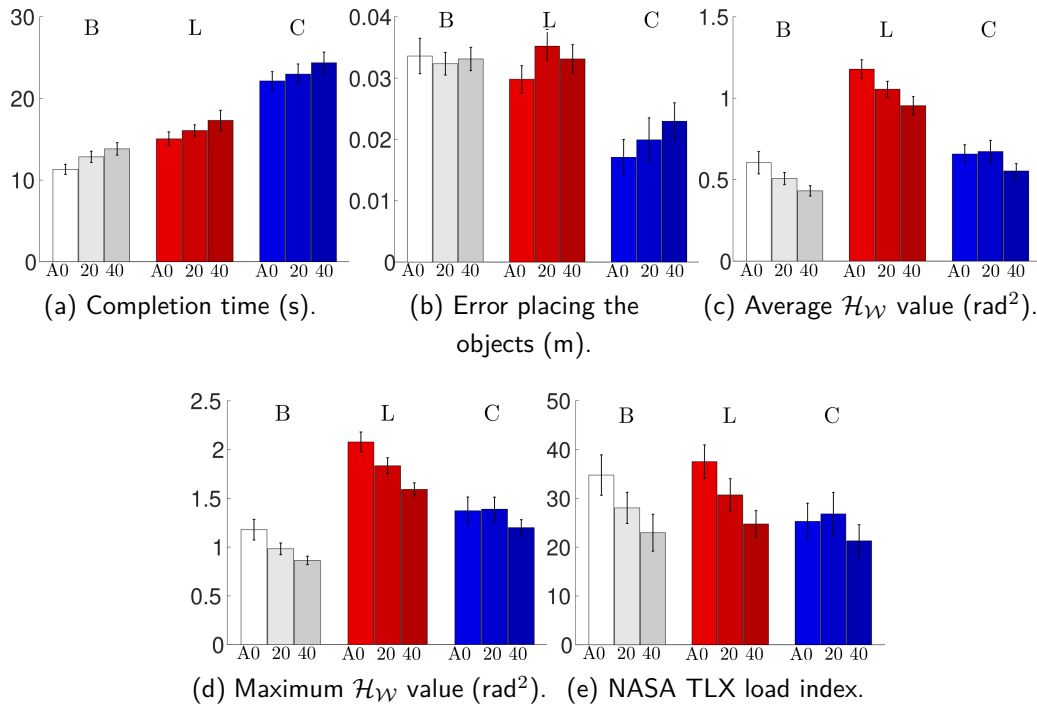


Figure 4.5 – Human subjects experiment. Mean and standard error of the mean of (a) completion time, (b) error in placing the objects, (c) average $\mathcal{H}_{\mathcal{W}}$, (d) maximum $\mathcal{H}_{\mathcal{W}}$, and (e) NASA TLX load index for the three control conditions (A0, A20, A40) and the three target objects (B, L, C).

at the target, (iii-iv) the mean and maximum $\mathcal{H}_{\mathcal{W}}$ registered, and (v) the NASA Task Load Index (NASA-TLX) [197]. To compare these metrics, we ran two-way repeated-measures ANOVA tests. The three weightings (A0 vs. A20 vs. A40) and the three sets of objects to move (B vs. C vs. L) were treated as within-subject factors. Data were transformed using the `arcsin` transformation whenever necessary to achieve normality. All data passed the Shapiro-Wilk normality test. A Greenhouse-Geisser correction was used when the assumption of sphericity was violated. Results of post hoc analysis with Bonferroni adjustments are reported in Table 4.1 (only significant p values are shown).

Fig. 4.5a shows the completion time, averaged across trials. All data passed the Mauchly’s Test of Sphericity. The two-way repeated-measure ANOVA revealed a statistically significant change for this metric across weighting conditions ($F(2, 28) = 14.898, p < 0.01$) and objects ($F(2,28) = 107.168, p < 0.001$). Fig. 4.5b shows the error in placing the objects, averaged across trials. It is calculated as the distance between the target position and where the objects were actually placed at the end of the task. All data passed the Mauchly’s Test of Sphericity. The two-way repeated-measure ANOVA revealed a statistically significant change

for this metric across objects only ($F(2,28) = 16.118, p < 0.001$). Fig. 4.5c shows the mean \mathcal{H}_W , averaged across trials. It is calculated as the value of \mathcal{H}_W averaged over the duration of the task. All data passed the Mauchly's Test of Sphericity. The two-way repeated-measure ANOVA revealed a statistically significant change for this metric across weighting conditions ($F(2,28) = 17.287, p < 0.001$) and objects ($F(2,28) = 58.534, p < 0.001$). Fig. 4.5d shows the maximum \mathcal{H}_W , averaged across trials. It is calculated as the maximum value of \mathcal{H}_W registered during the task. All data passed the Mauchly's Test of Sphericity. The two-way repeated-measure ANOVA revealed a statistically significant change for this metric across weighting conditions ($F(2,28) = 16.594, p < 0.001$) and objects ($F(2,28) = 32.418, p < 0.001$). Fig. 4.5e shows the overall workload score of the NASA TLX, registered using the official NASA TLX app. All data passed the Mauchly's Test of Sphericity. The two-way repeated-measure ANOVA revealed a statistically significant change for this metric across weighting conditions only ($F(2,28) = 13.340, p < 0.001$).

A linear regression was run to understand the effect of \mathcal{H}_W on the final NASA TLX. To assess linearity, a scatterplot of mean \mathcal{H}_W against NASA TLX with superimposed regression line was plotted. Visual inspection of these two plots indicated a linear relationship between the variables. There was homoscedasticity, independence, and normality of the residuals. Average \mathcal{H}_W accounted for 60.7% of the variation in NASA TLX with adjusted $R^2 = 60.3\%$, and it statistically significantly predicted NASA TLX, $F(1,133) = 265.123, p < 0.001$. A Pearson's product-moment correlation showed a statistically significant positive correlation between mean \mathcal{H}_W and NASA TLX, $r(135) = 0.779, p < 0.001$.

Fig. 4.6 shows a representative evolution of both cost functions vs. time for the A0 and A40 weighting schemes.

4.5 Discussion

Looking at the previous results, we can see that completion time showed a significant degradation when adding our human-centered guidance (A20, A40) vs. standard task-centered guided teleoperation (A0). This result is quite expected, and it is the major drawback of our approach, as the additional guidance inevitably deviates the user from the shortest path. However, this (small) performance degradation is compensated by a significant reduction of the estimated muscular discomfort (mean and max \mathcal{H}_W) and measured workload (NASA TLX). In fact, while the completion time and placing error degrade by 14% and 10%,

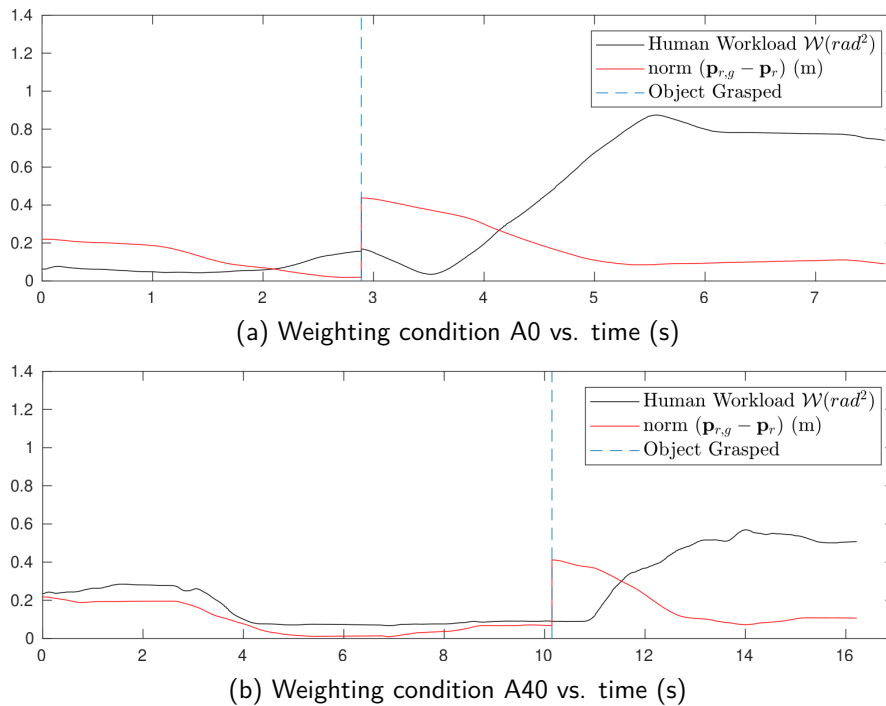


Figure 4.6 – Representative evolution of the human workload metric \mathcal{W} and the norm of the translational error between the current and the desired robot pose, for the A0 and A40 weighing conditions. The user is faster in completing the task using A0; however, a lower \mathcal{W} is recorded using A40, especially in the second part of the task (after grasping the object and moving towards the put-down location). The dashed line represents the moment the user grasps the object and the target position changes.

respectively, the NASA TLX value is improved by 30%. It is also important to highlight that we considered a rather short task (approx. 20 minutes in total), and we expect that the effect and usefulness of our approach increase with the duration of the task. Finally, we did not register any noticeable degradation of the performance due to implementing the haptic shared control at the master side. Indeed, where to implement haptic active constraints in robotic teleoperation is still an open question. There are arguments for both. Implementing the active constraint at the master side solves any issue related to the stability of the system, but it opens to the risk of badly controlling the robot. On the other hand, enforcing the active constraint at the remote side solves any issue related to the commanding of the robot, but it exposes to the risks of instabilities. This issue has been tackled in more details in Chapter 2, Sec. 2.2.2, and could open up the possibility to an interesting study in the future.

It would also be interesting to test other techniques to either directly measure the users' muscle effort (e.g., using Electromyography EMG) or better estimate their pose (e.g., using RGB-D cameras [198], machine-learning approaches [199],

or spatial tracking [200, 201]). Such approaches will solve the uncertainty related to the redundancy of our arm kinematic model. Another goal would also be to consider additional metrics (e.g. jerkiness of the motion, full-body kinematics, workload over a long task and multiple sessions).

Part III

Haptic Shared-Control Methods with Partial Human Authority

CHAPTER

5

Shared Control for Robotic Cutting

Contents

5.1	Related Works	79
5.2	Methods	81
5.2.1	Standard Haptic Teleoperation (Condition T)	82
5.2.2	Unicycle Approach (Condition U)	83
5.2.3	Car-like Approach (Condition C)	85
5.3	Experimental Evaluation	86
5.3.1	Setup	87
5.3.2	Task and Conditions	87
5.3.3	Participants	88
5.3.4	Results	88
5.4	Discussion	91

In Chapters 3 and 4, we presented haptic shared-control methods that are both directed towards minimizing the torques on the robot joints and towards maximizing the user comfort while performing the teleoperation task. In these methods, *soft* constraints were applied in the form of haptic information to the user on the master device side. These constraints could guide the operator while giving him/her the freedom to choose whether to comply. As such, the user had the final authority in commanding the robot. In this third part of the manuscript, we present novel system architectures with more authority given to the automation.

We start in this chapter by targeting a cutting application. Robotic cutting is a great example of applications where the specificity of the task could help us design a shared-control method that would alleviate the cognitive load on the user compared to simple teleoperation, while also improving the task execution. We therefore present two haptic shared-control methods that take into account the constraints particular to the cutting task. Given the nature of the constraints applied, which are *hard* constraints, less authority is given to the user whose motion is limited in space to some degrees of freedom. In the next chapter, we will instead demonstrate an autonomous architecture for grasping soft objects. The user input is in this case integrated in the learning data, providing the automation system with a human perspective on the best way to grasp with the help of haptic feedback.

The motivation behind this chapter stems from the fact that robot-assisted cutting is considered an important task in several fields, such as robotic surgery, nuclear decommissioning, waste management, and manufacturing. Despite the complex dexterity requirements of cutting tasks, very simple mechanically-linked master-remote manipulator systems still dominate many of the above fields (e.g., nuclear robotics). Moreover, even when more dexterous manipulators are available (e.g., in robot-assisted surgery), the employed systems show little or no autonomy, delegating all control to the experience of the human operator. To ameliorate this situation, we present two haptic shared-control approaches for robotic cutting. They are designed to assist the human operator by enforcing different nonholonomic-like constraints representative of the cutting kinematics. We validate our approach by carrying out a human-subject experiment in a real cutting scenario, and by comparing our shared-control techniques with each other and with a standard haptic teleoperation scheme.

This chapter contains work has been published and presented in [5, 8] and a video of the experiments is available at <https://youtu.be/DkW40cjgX9M>.

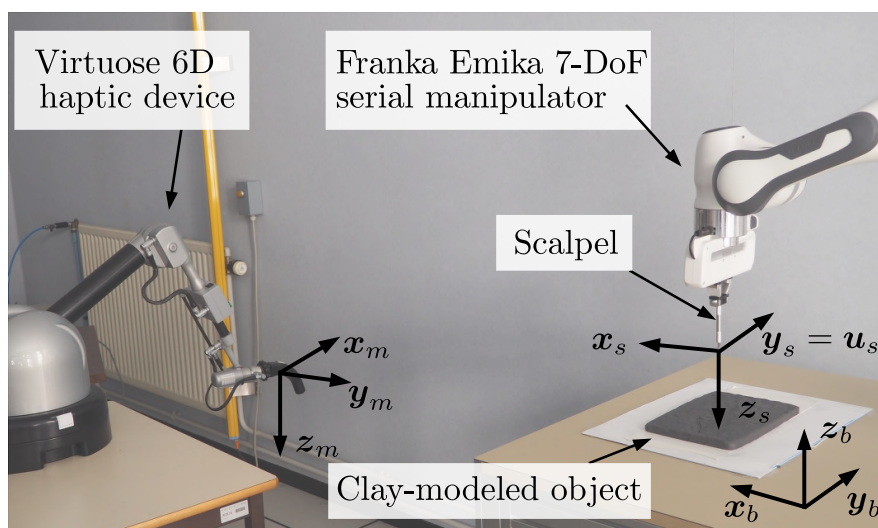


Figure 5.1 – Experimental setup and reference frames used for designing the shared-control techniques. Their objective is to help the operator cut the clay safely and intuitively. To do so, we enforced various nonholonomic-inspired constraints, limiting lateral motions, rotations in place, and sharp turns of the scalpel.

5.1 Related Works

Robotic cutting is particularly interesting for shared control, as it requires high dexterity and can have serious implications if it fails. It is in fact employed in various sensitive applications which range from surgical cutting [202] to nuclear decommissioning [78] and disaster response [203, 204]. Moreover, cutting applications feature a variety of constraints which can have a high impact on the task. For example, to avoid damaging the environment, the cutting tool should neither perform pure lateral motion nor rotate in place. Accounting for these constraints in the design of the control architecture can be key for a successful and safe task execution. Indeed, unicycle and car-like kinematic models have been used for modeling the cutting task to reflect its nonholonomic nature [205–207].

Several shared-control architectures have been proposed in the literature to tackle different cutting applications. For example, Prada and Payandeh [208] used geometric virtual fixtures for providing assistance during cutting. The user was guided towards a particular path using haptic feedback complemented with a visual interface. Experiments were performed in a virtual environment and no specific nonholonomic constraints were considered. Early work towards enforcing a nonholonomic behavior on robotic systems has also been proposed for cobots, where nonholonomy was ensured by mechanically limiting the DoF as to prevent any nonholonomic motion [209, 210]. The cobots then followed the forces applied

by the human operator along the available DoF. However, most scenarios require more flexible and dexterous robots, capable of performing different tasks which may not always be nonholonomic. Enforcing nonholonomic constraints on multi-purpose robots through control has been tackled, for example, by Arai et al. [211]. The authors propose a robotic control architecture that helps a human operator in handling long objects by imposing virtual nonholonomic constraints. More recently, Li and Kazanzides [212] proposed a shared-control architecture for cutting in satellite servicing scenarios under time delay. The task consisted of cutting a straight line in multi-layer insulation (MLI) blankets (a thermal insulation patch used to cover satellites). A semi-autonomous architecture helped the operator in keeping the blade normal to the blanket. Vozar et al. [213] addressed a similar problem by designing four shared-control approaches. The task again comprised cutting straight lines into MLI blankets under a time delay. In the first control approach, users were given control over all planar DoF. In the second one, lateral motion (away from the desired straight line) was scaled down to reduce its impact in comparison with the two other controlled DoF. In the third one, lateral motion was completely disregarded, i.e., the remote robot was forced to abide to nonholonomic constraints. In the fourth one, users were provided with visual guidance towards the desired straight line. In all modes, the master interface was free to move in any direction, and the constraints were implemented only at the remote side. The authors carried out a user study in which they compared the distance error over the trajectory, its “roughness,” and the completion time. Results showed no significant differences between the four modalities.

While the approaches of [213] and [212] are promising, they mainly focus on treating the time delay in the system rather than the cutting task itself. In fact, they all consider rather simple cutting tasks (straight lines). In real scenarios, the cutting trajectories might be significantly more complicated and the environment considerably sturdier. Moreover, they provide the user with little information about the constraints being enforced. While the robot was constrained to a non-holonomic motion, this restriction was not reflected on the master interface, that was free to move in all directions. This mismatch between remote robot and master may create confusion and it might have been the reason for the limited improvements shown by these modalities.

This chapter targets the limitations of the above-described architectures. It presents the design and evaluation of two shared-control approaches for commanding a torque-controlled manipulator in a cutting scenario. These approaches are designed to help the human operator complete the cutting task in an intuitive and safe way, by enforcing the constraints associated with the task itself, e.g.,

limiting lateral motions, rotations in place, and sharp turns of the tool. A key contribution of our system is that the user is provided with information about the enforced nonholonomic constraints (alongside contact forces) via haptic feedback on the master device. The constraints at the master's side are imposed only using information from the master position, limiting any unstable behavior due to communication delays between master and remote robot. We believe that this feedback is essential for the operator and can turn around the results of [213].

5.2 Methods

The robotic system is composed of the master 6-DoF haptic interface and the 7-DoF torque-controlled manipulator used in the previous chapters. In this setup, the robot is however equipped with a scalpel. The environment is composed of a planar object to cut, placed on a table.

We consider three reference frames, shown in Fig. 5.1: $\mathcal{F}_s : \{\mathcal{O}_s, \mathbf{x}_s, \mathbf{y}_s, \mathbf{z}_s\}$, attached to the remote scalpel; $\mathcal{F}_m : \{\mathcal{O}_m, \mathbf{x}_m, \mathbf{y}_m, \mathbf{z}_m\}$, attached to the end-effector of the master interface; and $\mathcal{F}_b : \{\mathcal{O}_b, \mathbf{x}_b, \mathbf{y}_b, \mathbf{z}_b\}$, our base frame attached to the environment, i.e., the object to cut. The environment is assumed to be fixed and planar, with \mathbf{z}_b being the normal to this plane. The scalpel (\mathcal{F}_s), as well as the end-effector of the master device (\mathcal{F}_m), are free to move along the three translational directions. However, their orientation is constrained via control, such that $\mathbf{z}_s = \mathbf{z}_m = -\mathbf{z}_b$. The system can thus only rotate around \mathbf{z}_b . This constraint is enforced in all the three control modalities described below.

Let $\mathbf{p}_s : (\mathbf{t}_s, \alpha_s) \in \mathbb{R}^4$ define the pose of the scalpel expressed in \mathcal{F}_b , where $\mathbf{t}_s \in \mathbb{R}^3$ encodes the three translational directions and $\alpha_s \in \mathbb{R}$ the rotation around \mathbf{z}_b . Similarly, let $\mathbf{p}_m : (\mathbf{t}_m, \alpha_m) \in \mathbb{R}^4$ define the pose of the master device expressed in \mathcal{F}_b . The master device is modeled as a generic (gravity pre-compensated) mechanical system,

$$\mathbf{M}_m(\mathbf{p}_m)\ddot{\mathbf{p}}_m + \mathbf{C}_m(\mathbf{p}_m, \dot{\mathbf{p}}_m)\dot{\mathbf{p}}_m = \boldsymbol{\tau}_m + \boldsymbol{\tau}_h, \quad (5.1)$$

where $\mathbf{M}_m(\mathbf{p}_m) \in \mathbb{R}^{4 \times 4}$ is the positive-definite and symmetric inertia matrix, $\mathbf{C}_m(\mathbf{p}_m, \dot{\mathbf{p}}_m) \in \mathbb{R}^{4 \times 4}$ accounts for Coriolis/centrifugal terms, and $\boldsymbol{\tau}_m, \boldsymbol{\tau}_h \in \mathbb{R}^4$ are the control and operator forces, respectively. Similarly, at the remote side,

$$\mathbf{M}_s(\mathbf{p}_s)\ddot{\mathbf{p}}_s + \mathbf{C}_s(\mathbf{p}_s, \dot{\mathbf{p}}_s)\dot{\mathbf{p}}_s = \boldsymbol{\tau}_s + \boldsymbol{\tau}_e, \quad (5.2)$$

where $\mathbf{M}_s(\mathbf{p}_s) \in \mathbb{R}^{4 \times 4}$ is the positive-definite and symmetric inertia matrix, $\mathbf{C}_s(\mathbf{p}_s, \dot{\mathbf{p}}_s) \in \mathbb{R}^{4 \times 4}$ accounts for Coriolis/centrifugal terms, and $\boldsymbol{\tau}_s, \boldsymbol{\tau}_e \in \mathbb{R}^4$ are the control and external forces, respectively.

We designed three different control approaches. The first one (T) is a simple human-in-the-loop teleoperation, with no added constraints related to the specificity of the cutting task. While this is a rather standard approach, we still deemed it important, as it still is the gold standard in many application scenarios, including robotic surgery. The second one (U) is a unicycle approach. It adds nonholonomic constraints to avoid any lateral motion of the knife tool, which may severely damage both the tool and the environment. However, this approach does not prevent the tool from rotating in place or performing sharp turns, which can also be dangerous. For this reason, we consider an additional mode C, in which the user has direct control over the radius of curvature of the trajectory, similar to the steering mechanism of a car. In addition to all the constraints enforced in U, this modality also ensures that the tool only rotates when a translation is commanded at the same time.

The general architecture of the system is summarized in Fig. 5.2. More details on each control mode are shown in Fig. 5.3 as well as in the video available at <https://youtu.be/DkW40cjgX9M>. We evaluated their performance against each other in the human subject study described in Sec. 5.3.

5.2.1 Standard Haptic Teleoperation (Condition T)

In this modality, the pose of the robot is linked to the pose of the master so as to replicate its motion. The manipulator receives torque commands that are calculated as

$$\boldsymbol{\tau}_s = \mathbf{K} (\mathbf{p}_{s,d} - \mathbf{p}_s) + \mathbf{D} (\dot{\mathbf{p}}_{s,d} - \dot{\mathbf{p}}_s), \quad (5.3)$$

where $\mathbf{p}_{s,d} = \mathbf{p}_m$ and $\dot{\mathbf{p}}_{s,d} = \dot{\mathbf{p}}_m$. $\mathbf{K} \in \mathbb{R}^{4 \times 4}$ is a proportional scaling term and $\mathbf{D} \in \mathbb{R}^{4 \times 4}$ is the corresponding derivative term. In our case, we choose \mathbf{K} and \mathbf{D} to be diagonal matrices with $\mathbf{K} = \text{diag}(500 \text{ N/m}, 350 \text{ N/m}, 150 \text{ N/m}, 15 \text{ Nm/rad})$ and $\mathbf{D} = \text{diag}(44 \text{ Ns/m}, 50 \text{ Ns/m}, 24 \text{ Ns/m}, 2 \text{ Nms/rad})$.

The external forces applied by the environment on the remote robot are fed back to the user through the master interface, such that

$$\boldsymbol{\tau}_m = \boldsymbol{\tau}_c + \boldsymbol{\tau}_{nc}, \quad (5.4)$$

where $\boldsymbol{\tau}_c$ represents the forces applied along the constrained directions, and $\boldsymbol{\tau}_{nc}$ the ones applied along the non-constrained directions. In this condition, since no constraints are added to the system, $\boldsymbol{\tau}_c = \mathbf{0}$ and $\boldsymbol{\tau}_{nc} = \mathbf{S}_x(\boldsymbol{\tau}_e - \mathbf{B}\dot{\mathbf{p}}_m)$, where \mathbf{S}_x is a selection matrix projecting the force feedback on the non-constrained directions (the identity matrix in this case), and $\mathbf{B} \in \mathbb{R}^{4 \times 4}$ is a damping matrix which improves the bilateral stability of the system. We chose $\mathbf{B} =$

$\text{diag}(4 \text{ Ns/m}, 4 \text{ Ns/m}, 4 \text{ Ns/m}, 0.05 \text{ Nms/rad})$ for a good trade-off between reactivity and stability (similarly to [124]).

5.2.2 Unicycle Approach (Condition U)

While T guarantees high flexibility, considering a cutting scenario enables us to introduce additional constraints which can make the teleoperation easier and safer. In particular, any pure lateral motion of the scalpel during cutting can induce significant damage on the material being cut (and even on the scalpel itself, if the material is hard enough). To limit this undesired behavior, we impose nonholonomic constraints on the robot motion, such that the scalpel is constrained to move along two translational directions only: (i) its cutting direction \mathbf{u}_s , and (ii) its vertical direction along \mathbf{z}_b . The scalpel can always rotate around its axis \mathbf{z}_s . In other words, it can move forward/backward, up/down, and rotate around its vertical axis; however, it cannot translate laterally, along the direction perpendicular to \mathbf{u}_s and \mathbf{z}_s (see Fig. 5.1). In our scenario, the scalpel was always oriented such that $\mathbf{u}_s = \mathbf{y}_s$.

To achieve this desired behavior, we constrain the master device such that the user is allowed to move along \mathbf{x}_m and \mathbf{z}_m in translation, as well as to rotate around \mathbf{z}_m . The motion around \mathbf{y}_m is, however, blocked. To enforce this blockage, we define a plane $S_{l,m}(t) : (\mathbf{n}_{l,m}(t), \mathbf{t}_{l,m}(t))$, in which the motion of the master is constrained at any time t . $\mathbf{n}_{l,m}(t) \in \mathbb{R}^3$ is the normal vector to the plane, and $\mathbf{t}_{l,m}(t) \in \mathbb{R}^3$ is a point in space through which the plane passes. We can easily define $\mathbf{n}_{l,m}(t)$ as $\mathbf{n}_{l,m}(t) = [\mathbf{x}_m(t)]_x \mathbf{z}_m$, where $[\]_x$ is the skew symmetric operator. The definition of $\mathbf{t}_{l,m}(t) \in \mathbb{R}^3$ is, however, more tricky, as it is not only dependent on the current pose of the master device but also on its previous pose and can be defined as $\mathbf{t}_{l,m}(t) = \mathbf{t}_{l,m}(t-1) + (\mathbf{t}_m(t) - \mathbf{t}_m(t-1))\mathbf{x}_m$. Finally, the master interface is constrained to remain in the plane $S_{l,m}(t)$ by providing a linear force

$$\boldsymbol{\tau}_{l,m} = -K_{l,m}d_{l,m}(t)\mathbf{n}_{l,m}(t) - B_{l,m}(\dot{\mathbf{t}}_m \cdot \mathbf{n}_{l,m}(t))\mathbf{n}_{l,m}(t), \quad (5.5)$$

where $d_{l,m}(t) = (\mathbf{t}_m - \mathbf{t}_{l,m}(t))\mathbf{n}_{l,m}(t)$ is the distance between the current master pose and the plane $S_{l,m}(t)$, $K_{l,m} \in \mathbb{R}$ is a (high) stiffness parameter, and $B_{l,m} \in \mathbb{R}$ is the corresponding damping term. For our application, $K_{l,m} = 500 \text{ N/m}$ and $B_{l,m} = 16 \text{ Ns/m}$.

The linear motion along \mathbf{x}_m is then mapped to the remote side as a motion along the cutting direction of the scalpel \mathbf{u}_s , defining the new desired pose of the

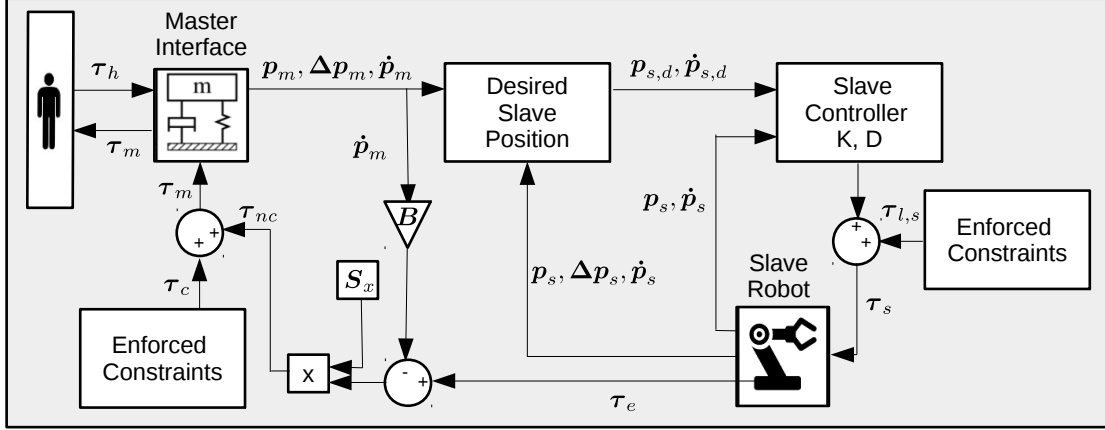


Figure 5.2 – Block diagram detailing the control architecture. In U and C, the *enforced constraints* intervene to account for the cutting task. In T, no constraint is enforced and therefore $\tau_c = \mathbf{0}$ and $\tau_{l,s} = \mathbf{0}$. In all conditions, along the non-constrained directions, the user receives haptic feedback reflecting the forces applied by the robot on the environment.

scalpel $\mathbf{p}_{s,d} : (\mathbf{t}_{s,d}, \alpha_{s,d})$ as

$$\mathbf{t}_{s,d}(t) = \underbrace{\begin{bmatrix} t_{sx}(t) \\ t_{sy}(t) \\ 0 \end{bmatrix}}_{\text{planar motion}} + d_{tot}(t)\mathbf{u}_s(t) + \underbrace{\begin{bmatrix} 0 \\ 0 \\ t_{mz}(t) \end{bmatrix}}_{\text{vertical motion}}, \quad (5.6)$$

where $\mathbf{t}_s(t) = [t_{sx}(t), t_{sy}(t), t_{sz}(t)]^T$, and $\mathbf{t}_m(t) = [t_{mx}(t), t_{my}(t), t_{mz}(t)]^T$. Moreover, $d_{tot}(t)$ is the total desired distance to be traveled by the robot at time t to match the change in position of the master. It is defined as $d_{tot}(t) = d_{tot}(t-1) + d_i(t)$, where $d_i(t)$ is the difference in the distance traveled by the master and remote manipulator in their last loop iteration,

$$d_i(t) = (\mathbf{t}_m(t) - \mathbf{t}_m(t-1))\mathbf{x}_m - (\mathbf{t}_s(t) - \mathbf{t}_s(t-1))\mathbf{u}_s. \quad (5.7)$$

This definition of $\mathbf{t}_{s,d}(t)$ ensures that the desired position of the robot is always along the pointing direction of the scalpel \mathbf{u}_s , guaranteeing the nonholonomic nature of the motion.

Forces τ_s controlling the robot are then defined as

$$\tau_s = \mathbf{K}(\mathbf{p}_{s,d} - \mathbf{p}_s) + \mathbf{D}(\dot{\mathbf{p}}_{s,d} - \dot{\mathbf{p}}_s) + \begin{bmatrix} \tau_{l,s} \\ 0 \end{bmatrix}, \quad (5.8)$$

where $\mathbf{p}_{s,d} = [\mathbf{t}_{s,d}^T(t), \alpha_m]^T$, $\dot{\mathbf{p}}_{s,d} = [((\dot{\mathbf{p}}_m\mathbf{x}_m)\mathbf{u}_s + (\dot{\mathbf{p}}_m\mathbf{z}_m)\mathbf{z}_s)^T, \dot{\alpha}_m]^T$, and $\tau_{l,s}$ is a lateral control force enforcing the nonholonomic motion constraints on the robot, defined similarly to $\tau_{l,m}$ in (5.5),

$$\tau_{l,s} = -K_{l,s}d_{l,s}(t)\mathbf{n}_{l,s}(t) - B_{l,s}(\dot{\mathbf{t}}_s \cdot \mathbf{n}_{l,s}(t))\mathbf{n}_{l,s}(t), \quad (5.9)$$

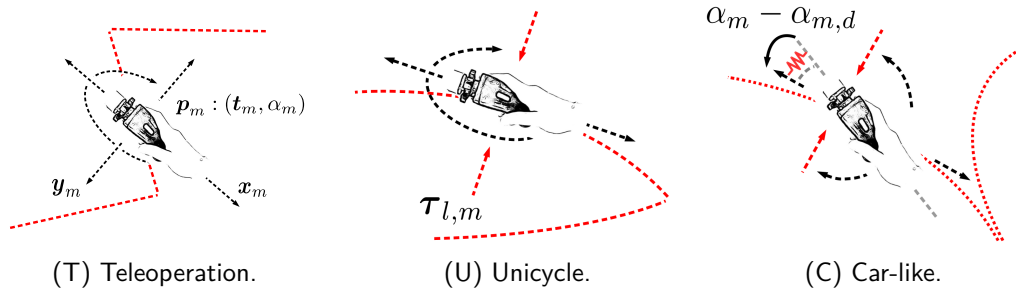


Figure 5.3 – Summary of the shared control modes. Black arrows are directions the user is allowed to control, red arrows directions which are blocked, dashed red lines sample trajectories. **(T) Teleoperation.** The user has control over all planar motions and the vertical movement. **(U) Unicycle.** Pure lateral motions are blocked. **(C) Car-like.** In addition to blocking the lateral motion, rotations in place and sharp turns are also avoided. The user controls the radius of curvature of the steering. A spring informs the user about the master position corresponding to a zero radius of curvature.

where $S_{l,s}(t) : (\mathbf{n}_{l,s}(t), \mathbf{t}_{l,s}(t))$ is the plane we want to constrain the robot in, $d_{l,s}(t) = (\mathbf{t}_s - \mathbf{t}_{l,s}(t))\mathbf{n}_{l,s}(t)$ is the distance between the current robot pose and the plane $S_{l,s}(t)$, $K_{l,s} \in \mathbb{R}$ is a (high) stiffness parameter, and $B_{l,s} \in \mathbb{R}$ is the corresponding damping term. In our application, $K_{l,s} = 1000$ N/m and $B_{l,s} = 63$ Ns/m.

In addition to $\boldsymbol{\tau}_{l,m}$ imposing the constraints on the master interface ($\boldsymbol{\tau}_c = [\boldsymbol{\tau}_{l,m}, 0]^T$), the user also receives haptic feedback $\boldsymbol{\tau}_{nc}$ from the environment along the directions not constrained by the control, similarly to (5.4).

5.2.3 Car-like Approach (Condition C)

The previous approach prevents the user from moving the scalpel laterally. However, the user is still free to rotate it in place, which may also lead to significant damage of the tissue. Moreover, even when moving, it is important to limit the rate of rotation of the scalpel, as to avoid very sharp turns. To limit these undesired behaviors (i.e., rotating in place and hairpin bends), we impose additional constraints w.r.t. the control discussed in Sec. 5.2.2, executing rotations only if the robot moves along \mathbf{u}_s . Moreover, in this approach, the user is given control over the radius of curvature of the trajectory, R_d . Similarly to driving a car, the user does not directly control the angular velocity of the robot but rather the steering angle.

As in Sec. 5.2.2, we constrain the master interface such that the user is allowed to move along \mathbf{x}_m and \mathbf{z}_m , with a hard spring blocking any lateral motion. Considering rotations, a soft spring is applied around \mathbf{z}_m so as to fix the orientation

of the master device at a particular pivot angle $\alpha_{m,d}$ (defined in the coming lines). As the user drives the master device away from $\alpha_{m,d}$, this divergence ($\alpha_m - \alpha_{m,d}$) is mapped as the desired radius of curvature of the trajectory R_d (i.e., the desired steering rate), such that

$$R_d = \frac{k}{(\alpha_m - \alpha_{m,d})^n}, \quad (5.10)$$

where $k \in \mathbb{R}$ and $n \in \mathbb{R}$ are control gains which depend on the range of the master device orientation, the tool attached to the remote robot, and the type of trajectories to cut. In our system, after pilot tests, we empirically chose $k = 1/40$ and $n = 2$. These parameters allowed us to map the angular motion of the master interface into a radius of curvature for the trajectory, with a suitable range.

Then, the angular velocity of the remote/slave robot, $\dot{\alpha}_s$, is designed to ensure that the curvature of the trajectory follows R_d when the user commands a linear velocity along \mathbf{u}_s , such that

$$\dot{\alpha}_{s,d} = \text{sgn}(\alpha_m - \alpha_{m,d}) \frac{|\dot{\mathbf{t}}_m \cdot \mathbf{x}_m|}{R_d}. \quad (5.11)$$

This technique ensures that the tool does not rotate in place, but it only rotates when a linear motion is commanded. Moreover, it also ensures that the motion of the robot follows the desired commanded radius of curvature, R_d .

The pivot master device angle $\alpha_{m,d}$ is updated at every iteration to account for $\dot{\alpha}_s$ and to ensure that the master and the remote robot are aligned at all times,

$$\alpha_{m,d}(t) = \alpha_{m,d}(t-1) + \dot{\alpha}_{s,d} \Delta t. \quad (5.12)$$

A similar integrator is used to retrieve the desired orientation $\alpha_{s,d}(t)$ of the scalpel, which is then commanded as in (5.8), now with $\mathbf{p}_{s,d} = [\mathbf{t}_{s,d}^T(t), \alpha_{s,d}]^T$ and $\dot{\mathbf{p}}_{s,d} = [((\dot{\mathbf{t}}_m \mathbf{x}_m) \mathbf{u}_s + (\dot{\mathbf{t}}_m \mathbf{z}_m) \mathbf{z}_s)^T, \dot{\alpha}_{s,d}]^T$.

As before, similarly to (5.4), the user receives $\boldsymbol{\tau}_{nc}$ along the directions not constrained by the control. And $\boldsymbol{\tau}_c = [\boldsymbol{\tau}_{l,m}, 0]^T + K_{z_m}(\alpha_{m,d} - \alpha_m)[0 \ 0 \ 0 \ 1]^T - B_{z_m} \dot{\alpha}_m [0 \ 0 \ 0 \ 1]^T$, where $K_{z_m} = 1.2 \text{ Nm/rad}$ is a stiffness constant and $B_{z_m} = 0.12 \text{ Nms/rad}$ a damping constant.

5.3 Experimental Evaluation

To evaluate the effectiveness and viability of our shared-control approaches, we carried out a human subject experiment.

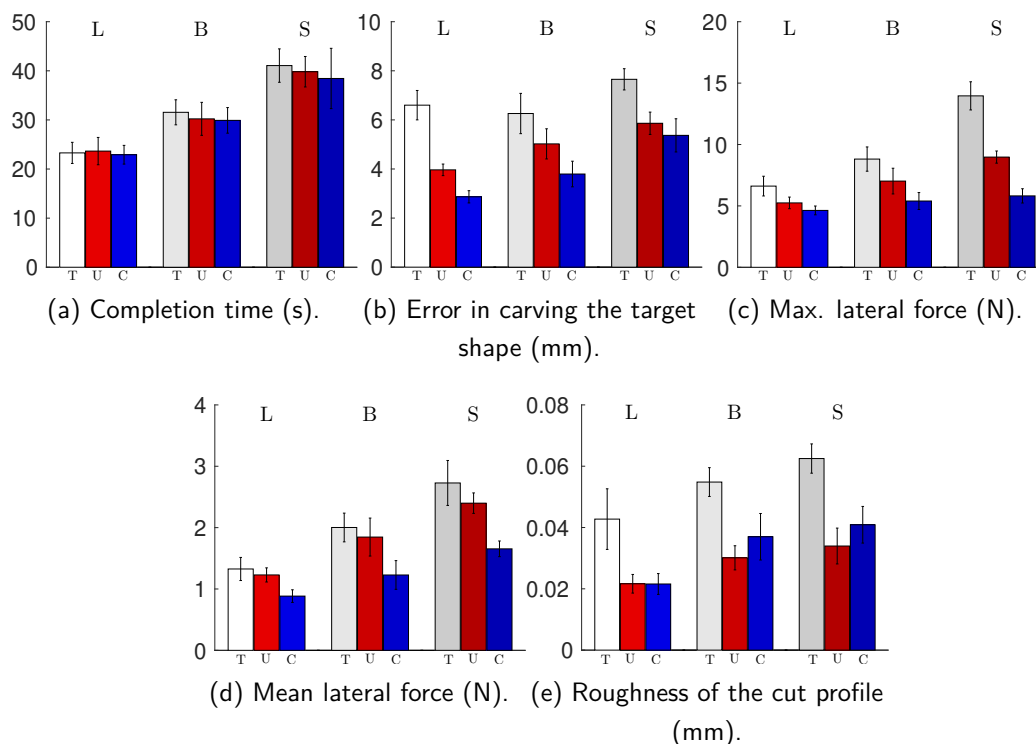


Figure 5.4 – Human subjects experiment. Objective metrics. Mean and standard error of the mean of (a) completion time, (b) error in carving the target shape, (c) max lateral force, (d) mean lateral force, and (e) roughness of the cut profile for the three control conditions (T, U, C) and the three target shapes (L, B, S).

5.3.1 Setup

The experimental setup is shown in Fig. 5.1, and it is described at the beginning of Sec. 5.2. The master side consisted of a Haption Virtuose 6-DoF haptic grounded interface. The remote side consisted of a Franka Panda 7-DoF serial manipulator equipped with a scalpel. The remote environment was composed of a $25 \times 17 \times 1.5$ cm surface made of modeling clay. To enable the operator to see the environment, the master interface was placed next to the robot manipulator.

5.3.2 Task and Conditions

Participants used the master interface to control the motion of the manipulator. The task consisted in cutting a target shape into the modeling clay. Participants were asked to complete the cutting task as precisely and fast as possible. Before each repetition, the experimenter used a pre-prepared plastic mold to draw the target shape on the clay, to make it visible to the user but without introducing any deformation to the material. The task started when the manipulator touched

the clay for the very first time and it was considered completed when the shape was totally carved (i.e., when the scalpel reached the end of the drawn shape). Participants were only allowed one pass on the shape. The task, environment, and target shapes have been chosen following a discussion with clinicians, which considered them as good representatives of surgical incisions [202]. The setup also reminds scenarios of sort and segregation of radioactive waste [214], where teleoperated robots are used to cut open old containers and sort the waste according to its radioactivity level.

We consider different ways of commanding the motion of the robot through the haptic interface: (T) standard teleoperation, (U) unicycle approach, and (C) car-like approach. See Sec. 5.2 for details on these control techniques.

For each control condition, participants were asked to carve three different shapes:

- L: a straight line, resembling sternotomy or upper midline incisions;
- B: a bent line, resembling Gibson, inguinal or femoral incisions;
- S: a sinusoidal shape, resembling Clamshell or sinusoidal coronal incisions;

Each subject carried out twelve randomized repetitions of the cutting task, one for each control condition and shape. Trials were randomized to avoid any learning effect. A video presenting the experiment and showing representative trials in the different conditions is available at <https://youtu.be/DkW40cjgX9M>.

5.3.3 Participants

Twelve subjects (average age 26.6, 8 males, 4 females) participated in the study. Four of them had previous experience with haptic interfaces. The experimenter explained the procedures and spent about one minute adjusting the setup to make it comfortable for the subject before beginning the experiment. Each subject then spent about two minutes practicing the control of the telemanipulation system before starting the experiment.

5.3.4 Results

To evaluate the effectiveness of our system in cutting the considered shapes and the usefulness of the proposed shared-control approaches, we recorded (*i*) the completion time, (*ii*) the error in following the target trajectory, (*iii-iv*) the maximum and mean lateral force applied by the scalpel on the environment, and (*v*) a measure of “roughness” of the cut profile. The latter indicates how clean the trajectory

is from irregularities and bends. Details on the calculation of these metrics are given below. To compare the metrics, we ran two-way repeated-measures ANOVA tests on the data. The control modality (T vs. U vs. C) and target shape (L vs. B vs. S) were treated as within-subject factors. All data passed the Shapiro-Wilk normality test. A Greenhouse-Geisser correction was used when the assumption of sphericity was violated. Results of post hoc analysis with Bonferroni adjustments or simple main effects are reported in Table 5.1 (only significant p values are shown).

Fig. 5.4a shows the completion time, $t_f - t_i$, averaged across user trials. It is calculated as the time elapsed between the instant t_i the manipulator touches the clay for the first time and the instant t_f the shape is completely carved. Mauchly's Test of Sphericity indicated that the assumption of sphericity had been violated for the shape variable ($\chi^2(2) = 8.242, p = 0.016$). The two-way repeated-measure ANOVA revealed no statistically significant change for this metric across control conditions ($F(2, 22) = 0.122, p > 0.05$), but it showed a statistically significant change across target shapes ($F(1.281, 14.090) = 26.831, p < 0.001$), with a higher completion time for more complex shapes.

Fig. 5.4b shows the mean error in following the target shape, averaged across trials. It is calculated as the mean distance between the profile cut by the user and the target shape, i.e., $(\sum_{k=1}^N \mathbf{t}_s(k) - \mathbf{t}_s^*(k))/N$, where $\mathbf{t}_s^*(k)$ is the closest point to $\mathbf{t}_s(k)$ on the target shape and N is the number of sample points in the user-cut trajectory. Mauchly's Test of Sphericity indicated that the assumption of sphericity had been violated for the control variable ($\chi^2(2) = 6.843, p = 0.033$) and for the interaction between variables ($\chi^2(9) = 30.031, p = 0.001$). The two-way repeated-measure ANOVA revealed statistically significant change for this metric across control conditions ($F(1.337, 14.710) = 16.556, p = 0.001$) and target shapes ($F(2, 22) = 8.281, p = 0.002$). The mean error decreased for conditions U and C with respect to simple teleoperation T.

Fig. 5.4c shows the maximum lateral force, averaged across trials. It is calculated as the maximum value of force sensed by the robot along the axis \mathbf{x}_s , which is perpendicular to the scalpel motion. Since moving the scalpel laterally with respect to its direction of motion can damage the tissue, this force should be as small as possible. Data passed the Mauchly's Test of Sphericity. The two-way repeated-measure ANOVA revealed a statistically significant change for this metric across control conditions ($F(2, 22) = 23.131, p < 0.001$) and target shapes ($F(2, 22) = 25.873, p < 0.001$). There was also a statistically significant two-way interaction between shapes and control conditions ($F(4, 44) = 5.075, p = 0.002$).

Fig. 5.4d shows the mean lateral force, averaged across trials. It is calculated

Table 5.1 – Summary of the experiment

Task	Control the haptic-enabled teleoperation system to cut a target shape into modeling clay (12 subjects enrolled).		
Conditions	<u>Control approaches</u> T (standard teleop.), U (unicycle-like), C (car-like) <u>Target shapes</u> L (straight line), B (bent line), S (sinusoidal shape)		
Statistical analysis (two-way repeated-measure ANOVA, $\alpha = 0.05$)			
<u>Completion time</u>			
Main effect of target shape			
L vs. B	$p = 0.001$	B vs. S	$p = 0.006$
L vs. S	$p < 0.001$		
<u>Error</u>			
Main effect of control approach			
T vs. U	$p = 0.022$	U vs. C	$p = 0.016$
T vs. C	$p = 0.002$		
Main effect of target shape			
L vs. S	$p = 0.002$		
<u>Max. lateral force</u>			
Simple main effect of control approach (condition/shape)			
T/B vs. C/B	$p = 0.040$	T/S vs. C/S	$p < 0.001$
T/S vs. U/S	$p = 0.025$		
Simple main effect of target shape (shape/condition)			
L/T vs. S/T	$p = 0.001$	L/U vs. S/U	$p < 0.001$
B/T vs. S/T	$p = 0.014$		
<u>Mean lateral force</u>			
Main effect of control approach			
T vs. C	$p = 0.004$	U vs. C	$p = 0.003$
Main effect of target shape			
L vs. B	$p = 0.034$	L vs. S	$p < 0.001$
<u>Roughness</u>			
Main effect of control approach			
T vs. U	$p = 0.001$	T vs. C	$p = 0.025$
Main effect of target shape			
L vs. B	$p = 0.003$	L vs. S	$p = 0.006$

as the mean value of force sensed by the robot along \mathbf{x}_s . As above, this force should be as small as possible. Mauchly’s Test of Sphericity indicated that the assumption of sphericity had been violated for the interaction between variables ($\chi^2(9) = 17.675, p = 0.042$). The two-way repeated-measure ANOVA revealed a statistically significant change for this metric across control conditions ($F(2, 22) = 10.208, p = 0.001$) and target shapes ($F(2, 22) = 14.085, p < 0.001$).

Fig. 5.4e shows a measure of “roughness” of the cut, averaged across trials. It is calculated as the mean difference between the profile carved by the user and the same profile smoothed using a low-pass Butterworth zero-phase digital filter [215], i.e., $(\sum_{k=1}^N \mathbf{t}_s(k) - \mathbf{t}_{s_{filt}}(k))/N$, where $\mathbf{t}_{s_{filt}}(k)$ is the closest point to $\mathbf{t}_s(k)$ on the filtered trajectory. Mauchly’s Test of Sphericity indicated that the assumption of sphericity had been violated for the interaction between variables ($\chi^2(9) = 17.225, p = 0.048$). The two-way repeated-measure ANOVA revealed a statistically significant change for this metric across control conditions ($F(2, 22) = 14.233, p < 0.001$) and target shapes ($F(2,22) = 13.200, p < 0.001$).

Finally, eight subjects out of twelve found control condition U to be the most effective at completing the cutting task. Three subjects preferred condition T while one preferred C.

5.4 Discussion

Results presented above show that the two proposed shared-control approaches significantly outperform standard teleoperation in most metrics. Specifically, C outperformed T in all metrics but completion time, and U outperformed T in all metrics but completion time and mean lateral force. These results are sustained across the three considered shapes (see Table 5.1). This proves our hypothesis that shared control can be a viable and effective approach to improve currently-available teleoperation systems for cutting tasks, which is in agreement with previous results in the literature. Comparing performance among the proposed shared-control techniques (U vs. C), we can see that limiting the maximum radius of curvature and preventing rotations in place (C) significantly lowers the lateral forces w.r.t. U, where these constraints were not enforced. Moreover, the error metric shows significant differences among all pairs, ranking C first (lowest error), followed by U and T (highest error). This latter result is partially in contrast with that of Vozar et al. [213], where imposing a virtual nonholonomic constraint on the end-effector motion did not significantly reduce the error in cutting a target path. However, Vozar et al. [213] did not use haptic feedback to inform the users about the constraints and carried out their experiment under a

4s delay. Finally, comparing performance among the target shapes, we can see that, as the shapes become more complex, their performance degrades. It is also interesting to notice that, for most metrics, as the shapes become more complex, the difference of T vs. U and C increases. This result is quite expected, as users need more help when cutting more complex shapes.

Surprisingly, the subjective metrics did not always agree with the above results. In fact, users preferred T and U over C. Indeed, the many constraints imposed in the C modality created the impression of conditions difficult to use. A common comment among subjects was that they often felt “limited” when using C, and that T and U made them feel “more in control” of the remote robot. However, it is important to notice that none of our subjects was experienced in using the experimental setup. In fact, the recorded subjective results might change in the presence of experienced users. This is something we plan to extensively study in the future, since all the operators in our target scenarios are skilled and experienced (e.g., surgeons). Another aspect to consider is the amount of information provided to the users. Although we took time to explain the procedure and the conditions, a more detailed explanation of how the shared control works and why it is important for certain applications might have led to a deeper understanding and acceptance by the users, who seemed reluctant to relinquish control.

Two sources of potential instability are present in the system, corresponding to the two sources of force feedback: τ_c , which imposes the nonholonomic constraints, and τ_{nc} , which reflects the interaction of the robot with the environment. However, τ_c raises no concern, as the constraints enforced at the master side are evaluated from the pose of the master interface only. This design allowed the use of high stiffness parameters ($K_{l,m} = 500$ N/m). On the other hand, since we experienced very small communication delays in our setup, a damping matrix was sufficient to avoid any undesired oscillation resulting from τ_{nc} . However, in cases where communication delays might be significant (e.g., space operations, remote robot-assisted surgery), stability could be enforced via passivity [216]. In fact, proving that the system is passive is sufficient to prove the stability of the system. Different methods to ensure stability have been presented in Sec. 2.1.2. For instance, one way to ensure stable behaviour of the system is through the use of energy tanks [12]. We plan to study in the future the effect of time delays on the performance of haptic shared-control techniques.

We also plan to carry out more human subject experiments in real scenarios, tailored for specific applications (e.g., cutting real tissue) and considering changes in other variables (e.g., different stiffness of the environment, communication delays, quality of the visual feedback).

CHAPTER

6

Human-Inspired Haptic Learning for Autonomous Grasping

Contents

6.1	Related Works	94
6.2	Contribution and Motivation	96
6.3	Grasping-Data Gathering	98
6.3.1	Direct Grasping by Hand	100
6.3.2	Teleoperated grasping by an expert operator	101
6.4	Machine Learning	104
6.4.1	Standard SVR	105
6.4.2	SVR with Time-Series	105
6.4.3	SVR with Heat-Map Weighting	106
6.5	Experimental Evaluation	107
6.5.1	Setup	107
6.5.2	Grasping Policies	107
6.5.3	Autonomous Grasping Task	109
6.5.4	Results and Discussion	110

In the previous chapter we presented a new shared-control system for a cutting task where the user was still in control of the teleoperation, but with less authority as some hard constraints were enforced on the user's motion. In this chapter, we present instead the design of an autonomous system for the grasping of soft and deformable objects. Unlike the previous chapters in this thesis where the haptic feedback is used as means of guidance, here the haptic feedback and teleoperation trials are used to train the autonomous system through a Learning from Demonstration (LfD) policy. As such, the user authority is more implicit in the system, and it is used to train an autonomous algorithm.

Research on robotic manipulation of fragile, compliant objects, such as food items, is gaining traction due to its game-changing potential within the food production and retailing sectors, currently characterized by manually-intensive and highly repetitive tasks. Food products exhibit high levels of frailness, biological variation, and complex 3D shapes and textures. For these reasons, introducing greater levels of robotic automation in the food and agricultural sectors remains an important challenge. This chapter addresses this challenge by developing a human-centred, haptic-based, Learning from Demonstration (LfD) policy that enables pre-trained autonomous grasping of food items using an anthropomorphic robotic system. The policy combines data from teleoperation and direct human manipulation of objects, embodying human intent and interaction areas of significance. We evaluated the proposed solution against a recent state-of-the-art LfD policy as well as against two standard impedance controller techniques. Results show that the proposed policy performs significantly better than the other considered techniques, leading to high grasping success rates while guaranteeing the integrity of the food at hand.

The work included in this chapter has been done in collaboration with Sintef, Norway. It is published in IEEE Transactions on System, Man, and Cybernetics: Systems and a video of the material is available at <https://youtu.be/OLaDPbGwZ1w>.

6.1 Related Works

Autonomous food processing and handling is gaining attention among researchers in the fields of robotics, automation, and machine learning. Reasons for this interest are three-fold: (i) compelling scientific and technological challenges linked to the handling of food, such as flexibility, frailness, friction, and high inter-object variability, (ii) increasing interest from public and private investors, and (iii) the possibility of impacting food quality and reducing waste. To address current chal-

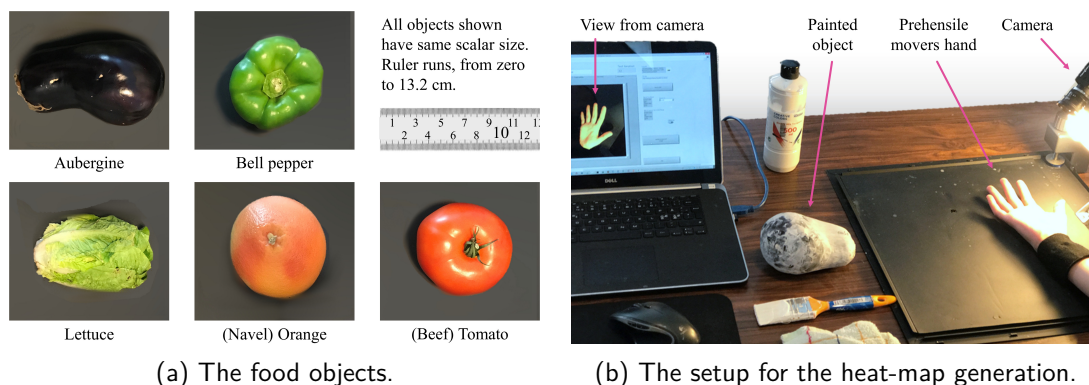


Figure 6.1 – *Food items and Heat-map capturing.* (a) The five food objects used in the experiments: average circumference 290 mm, height 75 mm. (b) Heat-map generation set-up. A laptop connected to a camera, a lighting system, water paint with a brush for application, and a cloth for wiping the subject’s hand after each trial.

lenges, the European Commission has recently funded the €7-million collaborative research project “SoMa,” which looks at innovative soft robotic manipulation for handling fragile objects such as fruits and vegetables [217]. Similarly, Amazon’s \$13.7-billion acquisition of the food retailer “Whole Foods” aims to promote an automation revolution in the food delivery market. According to Bloomberg [218], Amazon will soon introduce robots in Whole Food warehouses as a cost-cutting initiative. However, not only distributors need to automate the manipulation of delicate food items. Currently, food production, harvesting, and processing continue to be dominated by labour-intensive tasks. In addition, vital global suppliers have a constant need for more efficient operations, and improved HSSEQ (Health, Safety, Security, Environment, and Quality) practices linked to their workers *and* the safe handling of food. To address these issues, researchers need to focus on efficient and safe methods for the autonomous handling of food while preserving their quality.

Nowadays, (purely) vision-based techniques are the most widely applied approaches for autonomous robotic grasping and manipulation, either requiring a 3D-model of the item in question or constructing models using 3D-vision information, e.g. point clouds [219], [220], [221]. Although the knowledge of an object model may often be sufficient [222], the lack of precise information concerning its shape and mechanical properties may significantly affect the quality of the grasping [223, 224]. An issue of major importance when handling food is its frailness, which is an even more predominant problem when objects are moving, or when they are handled and grasped during harvesting, post-harvest processes, and on production lines. A representative example is strawberry harvesting, where even

the smallest excessive force can degrade and spoil the product.

Haptic sensations have been proven to play a key role in enhancing human fine manipulation [225] and precision grasping [226]. In robotics, haptic feedback is widely believed to be a valuable tool in teleoperation, and it has been shown to enhance operators' performance in a wide range of robotic applications, including microrobotics [227–229], needle and catheter insertion [123, 230], surgical knot tying [231], assembly [227], and palpation [123, 232]. The benefits of haptic feedback in this scenario include greater manipulation and perception accuracy, as well as lower levels of peak and mean force applied to food objects, thus lowering the impact on the food due to their handling.

A promising approach to autonomous grasping via robotic manipulators is Learning from Demonstration (LfD) [233]. This technique involves a robot learning a target policy from examples, or demonstrations, provided by an experienced human operator. LfD uses recorded datasets in the form of state-action pairs to derive policies that reproduce target behaviours. This methodology is in stark contrast to other learning techniques, such as Reinforcement Learning, where robots learn from direct self experience. The use of LfD to teach robots how to grasp is quite popular among researchers who make use of visual and/or haptic information to demonstrate tasks by means of teleoperation [133, 234–237] or direct interaction [238–240]. However, all of the aforementioned works involve human operators driving robots using non-intuitive and somewhat basic master interfaces such as teach pendants, non-haptic joysticks, single-point haptic interfaces, or by directly moving the robots around. It is our belief that, in order for robots to learn correctly from humans *how to grasp challenging, compliant, and fragile objects*, it is necessary to provide an intuitive and natural tool for controlling the remote manipulators. In other words, we believe that by achieving a high degree of dexterity and telepresence, human operators will be able to approach and grasp target objects in the same way as they would do if grasping barehanded.

6.2 Contribution and Motivation

This chapter presents a human-centered, haptic-based, LfD approach for teaching autonomous robotic systems the action of grasping delicate, fragile, and compliant food items.

First, five human subjects were asked to grasp five food items barehanded, recording the contact area between the users' hand and the objects' surface using paint transfer and machine vision techniques (see Sec. 6.3.1 and Fig. 6.1b). Paint-transfer approaches have already been used to detect contact areas when

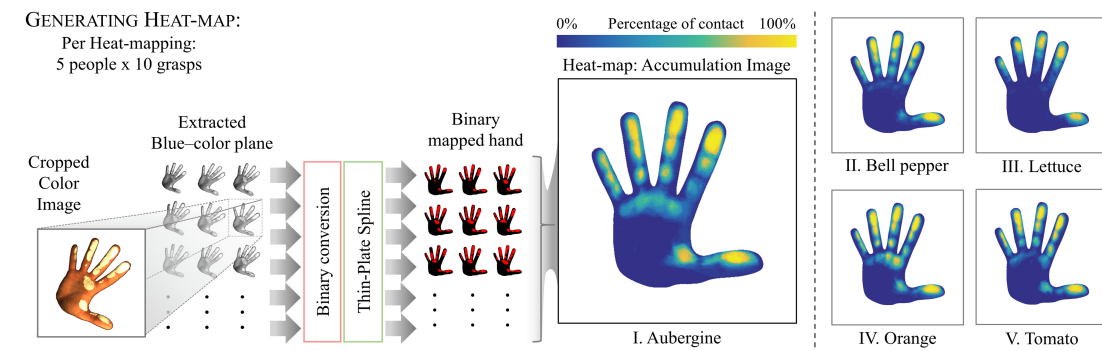


Figure 6.2 – Example of a heat-map generation (aubergine). The intensity of the RGB-image is extracted, converted to binary, then mapped to a generic hand using Thin-Plate spline interpolation, creating an intensity image for accumulated binary images. Active areas in the hand change with different objects.

humans grasp objects [241]. However, to the best of our knowledge, this is the first time that this approach is used to learn an LfD policy. This first step enables us to study *how humans grasp* the considered food items when they are endowed with maximum dexterity and feedback. However, these data alone are not sufficient to design an autonomous grasping policy for a robotic manipulator, which has significantly lower sensing and actuation capabilities than a human. For this reason, afterwards, we conducted *teleoperated* prehensile move experiments involving the same food object types (see Sec. 6.3.2). All relevant data on the grasping motion and exchanged forces were recorded. To achieve high levels of dexterity and telepresence, we devised a haptic-enabled high-degrees-of-freedom robotic teleoperation system, shown in Fig. 6.3a.

By using both direct interaction and teleoperation data, we then devised four Support Vector Regression (SVR) algorithms based on LfD policies, enabling a robotic manipulator to autonomously grasp a set of representative food items.

Finally, we validated our autonomous grasping policies by carrying out 2310 autonomous robotic grasping tasks on seven representative food items, not limited to those used during the training. We compared the proposed policies to each other, as well as, to a recently published LfD-based approach [234] and two standard impedance controllers. Misimi et al. [234] combines RGB-D images and tactile data to learn the required pose of the gripper, the gripper finger configuration, and the exerted forces. However, unlike our approach, it neither uses information derived from direct human interaction nor data supplied by high-dexterity haptic-enabled teleoperation.

With reference to related published work [234, 242–245], our study heavily

focuses on human input. By providing an intuitive and rich interface to control the remote robot, we enabled human operators to carry out the tasks naturally and intuitively, close to what they would do with their own hands. To the best of our knowledge, this is the first time an LfD approach is applied to enable autonomous grasping by making use of both (i) rich haptic-endowed teleoperation data and (ii) the mapping of direct hand interaction. Moreover, this is also the first time that such an approach is used for grasping raw food items. Our approach combines teleoperation data with real human interaction to build a robust learning policy based on LfD. This policy enables a continuous understanding of the interactions taking place between the human and the robot during a grasping sequence.

We have focused our research and validation on food items because they are excellent examples of 3D compliant objects that should not be degraded during manipulation. Robotic manipulation of 3D compliant objects is indeed a research field that still requires significant research input to achieve a robust manipulation of such objects.

6.3 Grasping-Data Gathering

This section provides details on the two data gathering experiments we carried out with the aim of building our LfD policies. In both cases, we asked our subjects to grasp the five different food items shown in Fig. 6.1a: an aubergine, a bell pepper, a lettuce, a navel orange, and a beef tomato. These items were selected as representative examples of 3D compliant objects because of their difference in size, shape, texture, and compliance properties, and as representatives of the most common fruits and vegetables consumed in global food markets. According to the Food and Agriculture Organization of the United Nations (FAO), tomatoes are one of the most cultivated fruits in the world, with more than 180M metric tonnes produced every year. Aubergines and oranges are also very popular, with 50M metric tonnes produced every year, bell peppers reach 35M metric tonnes, and lettuce 25M metric tonnes. Another important constraint for our choice of produce was the payload of our robotic system, which is only able to carry up to 2 kg. Employing a different robot could of course enlarge the set of food objects we are able to handle. However, it is important to highlight that our machine learning approach can easily be trained to handle any other type of compliant food objects, regardless of the robotic system being employed. A video of these experiments is available at <https://youtu.be/OLaDPbGwZlw>. Table 6.1 summarizes the main symbols and variables used in this chapter.

Table 6.1 – List of main symbols and variables.

Symbol	Definition/Description
$*_m, *_s$	related to the master or slave/remote robot, respectively
$\mathbf{x}_m, \mathbf{x}_s$	end-effector pose
$\mathbf{p}_m, \mathbf{p}_s$	end-effector position
$\mathbf{R}_m, \mathbf{R}_s$	end-effector orientation
W	world coordinate system
$\mathbf{v}_m, \mathbf{v}_s$	end-effector linear velocity
$\boldsymbol{\omega}_m, \boldsymbol{\omega}_s$	end-effector rotational velocity
$*_{MCP}, *_{PIP}$	related to the fingers' metacarpophalangeal joint and proximal-interphalangeal joint, respectively
θ_{r_i}	angular command to the MCP robotic joint i
θ_{e_i}	angular value of the MCP exoskeleton joint i
$\boldsymbol{\tau}_{MCP,i}, \boldsymbol{\tau}_{PIP,i}$	haptic feedback applied to finger i
$m_{pro,i}, m_{dis,i}$	average pressure on the proximal and distal phalanges of the robot finger i , respectively
\mathbf{g}_{pos}	pose of the gripper
\mathbf{f}_{prs}	tactile readings from the robotic hand pressure sensors
\mathbf{f}_{mot}	position of the motors of the robotic hand
\mathbf{f}_{ang}	joint angles of the exoskeleton
\mathbf{s}	observed robotic grasping action performed by the human teacher
\mathbf{a}	action-state, including gripper pose and motor positions
α, β, γ	discrete time-series steps
\mathbf{H}_j^k	heat-map values gathered during direct hand interaction for object k and action vector feature j

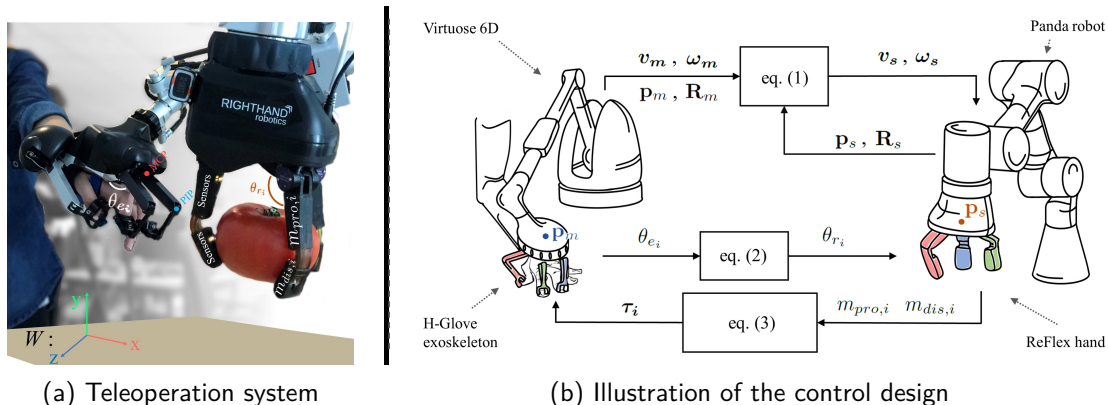


Figure 6.3 – *Teleoperation set-up and control design.* (a) The human operator teleoperates the remote robot to grasp a tomato. (b) Master-slave control: $[x_s, y_s, z_s, \mathbf{q}_s^T]^T$ are the end-effector coordinates defining the pose of the RHR hand. The difference between the previous and current master position is used to evaluate the velocity command, which is then sent to the remote manipulator. RHR finger movements are proportional to the positions registered by the H-Glove fingers.

6.3.1 Direct Grasping by Hand

Five subjects (four male and one female) were asked to grasp the five sample objects barehanded. Our objective was to understand *how humans grasp* objects when they are endowed with maximum dexterity and feedback (i.e. during direct hand interaction). Inspired by the work of Knopp et al. [241] and Kamakura et al. [246], we used a paint-transfer approach to identify the parts of the hand that are employed the most during this grasping.

Task and data gathering—Subjects were comfortably seated in front of a table. The experimenter placed the first object on the table and covered it in non-toxic water paint. Subjects were asked to grasp and lift the object as if they were moving it from one table to another. Then, they were asked to release the object and show their palm to a camera, which recorded the paint-transfer patterns (see Fig. 6.1a). Finally, subjects washed their hands and a new object was prepared for grasping. Each subject grasped each object ten times, yielding 50 grasps per subject, 50 grasps per object, and 250 paint-transfer trials in total.

Heat-map generation—Images of paint-transfer patterns were taken using a Grasshopper 3 camera (FLIR Systems, Canada), and the contact area was segmented using standard background subtraction and light intensity filtering. We then mapped the resulting contact area and constructed a heat-map using Thin-Plate Spline interpolation [247]. A heat-map is a graphical representation of individual values contained within a 2D matrix represented by colours. Brighter

colours indicate higher levels of accumulated contact, identifying which parts of the hand most used by the subjects when grasping the object in question. Establishing a human-grasp signature inferring innate sensor contact importance. An example of data derived from this heat-mapping process is shown in Fig. 6.2. Heat-map data are used in Sec. 6.4 as a basis for our human-inspired LfD grasping policy.

6.3.2 Teleoperated grasping by an expert operator

Although the heat-map data are interesting, they are not sufficient on their own to define an autonomous grasping policy for a robotic manipulator. For this reason, we gathered additional data from 250 *teleoperated* grasping trials (50 grasps per food item) using our target robotic manipulator as the remote robot of a haptic-enabled bilateral teleoperation system, shown in Fig. 6.3a. The master interface is composed of a 9-degrees-of-freedom (9-DoF) haptic hand exoskeleton (H-Glove by Haption), attached to the 6-DoF grounded haptic interface Virtuose. The remote system is composed of the Panda 7-DoF robotic manipulator endowed with a 4-DoF 3-fingered robotic hand equipped with matrix pressure sensors on all fingers (ReFlex TakkTile by Right-Hand-Robotics). This integrated system enables a human operator to grasp and manipulate compliant objects while receiving compelling haptic feedback of the forces applied by the remote system.

Teleoperation of the 7-DoF robotic manipulator—To achieve high motion fidelity, we mapped the velocity of the grounded haptic interface to that of the robotic end-effector, using an approach similar to that employed in [6, 110]. Let $\mathbf{x}_m = (\mathbf{p}_m, \mathbf{R}_m) \in \mathbb{R}^3 \times \mathcal{SO}(3)$ be the pose of the master interface end-effector, and $\mathbf{x}_s = (\mathbf{p}_s, \mathbf{R}_s) \in \mathbb{R}^3 \times \mathcal{SO}(3)$ the pose of the remote/slave end-effector, both expressed w.r.t. a common world frame W (see Fig. 6.3a). The velocity of the remote robot $[\mathbf{v}_s \ \boldsymbol{\omega}_s]^T$ is then calculated as a function of the master velocity $[\mathbf{v}_m \ \boldsymbol{\omega}_m]^T$ and the difference between the desired and current pose of the robot, i.e.

$$\begin{bmatrix} \mathbf{v}_s \\ \boldsymbol{\omega}_s \end{bmatrix} = \begin{bmatrix} \mathbf{v}_m \\ \boldsymbol{\omega}_m \end{bmatrix} + \lambda \begin{bmatrix} \mathbf{p}_{s,d} - \mathbf{p}_s \\ \mathbf{R}_s {}^s\theta\mathbf{u}_{s,d} \end{bmatrix}, \quad (6.1)$$

where λ is a gain parameter, and $\mathbf{p}_{s,d}$ the desired robot position derived from the current position of the haptic device, $\mathbf{p}_{s,d} = (\mathbf{p}_m - \mathbf{p}_{m0}) + \mathbf{p}_{s0}$, with \mathbf{p}_{m0} and \mathbf{p}_{s0} as the initial poses of the master and remote robot, respectively. Similarly, to establish orientation, ${}^s\theta\mathbf{u}_{s,d}$ is the angle-axis representation of the relative rotation

between the desired and current orientation of the manipulator, i.e. ${}^s\mathbf{R}_{s,d} = {}^{s_0}\mathbf{R}_s^T {}^{m_0}\mathbf{R}_m$, where ${}^{s_0}\mathbf{R}_s$ and ${}^{m_0}\mathbf{R}_m$ define the current orientation of the remote robot and the master, respectively, w.r.t their orientation at the start of a given experiment. Thus, the first term of eq. 6.1 ensures an adequate responsiveness of the system, while the second prevents drifts.

Of course, there are other ways we can map the motion of the human operator into that of the remote robot [73, 122, 248]. We chose a direct and straightforward way to control the robotic manipulator, as one of our hypotheses states that a human-like natural control can improve the quality of recorded data and, thus, of the learning policies.

Teleoperation of the 4-DoF robotic hand—To control the robotic hand, we mapped the positions of the exoskeleton fingers to the positions of the fingers of the remote robot.

The robotic hand has four active DoF: one DoF for each finger’s metacarpophalangeal (MCP) joint, and one to control the abduction of the two neighbouring fingers (see Fig. 6.3a). These fingers were chosen to correspond with the index and middle finger of the exoskeleton, together with an opposing thumb. The position command θ_{r_i} for the MCP joint in a robotic finger i is proportional to the recorded position θ_{e_i} of the MCP joint in the corresponding exoskeleton finger:

$$\theta_{r_i} = k_i\theta_{e_i} + \theta_{r_{i,s}}, \quad (6.2)$$

where k_i is a proportional gain, and $\theta_{r_{i,s}}$ is a safety offset, ensuring that the commanded position value is always within safe intervals.

Haptic feedback—The robotic hand is endowed with six matrix pressure sensors (TakkTile, USA), located on the proximal and distal phalanges of the three fingers. Force feedback at the MCP joint of the exoskeleton, $\boldsymbol{\tau}_{MCP,i}$, is computed by summing the pressure stimuli registered by sensors located at the proximal and distal phalanges in the corresponding remote manipulator fingers. At the proximal-interphalangeal (PIP) joint, forces $\boldsymbol{\tau}_{PIP,i}$ are computed only from pressure stimuli on sensors located on the distal phalanx of the remote robot. The total force feedback is computed as:

$$\boldsymbol{\tau}_i = \begin{bmatrix} \boldsymbol{\tau}_{MCP,i} \\ \boldsymbol{\tau}_{PIP,i} \end{bmatrix} = u_i \begin{bmatrix} m_{pro,i} + m_{dis,i} \\ m_{dis,i} \end{bmatrix}, \quad (6.3)$$

where u_i is a proportional gain, and $m_{pro,i}$ and $m_{dis,i}$ are average pressures recorded on the proximal and distal phalanges of the slave finger i , respectively.

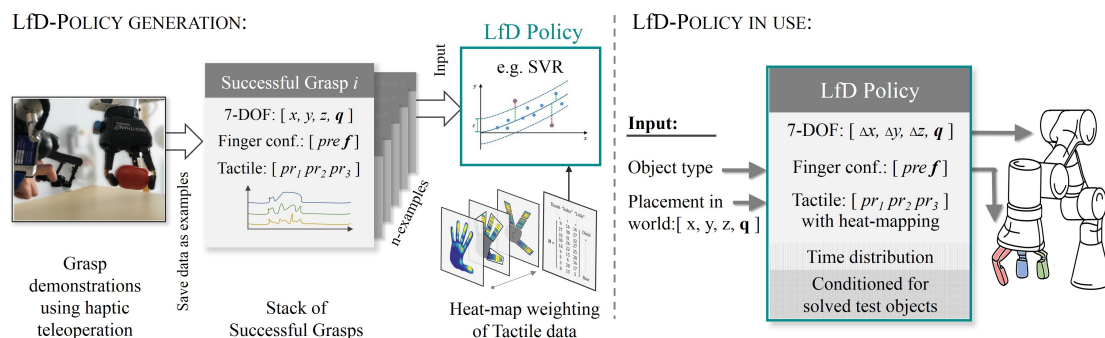


Figure 6.4 – *Generation of LfD policy from acquired data.* Finger tactile values coming from the RHR-hand were weighted according to heat-map data when generating the human-inspired LfD-policy. Temporal variation was captured by implementing time-series, where n previous values for the robot pose, finger configuration, and tactile stimuli were applied to the generation of predictions.

Each finger of the master exoskeleton is modeled as a gravity-compensated mechanical system with two active joints (MCP and PIP, see Fig. 6.3a), with force feedback τ_i . This approach enables the human operator to feel, on each finger, the forces exerted by the robotic hand on the environment.

Task and data collection—An expert operator used the teleoperation system for grasping and lifting the same five food items described in Sec. 6.3.1 and shown in Fig. 6.1a. Each item was placed on a table in front of the remote robot and lifted 50 times as part of a total of 250 trials (see Fig. 6.3a). To enable the operator to view the environment, the master interface was placed one metre in front of the robot workspace. For each trial, both the pose of the remote system and the forces exerted on the food items were saved. At the end of each task, the operator rated the quality of the grasp on a continuous scale from 0 (worst) to 4 (best). Zero (0) indicates that the operator was not able to grasp the object in the first place, while 4 means that the object was held firmly during the entire grasp sequence (see Table 6.2). This information was used to select the successful demonstration examples for training the LfD policy. The majority of the grasps were rated between 3 and 4. We also asked the expert operator to rate the quality of the food items after each grasp on a scale from 0 (worst) to 4 (best), carefully looking for bruises, cuts, changes in shape, and any other sign of degradation (see Table 6.2). The operator was gentle when handling the produce, resulting in a consistent quality rating of 4, reflecting the rich feedback and dexterity capabilities of the employed haptic teleoperation system. In comparison, Misimi et al. [234] provided no haptic feedback during their teleoperation trials, and operators reported that it was very challenging to not damage the items when not

Table 6.2 – Scales used in the evaluation of the teleoperated prehensile move and the quality of the food after the move, inspired from [250, 251]. Scale runs continuously from 0 (worst) to 4 (best), enabling the operator to select values between those indicated below.

Prehensile move	Food items
4 – Complete prehensile move	4 – No visible modifications
3 – Slips close to the landing	3 – Small, localized, light marks
2 – Slips mid-way	2 – Mid-sized, spread marks
1 – Slips right after lift-off	1 – Bruises, small tears in skin
0 – Robotic hand fails to clutch, action aborted	0 – Heavy bruises, spread marks and tears in skin

receiving any tactile information.

Finally, for each grasping repetition, we also registered the angle of approach, any significant synergy between the fingers, and the forces applied by the robotic hand on the object. The design of the robotic hand led to most grasps being precision ball (enveloping) grasps [249]. This type of grasp enabled the operator to receive haptic feedback to all the three fingers of the exoskeleton.

6.4 Machine Learning

Learning a task from scratch can be very challenging, even for humans. A good strategy for learning how to perform a brand new task is to be provided with a set of instructions by an expert, followed by a practical demonstration [252]. Indeed, most forms of machine learning (ML) applied in robotics are based on supervised learning (SL), typically using manually-crafted features as key to learning sought-after policies [234, 253]. Unsupervised learning methods, such as (deep) reinforcement learning, achieve objective functions by enabling learning agents to autonomously define actions that maximize specific reward functions [254]. Van Hoof et al. [255] illustrate such an approach with their tactile in-hand manipulation skills derived from reinforcement learning with tactile feedback. However, as SL can reduce the number of trials needed for sufficient implementation, i.e. also reducing food waste compared to a self-training algorithm, we opted for an LfD approach.

In this work, the prediction of a time-varying sequence of grasping features during the grasping task was performed using Support Vector Regression (SVR) time series. In addition, we tested the SVRs' response to the weighting of selected variables, and demonstrate how the imposition of human-inspired interaction in-

dicators (heat-map weights) affects performance. SVR is one of the most powerful and popular machine learning techniques to deal with non-linear prediction problems. It has a strict, well understood mathematical description, and it is widely used in various applications. Compared to recent NN-based methods, SVR is significantly less data-greedy, meaning that it does not require huge amounts of training data-sets to develop prediction models. Moreover, SVR is very robust to local minima problems. These aspects led us to choose SVR as the machine learning method for this application.

A detailed description of the proposed three variants of SVR techniques is given in the following subsections. Fig. 6.4 summarizes the process of generating these policies from the acquired data.

6.4.1 Standard SVR

Let $\mathbf{g}_{\text{pos}} = [x_s, y_s, z_s, \mathbf{q}_s^T]^T \in \mathbb{R}^3 \times \mathbb{H}$ represent the pose of the robotic gripper, where \mathbf{q}_s is a unit quaternion. Each robotic finger has nine tactile sensors, five on its proximal phalanx and four on the distal. Let $\mathbf{f}_{\text{prs}} \in \mathbb{R}^{27}$ be the vector containing all these tactile readings, $\mathbf{f}_{\text{mot}} \in \mathbb{R}^4$ the position of the motors in the robotic hand, and $\mathbf{f}_{\text{ang}} \in \mathbb{R}^7$ the joint angles of the exoskeleton. We can now define $\mathbf{s} \in \mathbf{S} \subseteq \mathbb{R}^3 \times \mathbb{H} \times \mathbb{R}^{27} \times \mathbb{R}^4 \times \mathbb{R}^7$ as an observed (demonstrated) robotic grasping action performed by a human teacher for a given object. Furthermore, let $\mathbf{a} \in \mathbf{A} \subseteq \mathbb{R}^3 \times \mathbb{H} \times \mathbb{R}^4$ be the corresponding action-state, which consists of a gripper pose and motor positions. We define the set of n demonstrations as ordered pairs $\mathcal{D} = \{(\mathbf{s}, \mathbf{a})_i : \forall i \in \mathbb{I}_n, \mathbf{s} \in \mathbf{S}, \mathbf{a} \in \mathbf{A}\}$. The goal is to instruct a policy function $\Pi_0(\mathbf{s}; \theta) : \mathbf{S} \rightarrow \mathbf{A}$, which is parameterized by $\theta \in \mathbb{R}^d$, using the set of human demonstrations. Let $l : \mathbf{A} \times \mathbf{A} \rightarrow \mathbb{R}$ be a loss function between two action-states and $\Pi^* : \mathbf{S}^* \rightarrow \mathbf{A}^*$ a robotic grasp policy demonstrated by a human. The objective is to find the parameterization θ that minimizes the expected loss across a set of human demonstrations, i.e. $\forall (\mathbf{s}, \mathbf{a}) \in \mathcal{D}^*$:

$$\arg \min_{\theta} \mathbf{E}[l(\Pi_0(\mathbf{s}; \theta), \Pi^*(\mathbf{s}))]. \quad (6.4)$$

6.4.2 SVR with Time-Series

For the implementation of an LfD policy based on SVR modelling, we used Vapnik’s \mathcal{E} -insensitive time-series [256], where the aim is to identify a policy Π_0 by minimization of an \mathcal{E} -function. In our case, this function is defined as

$$l_{\mathcal{E}}(\mathbf{s}, \mathbf{a}) = \sum_{k=1}^d l_{\mathcal{E}k}(\mathbf{s}_k, \mathbf{a}_k^*). \quad (6.5)$$

An SVR with time-series was chosen to generate a policy able to predict grasping actions in the form of action vectors with use of memory,

$$\hat{\mathbf{a}}_i(t + \Delta_t) = f(\mathbf{a}_i(t - \alpha), \mathbf{a}_i(t - \beta), \mathbf{a}_i(t - \gamma), \dots), \quad (6.6)$$

where $\hat{\mathbf{a}}_i$ is the predicted value of the action vector \mathbf{a}_i derived from its discrete grasping time-series values, and $\alpha = 0, \beta = 2, \gamma = 5$ are selected time-steps brought into the prediction equation, i.e. action predictions use current time sequence t together with shifted time sequences $(t - 2)$ and $(t - 5)$ as data input.

We organized and subdivided the data into predefined grasping stages: approach, grasp, lift, placement, and release (see [257, 258] for details). Then, we shifted \mathbf{g}_{pos} to make it relative to the position of the grasped object prior to finally normalizing all the data.

6.4.3 SVR with Heat-Map Weighting

We used heat-maps to represent action vector predictions by weighting the predicted tactile finger data using object-specific values generated by the heat-maps themselves. For a given object, we found little variability among the ten grasps performed by each subject (i.e. grasp practitioner). Although we registered a difference in heat-maps between subjects, this was negligible compared to the much larger differences identified between objects (i.e. the produce). Fig. 6.2 shows that the distal parts of the fingers experienced the most contact, whilst proximal parts yielded higher inter-object variation. As expected, the palm was more active in subjects with smaller hands, and when grasping larger objects such as the aubergine. However, since the RHR hand is not equipped with sensors on the palm, we did not use the palmar heat-map data.

In practice, we weighted each column of the sensor action vector (\mathbf{a} for $\mathbf{f}_{\text{prs}} \in \mathbb{R}^{27}$) with its respective heat-map values, represented by the matrix H :

$$\mathbf{a}_{ij}^{*k} = H_j^k \cdot \mathbf{a}_{ij}^k, \quad (6.7)$$

where k is the object type, i the sequence (row) values, and j a feature of the action vector. As mentioned above, this heat-map weighting was performed only on the sensor-covered area of the RHR hand, i.e., the RHR sensor placements were overlaid to the generic human hand heat-map generated during direct grasping. The human hand heat-map was thereby segmented into parcels which were averaged to create the matrix H (see also Fig. 6.4). This procedure enabled us to create a map of human-weighted grasp actions. It privileges the activation of specific tactile sensors according to the areas of the hand most used by the operator

during direct interaction with the objects. Of course, this mapping approach only works if the structure of the remote system resembles that of the human hand. Moreover, the more human-like the remote system is, the better we expect this mapping to perform.

6.5 Experimental Evaluation

This section presents the experimental evaluation of our LfD policy for autonomous grasping of compliant food. The execution-validation stage, conducted after the LfD-ML policy is learned, is illustrated on the right-hand side of Fig. 6.4.

6.5.1 Setup

The setup is comprised of the same remote system described in Sec. 6.3.2 and illustrated on the right-hand side of Fig. 6.3b, i.e. an RHR hand attached to a Panda manipulator. However, in this case, the robot is autonomously controlled by the learned LfD-ML policies and no human is involved in the loop. Feedback data derived from the RHR and the manipulator, such as tactile forces, joint positions, and velocity are continuously provided to the controller. The environment involves seven types of food objects: five (aubergine, bell pepper, lettuce, navel orange, and beef tomato) from the same categories used during training, and two (tangerine and plume tomato) which were not used in the training phase. These two latter objects are significantly different in size, approximately 50% smaller than the navel orange and beef tomato, respectively.

Food items were placed at a designated location within reachable working space of the robot. The location was carefully marked to ensure repeatability. The robot was placed in a starting position above the food item in question. Then, the grasping, lifting, and placement sequences were generated entirely from the autonomous LfD policy under consideration. While here we only focus on the interaction phase, in the future we also plan to consider the approaching phase by using, e.g., visual-servoing techniques to automatically reach the object from any position.

6.5.2 Grasping Policies

We carried out grasping experiments taking into account ((i)) standard human-in-the-loop teleoperation, ((ii)) standard SVR, ((iii)-(v)) three variants of our SVR-based policies, ((vi)) a recently-published haptic LfD approach, and ((vii)-(viii)) two standard impedance controllers:

- (i) *Human teleoperation (no automation)*. This approach considers the ground truth grasping data recorded during human teleoperation with the haptic interface (see Sec. 6.3.2). No machine learning is involved here.
- (ii) *SVR*. This approach uses normalized data (i.e. forces, positions, velocities) as input and directly maps them into grasping actions through a standard Support Vector Regression algorithm (see Sec. 6.4.1).
- (iii) *SVR-W (weighted as in [234])*. This approach is similar to the SVR above, but it privileges specific RHR sensor data as a mean of improving on the previous algorithm. The weighting is done as in the work of [234], not using any human direct grasping data (i.e. the heat-maps).
- (iv) *SVR-WH (weighted using heat-maps)*. This approach is similar to the SVR-W above, but it weights RHR sensor data according to our human-generated heat-maps (see Secs. 6.4.1 and 6.4.3).
- (v) *SVR-WHT (weighted using both heat-maps and time-series)*. Same as SVR-WH, but this approach takes into account the temporal variation in the finger configuration and sensor pressure during the grasping sequence (see Secs. 6.4.1, 6.4.2, and 6.4.3).
- (vi) *Misimi et al. [234] (state-of-the-art)*. This approach is a recent learning policy for autonomous grasping, published in 2018. It uses data derived from human teleoperation and tactile sensors on a robotic hand. It differs from our approach because it uses a simple non-haptic joystick during the teleoperation demonstrations, and it does not consider any human direct grasping information when weighting the tactile data.
- (vii) *Impedance controller (gentle grasp)*. This approach implements a standard impedance controller. The robotic hand increases the grasping force until the average force sensed by the tactile sensors reaches a set threshold. We set this threshold to the average value recorded during trials with haptic teleoperation.
- (viii) *Impedance controller (strong grasp)*. This approach is the same as ((vii)), but the threshold is here set to twice the average value recorded during trials with haptic teleoperation.

Fig. 6.5 summarizes the internal relative weights applied in these policies, illustrating how the different sensory input is valued.

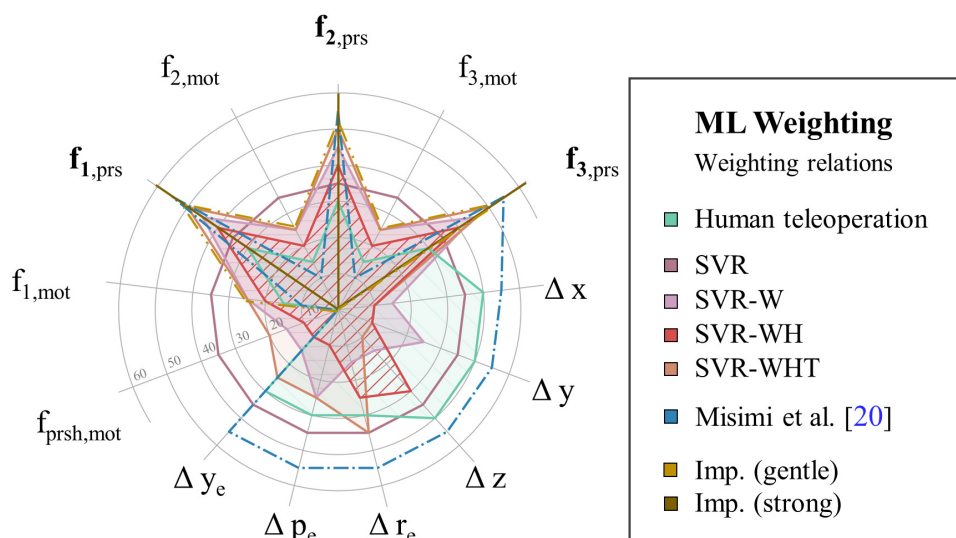


Figure 6.5 – *Weighting for each algorithm*: How these values relate to each other defines the SVRs work-space. Comparison of SVR weights gives an understanding of how they differ and relate to action inputs. For the abbreviations, see Sec. 6.5.2.

6.5.3 Autonomous Grasping Task

The task consisted in autonomously grasping seven types of food items using the learning policies cited above. We considered five food items (aubergine, bell pepper, lettuce, navel orange, and beef tomato) coming from the same categories of objects used during training, and two objects (tangerine and plume tomato) significantly different in size.

From the 50 teleoperated grasps per produce (see Sec. 6.3.2), it was possible to tailor our four grasping policies, ((ii)-(v)), for each produce used in Sec. 6.3.2, e.g. aubergine-trained SVR-WHT, pepper-trained SVR-WHT, lettuce-trained SVR-WHT, etc. This process yielded a total of 4 policies \times 5 (trained) objects = 20 tailored policies.

Each (trained) produce was grasped 30 times with its tailored policies. E.g., when grasping the aubergine, we used the four learning policies (ii)-(v) trained with data registered during the teleoperation of aubergines. To grasp the two food items whose category was not considered during training (tangerine and plume tomato), we used the four policies trained on navel orange and beef tomato, respectively. This task yielded 30 grasps \times 7 produce \times 4 policies = 840 grasps. For comparison, we also carried out the same task using the three standard controllers ((vi)-(viii)), yielding 30 grasps \times 7 produce \times 3 policies = 630 additional grasps.

In addition to the above grasping repetitions, we also wanted to study the adaptability of the proposed approach for different objects. To do so, we ran a

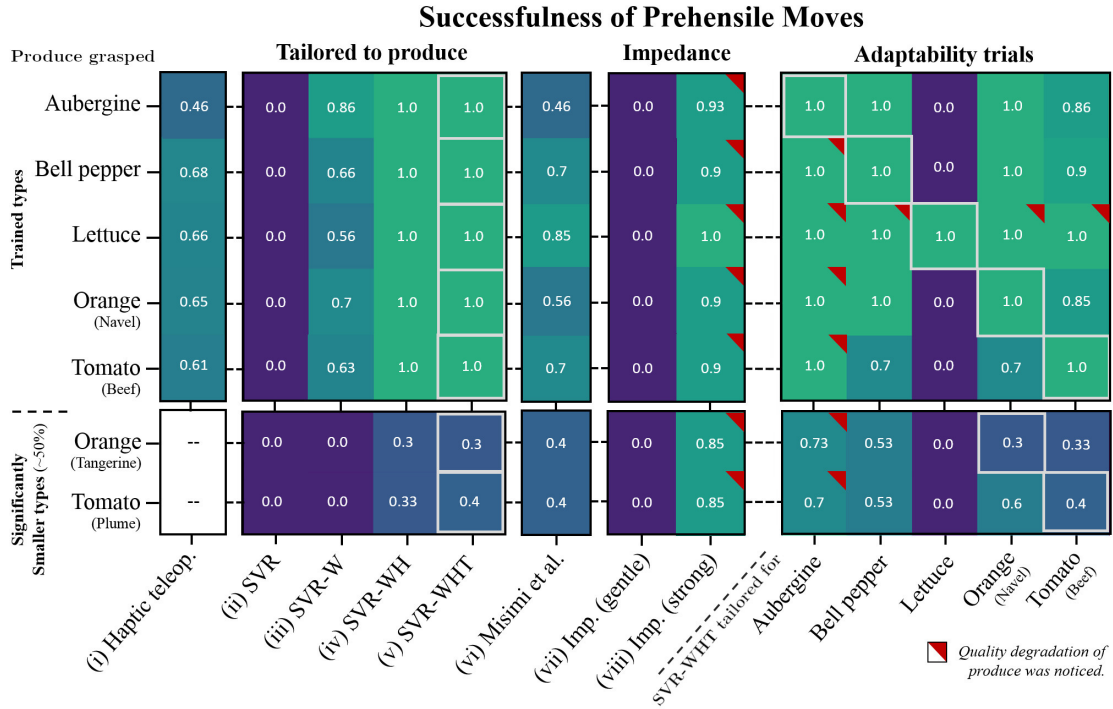


Figure 6.6 – *Success rate of grasping tasks.* Results are based on 30 grasp attempts per condition per food item. Autonomous grasping using LfD was implemented for a variety of SVRs. SVR with heat-map and time-series inputs had the best accuracy. We compared our approach to a recent state-of-the-art LfD from 2018, and two impedance controller techniques. Grasping variations and their abbreviations are described in Sec. 6.5.2.

second set of trials, using tailored SVR-WHT policies to grasp produce different than the one it was designed for. We only considered SVR-WHT policies because we expect them to be most effective. To avoid repeating grasps already considered in our first set of trials, each tailored policy only grasped the items it was not designed for, e.g., aubergine-trained SVR-WHT was used to autonomously grasp all items but aubergine. Each food item was grasped 30 times per policy, yielding $30 \text{ grasps} \times 6 \text{ produce} \times 5 \text{ tailored SVR-WHT} = 900 \text{ grasps}$.

In total, we carried out 2370 autonomous grasping actions.

6.5.4 Results and Discussion

Fig. 6.6 shows the average success rate for autonomous grasping actions for the different food items and policies. On the left-hand side, we can find the results of the first set of trials, which uses the four autonomous policies to grasp the seven objects. In this case, each policy was tailored for each food item, using data coming from grasping trials on the considered object only. For comparison, we also included success rates from ((i))–*human teleoperation*, ((vi))–*Misimi et al.*, and ((vii), (viii))–the two *impedance controllers*. On the right-hand side, we can

find the results of the second set of trials, using SVR-WHT policies trained on objects different than the one they grasped in the testing phase.

The left-hand side of Fig. 6.6 shows that, among the SVR-based approaches implemented, the SVR-weighted policy using heat-map and time-series data (SVR-WHT) was the one with the highest levels of accuracy. This confirmed our original hypothesis: *the addition of real human-interaction elements to the grasping policies increases the overall accuracy*, which peaked at 100% for SVR-WHT with all food items. We recall that this result was validated by 30 trial runs for each approach and food item. Both heat-map-based approaches ((iv)-(v)) outperformed *Misimi et al.* in all cases, performing on average 35% better. For SVR-WHT vs. *Misimi et al.*, a related-samples Wilcoxon-signed-rank-test showed a significant difference in the performance ($z = 1.997$ and $p = 0.046$). Considering [234] uses tactile sensing and a recent LfD approach (work published in 2018), this result strongly supports our hypothesis that combining direct hand interaction and high-dexterity haptic teleoperation is a winning technique (these are the two main differences between our system and that in [234]). For further comparison, we also included two standard impedance controllers. In this case, the robotic hand grasps until a certain threshold force is reached. We considered as thresholds one and two times the average force registered by the hand sensors during the teleoperation trials. The first approach (gentle grasp) did not damage the food, but it failed to successfully grasp the objects. On the other hand, the second approach (strong grasp) showed very good grasping performance. However, the high force applied severely damaged the considered food (see the red triangles in Fig. 6.6). Although impedance control could provide acceptable results through fine tuning (i.e. finding a custom force threshold for each item), we believe that LfD provides a more effective (and elegant) solution. Indeed, a simple force threshold approach still requires a significant amount of work from the human user, who needs to program the robot for each different set of objects, defeating the main purpose of our system: efficient non-programmatic automation for food processing.

After these first results, we carried out additional trials to study the adaptability of our approaches for other objects. In these trials, we used SVR-WHT to grasp food items different than the one used for the training, e.g. an SVR-WHT trained on the aubergine was used for grasping all other objects. The large difference between our food items enables us to evaluate the adaptability of our SVR algorithms to different situations. As mentioned above, five objects were in the same category as those used during training (aubergine, bell pepper, lettuce, orange, and beef tomato), while two were much smaller (tangerine and plum tomato). The results on the right-hand side of Fig. 6.6 suggest that we cannot

grasp heavy objects with an SVR policy trained with lighter ones, e.g. a policy trained using lettuce data fails to grasp an aubergine. However, the opposite often works quite well, e.g. a policy trained using aubergine data succeeds at grasping the lettuce. Of course, in general, results show that grasping objects using policies trained on other objects only works to a certain extent. As expected, as the difference between the target object and the training one increases, the success rate decreases. This degradation happens faster when grasping heavy objects with policies trained on lighter ones. However, even though it is possible to grasp lighter items (e.g. lettuce) using policies trained on heavier ones (e.g. aubergine), the higher force applied may risk to damage the object.

Finally, Fig. 6.6 shows that success rates for tangerines and plum tomatoes are quite low in respect to the others, demonstrating that our approach struggles to handle objects significantly smaller than those used during the training. As we are using both the positions and forces of the robotic fingers to learn our policies (see Fig. 6.5), this is an expected behaviour. In fact, while the combination of these two prevents the hand from squeezing items too hard, it also limits the capability of grasping objects with internally varying sizes (i.e. fruits or vegetables grown with higher ecological diversity). Results show that, if we had the opportunity to train LfD policies for each and every specific type of produce, this combined approach of finger position and tactile force sensing works well (see the high performance on the first five food objects Fig. 6.6). On the other hand, if we plan to autonomously grasp objects where size and shape span a wider range (i.e. produces is less uniformed/higher diversity) we need to make further adjustments, such as using finger force only. However, finger positions seem important and leaving this information out might not be viable, in regards to damages. Our grasps have all been made blindly, picking up a produce at position X. Adding further information about the produce through machine vision could be one way to unify finger positioning and variations size and shape.

It is also interesting to notice that the success rate for the teleoperation trials is not as high as one might expect (between 0.46 and 0.68). A grasping task was deemed successful only when the user was able to successfully grasp, lift, and move the object. Often the operator was able to grasp and lift the object, but then it slipped during transport. Upon asking, the operator said that it was not easy to always maintain the right amount of force needed for a robust grasp, as she was afraid of damaging the produce.

As a conclusion, after comparing our four different LfD variants, the best proposed approach combines (a) data collected during demonstrations using a haptic-enabled high-dexterity teleoperation interface, and (b) heat-map knowl-

edge acquired from humans directly grasping the items in question. Results indicated that the use of tactile data, weighted according to experience gathered during direct interaction trials, yielded the best performance. Compared to a recent LfD method for grasping compliant objects and two standard impedance controllers, results also showed that our approach performed better, proving our hypothesis—that to properly learn from humans how to grasp challenging, compliant, and fragile objects, it is beneficial to carry out the demonstrations using an intuitive and natural tool for controlling the remote manipulator. A key aspect of our approach is the inspiration from direct human grasping actions, represented in the LfD model by the use of heat-maps as an input variable, privileging and activating the “right” sensors on the robotic hand.

The proposed approach has a vast range of potential applications in the agricultural and food sectors, as well as in other industries that deal with compliant and fragile objects and where a knowledge of the applied tactile forces is crucial to achieving successful grasping actions. Our system contributes to a better understanding of the input required during the development of grasping ML policies. Furthermore, it is an added contribution to the topic of *LfD through teleoperation*, which highlights (a) the necessity of improved operator interaction by means of high-fidelity high-dexterity interfaces, and (b) the importance of combining these teleoperation data with barehanded prehensile movements. These results have the potential to advance the capabilities of robotic interaction, combining human puppetry with inherent intentions. We also believe that in the future, a more intuitive interaction system with strong learning capabilities can even avoid the need of expert human operators pre-training the robots. If the interface is intuitive enough, anyone able to carry out the target task will be able to also train the robot, allowing for an easier deployment.

Part IV

Conclusions and Future Work

CHAPTER

7

Concluding Remarks

Contents

7.1	Discussion and Conclusions	118
7.1.1	Part II	118
7.1.2	Part III	120
7.2	Additional Remarks and Future Directions	121

7.1 Discussion and Conclusions

In this thesis, we presented multiple shared-control architectures that utilize haptic feedback to convey information to the user and interact with him/her. The different results allowed us to showcase the advantages of shared autonomy versus standard teleoperation, which is in many cases too cognitively demanding and even physically tiring for the operator. In Part I, we started by introducing the main existing works in the literature related to the thesis, mainly in the fields of teleoperation and shared autonomy (Chapter 2), highlighting the current limitations and potential for development. We then presented the main contributions of this thesis in two separate parts, which will be summarized below.

7.1.1 Part II

In Part II, we presented two shared-control methods which provide the user with haptic guidance while keeping him/her in control. As such, these are referred to as shared-control methods with *high human authority*. In fact, the human and the automation intentions were mixed at the level of the haptic interface. The user then utilized this information to perform the task in a way that minimizes the cost function at hand, always being in control of the final robot movement.

In Chapter 3, we presented a haptic shared-control technique for robotic telemanipulation that provides the human operator with information on how to grasp an object for optimizing some future metrics, which might be unintuitive or difficult for the operator to predict. We specifically considered minimizing the torques the manipulator will exert to carry out an autonomous manipulation on the object after the grasp. This metric is important because it helps reducing the system's operating cost while extending the range of objects it can manipulate.

We demonstrated the effectiveness of the proposed approach in a series of representative real-world experiments as well as a human subjects study enrolling 15 subjects. Results proved the effectiveness of our shared-control techniques vs. standard human-in-the-loop teleoperation in most performance metrics. Moreover, haptic-only guidance performed better than visual-only guidance, although combined visuo-haptic guidance led to the best overall results.

While this chapter focused on minimizing the expected torque, the framework can be easily adapted to consider any other type of metric able to provide a cost for the set of feasible grasps. Similarly, while our post-grasp manipulation consisted in picking the object up and placing it somewhere else, the framework

can be adapted to consider to any other type of manipulation action.

Automation is present in our system on different levels: First, the system automatically identifies the feasible grasp poses from the object's 3-dimensional model. Second, the post-grasp manipulative action is defined, in our case, as autonomously moving the grasped object along a pre-planned desired trajectory. However, the human cognitive capabilities are still given the higher authority in the pre-grasp and grasping phase. In fact, we believe that the human judgement is necessary in this case to choose the grasp, even if the automation can successfully accomplish the post-grasp task alone. As such, during the teleoperation, the system provides the human operator with navigation guidance towards the grasp locally minimizing the expected torque effort. The user is therefore free to grasp the object from the side he/she wants, and the algorithm adapts by changing the force cues towards the local optimal grasping pose.

In **Chapter 4**, we presented a haptic shared control for robotic teleoperation that combines human-centered and task-centered cost functions, so as to consider together the need of the human operator as well as the objective of the teleoperation. First, we devised an innovative approach to estimate the user's muscular comfort during the task. Then, we combined this workload measure with a cost function related to the task at hand or the status of the robotic system. As an example, in our experiments, we considered a cost function indicating the distance from a target position. However, it is important to highlight that the proposed framework supports *any* other task- or system-related cost function (e.g., minimizing the joint torques as in Chapter 3, displacement, risks of encountering singularities). The one used here was chosen because representative, effective, and simple to implement. From the combination of both, we then generated a dynamic active constraint guiding the user towards a successful completion of the task along directions maximizing the user comfort.

To prove the effectiveness of the proposed approach, we carried out a robotic telemanipulation experiment enrolling 15 participants. Subjects were asked to pick and place three different sets of objects while receiving three different haptic guidance profiles. We evaluated the performance of the task considering five metrics, and the results showed that a small decrease in the task performance in terms of completion time and error to the target has been accompanied by a significant improvement in the NASA TLX test results, proving that our method does increase the user's perceived comfort.

This chapter sheds the light on how the automation component can act in the benefit of the human user, improving the comfort during robotic teleoperation.

While the operator can decide to override the haptic guidance provided, and thus remains in final control of the remote robot motion, following the haptic cues would decrease both the cognitive and the physical workload incurred.

7.1.2 Part III

In Part III, we presented two system designs with less control authority given to the user. The first one (Chapter 5) was applied to robotic cutting, and falls under the shared control category, while the second one (Chapter 6) suggested a new type of human-robot interaction where the human demonstrations and haptic interactions during teleoperation are used to learn the autonomous grasping of deformable fragile objects.

In Chapter 5, we designed and evaluated two shared-control approaches for assisting a human operator in various robot-assisted cutting tasks. The first shared-control technique resembled the behavior of a unicycle. We imposed non-holonomic constraints on the motion of the robotic system, such that the scalpel translation was limited to its cutting direction (forward/backward) and its vertical direction (up/down). These constraints prevented the operator from inadvertently applying high lateral forces during the cutting, which would result in dangerous ruptures of the environment. Although effective, in this condition the operator was still able to rotate the scalpel in place, which could also lead to significant damage. For this reason, we designed an additional shared-control technique, the car-like method, enforcing an additional constraint on the unicycle motion that ensured the scalpel rotation was coupled with a linear motion.

To validate our approach, we carried out a human-subject experiment in a real cutting scenario, considering the two shared-control techniques as well as a standard teleoperation approach. Results showed that shared-control methods outperformed teleoperation in most metrics considered, which proves that shared control improves the task execution compared to simple teleoperation.

However, as discussed in the chapter, subjective metrics showed that users preferred teleoperation and the unicycle approach over the car-like method, which had many constraints and made the users feel limited in action. In fact, the nonholonomic constraints applied in this chapter were *hard* constraints, and as such the user motion was limited along some directions.

In Chapter 6, we presented an extension to the work in previous chapters where we proposed a new method of using haptic feedback and teleoperation to

teach an autonomous system how to grasp. While the final objective is to achieve a fully-autonomous system, the grasping policy is defined from human teleoperated demonstrations. For this reason, we place this chapter under the *partial authority* framework, similarly to the previous one.

In this chapter, we proposed a novel human-inspired, haptic-enabled learning policy designed to handle compliant food items, originating from the agricultural automation domain. Four LfD learning policies were presented which, after training, were capable of gently and autonomously grasping a representative set of compliant produce such as aubergines, bell peppers, lettuces, oranges, and tomatoes without damaging them.

According to the experiments performed to test the different LfD methods policies presented, the best approach was the one combining both teleoperation data from human demonstrations performed with haptic feedback, and heat-map data acquired from humans directly grasping the items in question. As such, the use of tactile data improved the autonomous grasping, especially when weighted according to the results of direct human interaction trials. Our method also performed better than the state of the art methods, proving our hypothesis that learning from the human is essential to perform the grasping of compliant objects in an optimal way.

Unlike in the previous chapters, where the human is helped by the automation component to optimize some measure, this system uses the human input to help the autonomous system learn the right way to grasp. This automation of the grasping process would have, on the long term, a beneficial effect to the human operator since the robot would be able to replace the human in a highly repetitive and tiring task.

7.2 Additional Remarks and Future Directions

Each chapter of this thesis presents a different way of dividing the authority between the human and the automation system to successfully perform tasks such as grasping, manipulation and robotic cutting.

Three chapters of the thesis present shared-control methods for robotic teleoperation:

- a method with soft constraints, which focuses on the task execution. The result is an improvement in the task execution as measured by the metric of interest: the robot joint torques in the post-grasp trajectory.
- a method with soft constraints, which focuses both on the task execution

and the user's comfort. This human-oriented approach was appreciated by the users even though it led to a decrease in the task performance.

- two methods employing both hard and soft constraints, which focus on the task execution. While the architecture led to a better performance in terms of task-related parameters, the subjective data showed the users preferred the less constrained methods over the most constrained one, with a reluctance from their side to hand over control to the automation.

These results are interesting from different perspectives, and raise many questions which are still not fully answered despite the progress in the domain:

(1) Who should be the ultimate decision maker in a robotic system, the human or the robot? And what is the desirable strength of haptic feedback to apply so that the user follows the automation recommendation but does not feel hindered or not in control?

(2) Can task-related parameters and human comfort both be optimized at the same time, or does a compromise always has to be done to ensure satisfactory results for both parameters?

As already mentioned in Chapter 2, question (1) is not easy to answer, and the *optimal* distribution of authority between the human and the robot is far from being achieved. The best combination depends on many factors that are often unknown to the system engineer, such as the specificity of the task and environment, or the experience of the operator. In addition, it is important to combine the system performance with the user acceptance of the system. To do this, a policy needs to be designed to deal with the cases where the human and the automation components disagree. One way to tune the strength of haptic feedback is through an adaptive system that takes the confidence of each actor into account. For example, we could adapt the guidance strength to the operator's performance or experience, e.g., a system could use a stiff navigation approach (i.e., less freedom for the operator) when operated by novices, while it could employ a soft navigation approach (i.e., more freedom for the operator) when operated by experts. This approach could be also useful when teaching new operators, employing different levels of autonomy according to the operator's experience and learning process. This idea is an interesting extension to the contribution presented in Chapter 5, which I have started during my short stay at the Technical University of Munich, and it could lead to many interesting future

works on finding the right authority allocation scheme in a shared control scenario.

Beyond the cognitive level, the user should also feel physical comfort while operating the remote manipulator, and this brings us to question (2). A lot of the previous works in the field of assisted control are focused on the task itself, and they provide guidance information that would decrease the cognitive load on the user while teleoperating the robot. However, very few works address the problem of physical discomfort during teleoperation, even though this is an important consideration in the field. We hope that our work in Chapter 4 encourages future contributions where shared-control methods would compromise between task execution and user comfort. We believe that this is particularly important in long and repetitive tasks, as the user performance is often affected by the fatigue they experience.

On this level, Chapter 6 presents an innovative approach to automate a task that is still widely performed by human operators in a manual and repetitive task, in an attempt to decrease the load on them. The system uses teleoperated grasping actions, as well as barehanded human prehensile moves, to teach the robot to grasp soft and fragile objects, which is still a problematic task to execute autonomously given their sensitivity to the applied force by the robotic hand. The haptic interaction information is integrated in the LfD policy, and the results show that our system performs better than previous systems that are less intuitive for the human and that do not fully utilize the human experience in prehensile moves. Of course, the more naturally a human operator carries out a task, the more useful the data will be, enabling effective and true learning of the task in question. As such, it is important in the future to keep improving the teleoperation system to provide the human operators with intuitive and natural approaches to control the remote manipulator. As an example, one way to do so is by designing a multisensory bi-manual teleoperation system that will provide a wide range of haptic feedback features (kinesthetic, contact pressure, skin stretch and vibratory), which would also extend the range of tasks that the robotic system can perform. It would also be interesting to map the motion of the human operator into that of the robotic manipulator, so as to understand how different mapping techniques can affect the performance of the learning policies. Another important point to further study is the type and amount of information we need during the training, especially to understand what is most important when it comes to grasping objects with a different size than those used during the training. For this reason, it will be fundamental to also extend the

evaluation that we did to a wider range of compliant objects. Furthermore, our technique for heat-mapping, though functional for our small scale, should get a simpler and faster interface in future works. Sundaram et al. [259] could be one avenue to explore with a promising technique for collection of digital heat-maps and human-object-interaction signatures, when their interface becomes available for research use.

The work of this thesis opens the door to many other discussion points along the same line of research. One such topic is related to the nature of the feedback provided to the user. For instance, in the different systems we presented, haptic interaction was essential to give the operator a feeling of telepresence by providing contact forces from the environment. It was also used to convey guidance cues, and inform the user of hard constraints in the case of the cutting scenario. We would like, in the future, to explore the possibility of using both (wearable) cutaneous feedback and kinesthetic force feedback. This could be used to provide two pieces of information separately, to make it easier for the human operator to differentiate the source of the guidance (for example, the human-related guidance and the task-related guidance) such as in Chapter 4. It could also be used to give the user guidance cues while allowing him/her to feel the environment without limiting the control capabilities of the human users, who are not able to freely move the robot wherever they prefer, such as in Chapter 5. Another option is to provide *all* feedback information using wearable cutaneous feedback, to inform users about which composite trajectory the system would like them to follow while still leaving them completely free to move wherever they find suitable. In addition to haptic feedback, our experiments in Chapter 3 showed that the addition of visual feedback to the haptic guidance helped the user perform the task. Therefore, the combination of different types of feedback (e.g., visual, haptic or auditory) is another interesting topic to study.

Finally, the thesis also raises an important question concerning the point of application of the virtual fixtures in shared-control methods. In our cutting system (Chapter 5), we implemented both soft and hard constraints in the shared-control architecture. The virtual fixtures related to the nonholonomic constraints were applied on both the master and the remote sides. Virtual fixtures on the master interface only used the master pose, which ensured that no instabilities occur in the system due to this hard constraint. The same strategy was adopted in Chapter 4 for defining the haptic feedback related to the task cost function. The virtual fixtures were rendered on the master side, based on the master desired

pose, assuming no significant error is present between the master and the remote robot. Of course, implementing the constraints on each side separately can lead to less precision in the tracking of the master motion by the remote manipulator, reducing the performance in the task, which could be a problem in applications that require high levels of precision. Previous works rarely targeted this issue. As we have mentioned in Chapter 2, some works applied the constraints on the master, while others applied them on the remote side. It would be interesting to further study this issue in the future, by comparing the application of VF on the master based on the slave or the master data, in terms of both precision and stability.

Bibliography

- [1] T. B. Sheridan, “Human-robot interaction: Status and challenges,” *Human Factors*, vol. 58, no. 4, pp. 525–532, 2016, pMID: 27098262.
- [2] R. C. Goertz, “A force-reflecting positional servomechanism,” *Nucleonics*, vol. 10, no. 11, pp. 43–45, 1952.
- [3] G. Niemeyer, C. Preusche, S. Stramigioli, and D. Lee, “Telerobotics,” in *Springer handbook of robotics*. Springer, 2016, pp. 1085–1108.
- [4] T. B. Sheridan, “Telerobotics,” *Automatica*, vol. 25, no. 4, pp. 487–507, 1989.
- [5] R. Rahal, F. Abi-Farraj, P. R. Giordano, and C. Pacchierotti, “Haptic shared-control methods for robotic cutting under nonholonomic constraints,” in *2019 IEEE/RSJ International Conference on Intelligent Robots and Systems (IROS)*. IEEE, 2019, pp. 8151–8157.
- [6] R. Rahal, G. Matarese, M. Gabiccini, A. Artoni, D. Prattichizzo, P. Robuffo Giordano, and C. Pacchierotti, “Caring about the human operator: haptic shared control for enhanced user comfort in robotic telemanipulation,” *IEEE Transactions on Haptics*, vol. 13, no. 1, pp. 197–203, 2020.
- [7] —, “Haptic shared control for enhanced user comfort in robotic telemanipulation,” *IEEE ICRA workshop on Shared Autonomy: Learning and Control*, 2020.
- [8] R. Rahal, F. Abi-Farraj, P. Robuffo Giordano, and C. Pacchierotti, “Haptic shared-control methods for robotic cutting under nonholonomic constraints,” *12th International Workshop on Human-Friendly Robotics*, 2019.
- [9] B. Siciliano and O. Khatib, *Springer handbook of robotics*. Springer, 2016.
- [10] H. A. Ernst, “Mh-1, a computer-operated mechanical hand,” in *Proceedings of the May 1-3, 1962, spring joint computer conference*, 1962, pp. 39–51.

- [11] M. Goodrich and A. Schultz, “Human-robot interaction: A survey,” *Foundations and Trends in Human-Computer Interaction*, vol. 1, no. 3, pp. 203–275, 2007.
- [12] F. Ferraguti, N. Preda, A. Manurung, M. Bonfe, O. Lambercy, R. Gassert, R. Muradore, P. Fiorini, and C. Secchi, “An energy tank-based interactive control architecture for autonomous and teleoperated robotic surgery,” *IEEE Transactions on Robotics*, vol. 31, no. 5, pp. 1073–1088, 2015.
- [13] A. Franchi, C. Secchi, H. I. Son, H. H. Bulthoff, and P. R. Giordano, “Bilateral teleoperation of groups of mobile robots with time-varying topology,” *IEEE Transactions on Robotics*, vol. 28, no. 5, pp. 1019–1033, 2012.
- [14] D. Lee and P. Y. Li, “Passive coordination control of nonlinear bilateral teleoperated manipulators,” in *Proceedings 2002 IEEE International Conference on Robotics and Automation (Cat. No. 02CH37292)*, vol. 3. IEEE, 2002, pp. 3278–3283.
- [15] C. Schindlbeck and S. Haddadin, “Unified passivity-based cartesian force/impedance control for rigid and flexible joint robots via task-energy tanks,” in *2015 IEEE international conference on robotics and automation (ICRA)*. IEEE, 2015, pp. 440–447.
- [16] G. Bianchini, J. Bimbo, C. Pacchierotti, D. Prattichizzo, and O. A. Moreno, “Transparency-oriented passivity control design for haptic-enabled teleoperation systems with multiple degrees of freedom,” in *2018 IEEE Conference on Decision and Control (CDC)*. IEEE, 2018, pp. 2011–2016.
- [17] D. Lee and K. Huang, “Passive-set-position-modulation framework for interactive robotic systems,” *IEEE Transactions on Robotics*, vol. 26, no. 2, pp. 354–369, 2010.
- [18] B. Hannaford and J.-H. Ryu, “Time-domain passivity control of haptic interfaces,” *IEEE transactions on Robotics and Automation*, vol. 18, no. 1, pp. 1–10, 2002.
- [19] J. Ryu, D. Kwon, and B. Hannaford, “Stable teleoperation with time-domain passivity control,” *IEEE Transactions on Robotics and Automation*, vol. 20, no. 2, pp. 365–373, 2004.
- [20] J.-H. Ryu, Y. S. Kim, and B. Hannaford, “Sampled-and continuous-time passivity and stability of virtual environments,” *IEEE Transactions on Robotics*, vol. 20, no. 4, pp. 772–776, 2004.

-
- [21] J.-H. Ryu, C. Preusche, B. Hannaford, and G. Hirzinger, “Time domain passivity control with reference energy following,” *IEEE Transactions on Control Systems Technology*, vol. 13, no. 5, pp. 737–742, 2005.
- [22] R. C. Goertz, “Mechanical master-slave manipulator,” *Nucleonics (US) Ceased publication*, vol. 12, 1954.
- [23] J. Vertut and P. C. Coeffet, “Robot technology; vol. 3a teleoperation and robotics evolution and development,” 1986.
- [24] J. Vertut, *Teleoperation and robotics: applications and technology*. Springer Science & Business Media, 2013, vol. 3.
- [25] T. H. Massie, J. K. Salisbury *et al.*, “The phantom haptic interface: A device for probing virtual objects,” in *Proceedings of the ASME winter annual meeting, symposium on haptic interfaces for virtual environment and teleoperator systems*, vol. 55, no. 1. Chicago, IL, 1994, pp. 295–300.
- [26] J. Marescaux, J. Leroy, F. Rubino, M. Smith, M. Vix, M. Simone, and D. Mutter, “Transcontinental robot-assisted remote telesurgery: feasibility and potential applications,” *Annals of surgery*, vol. 235, no. 4, p. 487, 2002.
- [27] S. Panesar, Y. Cagle, D. Chander, J. Morey, J. Fernandez-Miranda, and M. Kliot, “Artificial intelligence and the future of surgical robotics,” *Annals of surgery*, vol. 270, no. 2, pp. 223–226, 2019.
- [28] T. Pardi, V. Ortenzi, C. Fairbairn, T. Pipe, A. Ghalamzan-E, and R. Stolkin, “Planning maximum-manipulability cutting paths,” *IEEE Robotics and Automation Letters*, vol. accepted, no. –, pp. —, 2020.
- [29] M. Talha, E. Ghalamzan, C. Takahashi, J. Kuo, W. Ingamells, and R. Stolkin, “Towards robotic decommissioning of legacy nuclear plant: Results of human-factors experiments with tele-robotic manipulation, and a discussion of challenges and approaches for decommissioning,” in *2016 IEEE International Symposium on Safety, Security, and Rescue Robotics (SSRR)*. IEEE, 2016, pp. 166–173.
- [30] M. Selvaggio, A. Ghalamzan Esfahani, R. Moccia, F. Ficuciello, B. Siciliano *et al.*, “Haptic-guided shared control for needle grasping optimization in minimally invasive robotic surgery,” in *IEEE/RSJ International Conference Intelligent Robotic System*, 2019.

- [31] F. Corucci and E. Ruffaldi, “Toward autonomous robots for demolitions in unstructured environments,” in *Intelligent Autonomous Systems 13*. Springer, 2016, pp. 1515–1532.
- [32] L. Meli, C. Pacchierotti, and D. Prattichizzo, “Experimental evaluation of magnified haptic feedback for robot-assisted needle insertion and palpation,” *The International Journal of Medical Robotics and Computer Assisted Surgery*, vol. 13, no. 4, p. e1809, 2017.
- [33] C. Pacchierotti, L. Meli, F. Chinello, M. Malvezzi, and D. Prattichizzo, “Cutaneous haptic feedback to ensure the stability of robotic teleoperation systems,” *The International Journal of Robotics Research*, vol. 34, no. 14, pp. 1773–1787, 2015.
- [34] A. Baheti, S. Seshadri, A. Kumar, G. Srimathveeravalli, T. Kesavadas, and K. Guru, “Ross: Virtual reality robotic surgical simulator for the da vinci surgical system,” in *IEEE Haptics Symposium 2008*. IEEE Computer Society, 2008, pp. 479–480.
- [35] M. Ferro, D. Brunori, F. Magistri, L. Saiella, M. Selvaggio, and G. A. Fontanelli, “A portable da vinci simulator in virtual reality,” in *2019 Third IEEE International Conference on Robotic Computing (IRC)*. IEEE, 2019, pp. 447–448.
- [36] M. Sagardia, K. Hertkorn, T. Hulin, S. Schätzle, R. Wolff, J. Hummel, J. Dodiya, and A. Gerndt, “Vr-oos: The dlr’s virtual reality simulator for telerobotic on-orbit servicing with haptic feedback,” in *2015 IEEE Aerospace Conference*. IEEE, 2015, pp. 1–17.
- [37] A. Bolopion, G. Millet, C. Pacoret, and S. Régnier, “Haptic feedback in teleoperation in micro-and nanoworlds,” *Reviews of Human Factors and Ergonomics*, vol. 9, no. 1, pp. 57–93, 2013.
- [38] T. B. Sheridan, “Telerobotics,” *Automatica*, vol. 25, no. 4, pp. 487–507, 1989.
- [39] J. V. Draper, D. B. Kaber, and J. M. Usher, “Telepresence,” *Human Factors: The Journal of the Human Factors and Ergonomics Society*, vol. 40, no. 3, pp. 354–375, 1998.
- [40] K. Hashtrudi-Zaad and S. E. Salcudean, “Transparency in time-delayed systems and the effect of local force feedback for transparent teleoperation,”

-
- IEEE Transactions on Robotics and Automation*, vol. 18, no. 1, pp. 108–114, 2002.
- [41] D. A. Lawrence, “Stability and transparency in bilateral teleoperation,” *IEEE Transactions on Robotics and Automation*, vol. 9, no. 5, pp. 624–637, 1993.
- [42] —, “Stability and transparency in bilateral teleoperation,” in *[1992] Proceedings of the 31st IEEE Conference on Decision and Control*. IEEE, 1992, pp. 2649–2655.
- [43] P. F. Hokayem and M. W. Spong, “Bilateral teleoperation: An historical survey,” *Automatica*, vol. 42, no. 12, pp. 2035–2057, 2006.
- [44] B. Hannaford and A. M. Okamura, “Haptics,” in *Springer Handbook of Robotics*. Springer, 2016, pp. 1063–1084.
- [45] E. Abdi, D. Kuli, and E. Croft, “Haptics in teleoperated medical interventions: Force measurement, haptic interfaces and their influence on users performance,” *IEEE Transactions on Biomedical Engineering*, 2020.
- [46] C. Pacchierotti, *Cutaneous haptic feedback in robotic teleoperation*. Springer, 2015.
- [47] L. Meli, C. Pacchierotti, and D. Prattichizzo, “Sensory subtraction in robot-assisted surgery: fingertip skin deformation feedback to ensure safety and improve transparency in bimanual haptic interaction,” *IEEE Transactions on Biomedical Engineering*, vol. 61, no. 4, pp. 1318–1327, 2014.
- [48] F. Chinello, M. Malvezzi, D. Prattichizzo, and C. Pacchierotti, “A modular wearable finger interface for cutaneous and kinesthetic interaction: control and evaluation,” *IEEE Transactions on Industrial Electronics*, vol. 67, no. 1, pp. 706–716, 2019.
- [49] C. Pacchierotti, D. Prattichizzo, and K. J. Kuchenbecker, “Cutaneous feedback of fingertip deformation and vibration for palpation in robotic surgery,” *IEEE Transactions on Biomedical Engineering*, vol. 63, no. 2, pp. 278–287, 2015.
- [50] H. Culbertson, S. B. Schorr, and A. M. Okamura, “Haptics: The present and future of artificial touch sensation,” *Annual Review of Control, Robotics, and Autonomous Systems*, vol. 1, pp. 385–409, 2018.

- [51] M. Y. Tsalamlal, N. Ouarti, and M. Ammi, “Non-intrusive haptic interfaces: State-of-the art survey,” in *International Workshop on Haptic and Audio Interaction Design*. Springer, 2013, pp. 1–9.
- [52] T. Howard, M. Marchal, A. Lécuyer, and C. Pacchierotti, “Pumah: Pantilt ultrasound mid-air haptics for larger interaction workspace in virtual reality,” *IEEE Transactions on Haptics*, vol. 13, no. 1, pp. 38–44, 2019.
- [53] I. Rakkolainen, E. Freeman, A. Sand, R. Raisamo, and S. Brewster, “A survey of mid-air ultrasound haptics and its applications,” *IEEE Transactions on Haptics*, 2020.
- [54] L. Moody, C. Baber, T. N. Arvanitis *et al.*, “Objective surgical performance evaluation based on haptic feedback,” *Studies in health technology and informatics*, pp. 304–310, 2002.
- [55] C. Pacchierotti, F. Chinello, M. Malvezzi, L. Meli, and D. Prattichizzo, “Two finger grasping simulation with cutaneous and kinesthetic force feedback,” *Haptics: Perception, Devices, Mobility, and Communication*, pp. 373–382, 2012.
- [56] C. R. Wagner, R. D. Howe, and N. Stylopoulos, “The role of force feedback in surgery: analysis of blunt dissection,” in *Haptic Interfaces for Virtual Environment and Teleoperator Systems, International Symposium on*. Citeseer, 2002, pp. 73–73.
- [57] A. Bolopion, C. Stolle, R. Tunnell, S. Haliyo, S. Régnier, and S. Fatikow, “Remote microscale teleoperation through virtual reality and haptic feedback,” in *2011 IEEE/RSJ International Conference on Intelligent Robots and Systems*. IEEE, 2011, pp. 894–900.
- [58] C. Pacchierotti, A. Tirmizi, G. Bianchini, and D. Prattichizzo, “Enhancing the performance of passive teleoperation systems via cutaneous feedback,” *IEEE transactions on haptics*, vol. 8, no. 4, pp. 397–409, 2015.
- [59] W. R. Ferrell and T. B. Sheridan, “Supervisory control of remote manipulation,” *IEEE spectrum*, vol. 4, no. 10, pp. 81–88, 1967.
- [60] A. Madni, Y.-y. Chu, and A. Freedy, “Intelligent interface for remote supervision and control of underwater manipulation,” in *Proceedings OCEANS’83*. IEEE, 1983, pp. 106–110.

-
- [61] F. Miyazaki, S. Matsubayashi, T. Yoshimi, and S. Arimoto, "A new control methodology toward advanced teleoperation of master-slave robot systems," in *Proceedings. 1986 IEEE International Conference on Robotics and Automation*, vol. 3. IEEE, 1986, pp. 997–1002.
- [62] B. Hannaford, "A design framework for teleoperators with kinesthetic feedback," *IEEE transactions on Robotics and Automation*, vol. 5, no. 4, pp. 426–434, 1989.
- [63] T. B. Sheridan and W. L. Verplank, "Human and computer control of undersea teleoperators," Massachusetts Inst of Tech Cambridge Man-Machine Systems Lab, Tech. Rep., 1978.
- [64] D. B. Kaber and M. R. Endsley, "The effects of level of automation and adaptive automation on human performance, situation awareness and workload in a dynamic control task," *Theoretical Issues in Ergonomics Science*, vol. 5, no. 2, pp. 113–153, 2004.
- [65] C. A. Miller and R. Parasuraman, "Beyond levels of automation: An architecture for more flexible human-automation collaboration," in *Proceedings of the human factors and ergonomics society annual meeting*, vol. 47, no. 1. SAGE Publications Sage CA: Los Angeles, CA, 2003, pp. 182–186.
- [66] G. Hirzinger, B. Brunner, J. Dietrich, and J. Heindl, "Rotex-the first remotely controlled robot in space," in *Proceedings of the 1994 IEEE international conference on robotics and automation*. IEEE, 1994, pp. 2604–2611.
- [67] G. Ferretti, G. Magnani, and P. Rocco, "Web-based industrial robot teleoperation: An application," in *Web-Based Control and Robotics Education*. Springer, 2009, pp. 249–266.
- [68] P. Schmaus, D. Leidner, T. Krüger, A. Schiele, B. Pleintinger, R. Bayer, and N. Y. Lii, "Preliminary insights from the meteron supvis justin space-robotics experiment," *IEEE Robotics and Automation Letters*, vol. 3, no. 4, pp. 3836–3843, 2018.
- [69] P. C. Leger, A. Trebi-Ollennu, J. R. Wright, S. A. Maxwell, R. G. Bonitz, J. J. Biesiadecki, F. R. Hartman, B. K. Cooper, E. T. Baumgartner, and M. W. Maimone, "Mars exploration rover surface operations: Driving spirit at gusev crater," in *2005 IEEE international conference on systems, man and cybernetics*, vol. 2. IEEE, 2005, pp. 1815–1822.

- [70] J. Funda, T. S. Lindsay, and R. P. Paul, “Teleprogramming: Toward delay-invariant remote manipulation,” *Presence: Teleoperators & Virtual Environments*, vol. 1, no. 1, pp. 29–44, 1992.
- [71] T. Xia, S. Léonard, A. Deguet, L. Whitcomb, and P. Kazanzides, “Augmented reality environment with virtual fixtures for robotic telemanipulation in space,” in *2012 IEEE/RSJ International Conference on Intelligent Robots and Systems*. IEEE, 2012, pp. 5059–5064.
- [72] D. Nicolis, M. Palumbo, A. M. Zanchettin, and P. Rocco, “Occlusion-free visual servoing for the shared autonomy teleoperation of dual-arm robots,” *IEEE Robotics and Automation Letters*, vol. 3, no. 2, pp. 796–803, 2018.
- [73] M. Selvaggio, F. Abi-Farraj, C. Pacchierotti, P. Robuffo Giordano, and B. Siciliano, “Haptic-based shared-control methods for a dual-arm system,” *IEEE Robotics and Automation Letters*, vol. 3, no. 4, pp. 4249–4256, 2018.
- [74] N. Pedemonte, F. Abi-Farraj, and P. Robuffo Giordano, “Visual-based shared control for remote telemanipulation with integral haptic feedback,” in *IEEE Int. Conf. Robotics and Automation*, 2017, pp. 5342–5349.
- [75] F. Abi-Farraj, “Contributions to shared control architectures for advanced telemanipulation,” Ph.D. dissertation, Université Rennes 1, 2018.
- [76] A. Leeper, K. Hsiao, M. Ciocarlie, L. Takayama, and D. Gossow, “Strategies for human-in-the-loop robotic grasping,” in *Proc. ACM/IEEE Int. Conf. Human-Robot Interaction*, 2012, pp. 1–8.
- [77] H. Boessenkool, D. A. Abbink, C. J. Heemskerk, F. C. van der Helm, and J. G. Wildenbeest, “A task-specific analysis of the benefit of haptic shared control during telemanipulation,” *IEEE Trans. Haptics*, vol. 6, no. 1, pp. 2–12, 2013.
- [78] Y. S. Park, H. Kang, T. F. Ewing, E. L. Faulring, J. E. Colgate, and M. A. Peshkin, “Enhanced teleoperation for d and d,” in *Proc. IEEE Int. Conf. Robotics and Automation*, vol. 4, 2004, pp. 3702–3707 Vol.4.
- [79] L. B. Rosenberg, “Virtual fixtures: Perceptual tools for telerobotic manipulation,” in *Proc. IEEE Virtual Reality Annual Intl. Symp.*, 1993, pp. 76–82.
- [80] F. Abi-Farraj, C. Pacchierotti, and P. Robuffo Giordano, “User evaluation of a haptic-enabled shared-control approach for robotic telemanipulation,” in *Proc. IEEE/RSJ Int. Conf. on Intelligent Robots and Systems*, 2018.

-
- [81] F. Abi-Farraj, C. Pacchierotti, O. Arenz, G. Neumann, and P. Robuffo Giordano, “A haptic shared-control architecture for guided multi-target robotic grasping,” *IEEE Trans. Haptics*, pp. 1–1, 2019.
- [82] L. Devigne, M. Aggravi, M. Bivaud, N. Balix, C. S. Teodorescu, T. Carlson, T. Spreters, C. Pacchierotti, and M. Babel, “Power wheelchair navigation assistance using wearable vibrotactile haptics,” *IEEE Transactions on Haptics*, vol. 13, no. 1, pp. 52–58, 2020.
- [83] M. Babel, F. Pasteau, S. Guégan, P. Gallien, B. Nicolas, B. Fraudet, S. Achille-Fauveau, and D. Guillard, “Handiviz project: clinical validation of a driving assistance for electrical wheelchair,” in *2015 IEEE International Workshop on Advanced Robotics and its Social Impacts (ARSO)*. IEEE, 2015, pp. 1–6.
- [84] D. A. Bell, S. P. Levine, Y. Koren, L. A. Jaros, and J. Borenstein, “Design criteria for obstacle avoidance in a shared-control system,” in *Proceedings of the RESNA*, vol. 94, 1994, pp. 17–24.
- [85] S. Payandeh, “Application of shared control strategy in the design of a robotic device,” in *American Control Conference, 2001. Proceedings of the 2001*, vol. 6. IEEE, 2001, pp. 4532–4536.
- [86] K. Lindgren, K. Huang, and B. Hannaford, “Towards real-time surface tracking and motion compensation integration for robotic surgery,” in *2017 IEEE/SICE International Symposium on System Integration (SII)*. IEEE, 2017, pp. 450–456.
- [87] M. Steele and R. B. Gillespie, “Shared control between human and machine: Using a haptic steering wheel to aid in land vehicle guidance,” *Proceedings of the Human Factors and Ergonomics Society Annual Meeting*, vol. 45, no. 23, pp. 1671–1675, 2001. [Online]. Available: <https://doi.org/10.1177/154193120104502323>
- [88] S. Anderson, S. Peters, K. Iagnemma, and J. Overholt, “Semi-autonomous stability control and hazard avoidance for manned and unmanned ground vehicles,” in *the 27th Army Science Conference, Orlando, Florida, USA, November 29-December 02, 2010*, 2010, pp. 1–8.
- [89] K. H. Goodrich, P. C. Schutte, F. O. Flemisch, and R. A. Williams, “Application of the h-mode, a design and interaction concept for highly automated

- vehicles, to aircraft,” in *2006 IEEE/AIAA 25TH Digital Avionics Systems Conference*. IEEE, 2006, pp. 1–13.
- [90] A. Franchi, C. Secchi, M. Ryll, H. H. Büthoff, and P. Robuffo Giordano, “Shared control : Balancing autonomy and human assistance with a group of quadrotor uavs,” *IEEE Robotics Automation Magazine*, vol. 19, no. 3, pp. 57–68, 2012.
- [91] C. Masone, A. Franchi, H. H. Büthoff, and P. R. Giordano, “Interactive planning of persistent trajectories for human-assisted navigation of mobile robots,” in *2012 IEEE/RSJ international conference on intelligent robots and systems*. IEEE, 2012, pp. 2641–2648.
- [92] C. Masone, P. R. Giordano, H. H. Büthoff, and A. Franchi, “Semi-autonomous trajectory generation for mobile robots with integral haptic shared control,” in *2014 IEEE International Conference on Robotics and Automation (ICRA)*. IEEE, 2014, pp. 6468–6475.
- [93] M. Aggravi, C. Pacchierotti, and P. R. Giordano, “Connectivity-maintenance teleoperation of a uav fleet with wearable haptic feedback,” *IEEE Transactions on Automation Science and Engineering*, 2020.
- [94] N. Yu, K. Wang, Y. Li, C. Xu, and J. Liu, “A haptic shared control approach to teleoperation of mobile robots,” in *2015 IEEE International Conference on Cyber Technology in Automation, Control, and Intelligent Systems (CYBER)*. IEEE, 2015, pp. 31–35.
- [95] F. Janabi-Sharifi and I. Hassanzadeh, “Experimental analysis of mobile-robot teleoperation via shared impedance control,” *IEEE Transactions on Systems, Man, and Cybernetics, Part B (Cybernetics)*, vol. 41, no. 2, pp. 591–606, 2010.
- [96] S. Park, R. D. Howe, and D. F. Torchiana, “Virtual fixtures for robotic cardiac surgery,” in *International Conference on Medical Image Computing and Computer-Assisted Intervention*. Springer, 2001, pp. 1419–1420.
- [97] S. Payandeh and Z. Stanicic, “On application of virtual fixtures as an aid for telemanipulation and training,” in *Proceedings 10th Symposium on Haptic Interfaces for Virtual Environment and Teleoperator Systems. HAPTICS 2002*. IEEE, 2002, pp. 18–23.

-
- [98] A. Bettini, P. Marayong, S. Lang, A. M. Okamura, and G. D. Hager, “Vision-assisted control for manipulation using virtual fixtures,” *Robotics, IEEE Trans.*, vol. 20, no. 6, pp. 953–966, 2004.
- [99] M. Ammi and A. Ferreira, “Realistic visual and haptic rendering for biological-cell injection,” in *Proceedings of the 2005 IEEE International Conference on Robotics and Automation*. IEEE, 2005, pp. 918–923.
- [100] ———, “Robotic assisted micromanipulation system using virtual fixtures and metaphors,” in *Proceedings 2007 IEEE International Conference on Robotics and Automation*. IEEE, 2007, pp. 454–460.
- [101] J. van Oosterhout, J. G. Wildenbeest, H. Boessenkool, C. J. Heemskerk, M. R. de Baar, F. C. van der Helm, and D. A. Abbink, “Haptic shared control in tele-manipulation: Effects of inaccuracies in guidance on task execution,” *IEEE transactions on haptics*, vol. 8, no. 2, pp. 164–175, 2015.
- [102] J. J. Abbott, P. Marayong, and A. M. Okamura, “Haptic virtual fixtures for robot-assisted manipulation,” in *Robotics research*. Springer, 2007, pp. 49–64.
- [103] S. A. Bowyer, B. L. Davies, and F. Rodriguez y Baena, “Active constraints/virtual fixtures: A survey,” *IEEE Trans. Robotics*, vol. 30, no. 1, pp. 138–157, 2014.
- [104] D. Nicolis, A. M. Zanchettin, and P. Rocco, “A hierarchical optimization approach to robot teleoperation and virtual fixtures rendering,” *IFAC-PapersOnLine*, vol. 50, no. 1, pp. 5672–5679, 2017.
- [105] J. J. Abbott and A. M. Okamura, “Virtual fixture architectures for telemanipulation,” in *2003 IEEE International Conference on Robotics and Automation (Cat. No. 03CH37422)*, vol. 2. IEEE, 2003, pp. 2798–2805.
- [106] D. Abbink and M. Mulder, “Exploring the dimensions of haptic feedback support in manual control,” *Journal of Computing and Information Science in Engineering*, vol. 9, no. 1, 2009.
- [107] C. T. Landi, V. Villani, F. Ferraguti, L. Sabattini, C. Secchi, and C. Fantuzzi, “Relieving operators’ workload: Towards affective robotics in industrial scenarios,” *Mechatronics*, vol. 54, pp. 144–154, 2018.

- [108] M. M. Marinho, B. V. Adorno, K. Harada, K. Deie, A. Deguet, P. Kazanzides, R. H. Taylor, and M. Mitsuishi, “A unified framework for the teleoperation of surgical robots in constrained workspaces,” in *2019 International Conference on Robotics and Automation (ICRA)*. IEEE, 2019, pp. 2721–2727.
- [109] W. Liu, Y. Su, W. Wu, C. Xin, Z.-G. Hou, and G.-B. Bian, “An operating smooth man–machine collaboration method for cataract capsulorhexis using virtual fixture,” *Future Generation Computer Systems*, vol. 98, pp. 522–529, 2019.
- [110] F. Abi-Farraaj, C. Pacchierotti, O. Arenz, G. Neumann, and P. R. Giordano, “A haptic shared-control architecture for guided multi-target robotic grasping,” *IEEE Trans. Haptics*, 2019.
- [111] Y. Yang, Z. Jiang, Y. Yang, X. Qi, Y. Hu, J. Du, B. Han, and G. Liu, “Safety control method of robot-assisted cataract surgery with virtual fixture and virtual force feedback,” *Journal of Intelligent & Robotic Systems*, vol. 97, no. 1, pp. 17–32, 2020.
- [112] M. Selvaggio, F. Chen, B. Gao, G. Notomista, F. Trapani, and D. Caldwell, “Vision based virtual fixture generation for teleoperated robotic manipulation,” in *2016 International Conference on Advanced Robotics and Mechatronics (ICARM)*. IEEE, 2016, pp. 190–195.
- [113] V. Pruks and J.-H. Ryu, “A framework for interactive virtual fixture generation for shared teleoperation in unstructured environments,” in *2020 IEEE International Conference on Robotics and Automation (ICRA)*. IEEE, 2020, pp. 10 234–10 241.
- [114] D. A. Abbink, M. Mulder, and E. R. Boer, “Haptic shared control: smoothly shifting control authority?” *Cognition, Technology & Work*, vol. 14, no. 1, pp. 19–28, 2012.
- [115] D. A. Abbink and M. Mulder, “Neuromuscular analysis as a guideline in designing shared control,” *Advances in Haptics, Mehrdad Hosseini Zadeh (Ed.)*, ISBN: 9789533070933, 2010.
- [116] H. Boessenkool, D. A. Abbink, C. J. Heemskerk, and F. C. van der Helm, “Haptic shared control improves tele-operated task performance towards performance in direct control,” in *Proc. IEEE World Haptics Conference*, 2011, pp. 433–438.

-
- [117] H. Boessenkool, D. A. Abbink, C. J. Heemskerk, F. C. van der Helm, and J. G. Wildenbeest, “A task-specific analysis of the benefit of haptic shared control during telemanipulation,” *IEEE Transactions on Haptics*, vol. 6, no. 1, pp. 2–12, 2012.
- [118] A. W. de Jonge, J. G. Wildenbeest, H. Boessenkool, and D. A. Abbink, “The effect of trial-by-trial adaptation on conflicts in haptic shared control for free-air teleoperation tasks,” *IEEE transactions on haptics*, vol. 9, no. 1, pp. 111–120, 2015.
- [119] M. Mulder, D. A. Abbink, and E. R. Boer, “Sharing control with haptics: Seamless driver support from manual to automatic control,” *Human factors*, vol. 54, no. 5, pp. 786–798, 2012.
- [120] C. Passenberg, R. Groten, A. Peer, and M. Buss, “Towards real-time haptic assistance adaptation optimizing task performance and human effort,” in *Proc. IEEE World Haptics Conference*, 2011, pp. 155–160.
- [121] M. Abayazid, C. Pacchierotti, P. Moreira, R. Alterovitz, D. Prattichizzo, and S. Misra, “Experimental evaluation of co-manipulated ultrasound-guided flexible needle steering,” *International J. Medical Robotics and Computer Assisted Surgery*, vol. 12, no. 2, pp. 219–230, 2016.
- [122] J. Bimbo, C. Pacchierotti, M. Aggravi, N. Tsagarakis, and D. Prattichizzo, “Teleoperation in cluttered environments using wearable haptic feedback,” in *IEEE/RSJ Intl. Conf. Intell. Robots and Systems*, 2017, pp. 3401–3408.
- [123] L. Meli, C. Pacchierotti, and D. Prattichizzo, “Experimental evaluation of magnified haptic feedback for robot-assisted needle insertion and palpation,” *International Journal of Medical Robotics and Computer Assisted Surgery*, vol. 13, pp. 1809–1809, 2017.
- [124] F. Abi-Farraj, C. Pacchierotti, and P. Robuffo Giordano, “User evaluation of a haptic-enabled shared-control approach for robotic telemanipulation,” in *Proc. IEEE/RSJ Intl. Conf. Intell. Robots and Systems*, 2018, pp. 1–9.
- [125] L. Marchal-Crespo, M. Bannwart, R. Riener, and H. Vallery, “The effect of haptic guidance on learning a hybrid rhythmic-discrete motor task,” *IEEE Trans. Haptics*, vol. 8, no. 2, pp. 222–234, 2015.
- [126] E. A. M. Ghalamzan, F. Abi-Farraj, P. Robuffo Giordano, and R. Stolkin, “Human-in-the-loop optimisation: mixed initiative grasping for optimally

- facilitating post-grasp manipulative actions,” in *2017 IEEE/RSJ International Conference on Intelligent Robots and Systems (IROS)*. IEEE, 2017, pp. 3386–3393.
- [127] D. J. Bruemmer, D. A. Few, R. L. Boring, J. L. Marble, M. C. Walton, and C. W. Nielsen, “Shared understanding for collaborative control,” *IEEE Trans. Systems, Man, and Cybernetics-Part A: Systems and Humans*, vol. 35, no. 4, pp. 494–504, 2005.
- [128] M. Hong and J. W. Rozenblit, “A haptic guidance system for computer-assisted surgical training using virtual fixtures,” in *Proc. IEEE Int. Conf. Systems, Man, and Cybernetics*, 2016, pp. 002 230–002 235.
- [129] A. M. Ghalamzan, F. Abi-Farraj, P. Robuffo Giordano, and R. Stolkin, “Human-in-the-loop optimisation: mixed initiative grasping for optimally facilitating post-grasp manipulative actions,” in *Proc. IEEE/RSJ Int. Conf. Intelligent Robots and Systems*, 2017, pp. 3386–3393.
- [130] I. Havoutis and S. Calinon, “Learning from demonstration for semi-autonomous teleoperation,” *Autonomous Robots*, vol. 43, no. 3, pp. 713–726, 2019.
- [131] —, “Supervisory teleoperation with online learning and optimal control,” in *2017 IEEE International Conference on Robotics and Automation (ICRA)*. IEEE, 2017, pp. 1534–1540.
- [132] P. Berthet-Rayne, M. Power, H. King, and G.-Z. Yang, “Hubot: A three state human-robot collaborative framework for bimanual surgical tasks based on learned models,” in *2016 IEEE International Conference on Robotics and Automation (ICRA)*. IEEE, 2016, pp. 715–722.
- [133] M. J. Zeestraten, I. Havoutis, and S. Calinon, “Programming by demonstration for shared control with an application in teleoperation,” *IEEE Robotics and Automation Letters*, vol. 3, pp. 1848–1855, 2018.
- [134] I. Havoutis and S. Calinon, “Learning assistive teleoperation behaviors from demonstration,” in *2016 IEEE International Symposium on Safety, Security, and Rescue Robotics (SSRR)*. IEEE, 2016, pp. 258–263.
- [135] A. Pervez, H. Latifee, J.-H. Ryu, and D. Lee, “Motion encoding with asynchronous trajectories of repetitive teleoperation tasks and its extension to

-
- human-agent shared teleoperation,” *Autonomous Robots*, vol. 43, no. 8, pp. 2055–2069, 2019.
- [136] F. Abi-Farraj, T. Osa, N. Pedemonte, J. Peters, G. Neumann, and P. Robuffo Giordano, “A learning-based shared control architecture for interactive task execution,” in *IEEE Int. Conf. Robotics and Automation*, 2017, pp. 329–335.
- [137] H. Latifee, A. Pervez, J.-H. Ryu, and D. Lee, “Mini-batched online incremental learning through supervisory teleoperation with kinesthetic coupling,” in *2020 IEEE International Conference on Robotics and Automation (ICRA)*. IEEE, 2020, pp. 5453–5459.
- [138] C. J. Pérez-del Pulgar, J. Smisek, V. F. Munoz, and A. Schiele, “Using learning from demonstration to generate real-time guidance for haptic shared control,” in *2016 IEEE International Conference on Systems, Man, and Cybernetics (SMC)*. IEEE, 2016, pp. 003 205–003 210.
- [139] G. Raiola, X. Lamy, and F. Stulp, “Co-manipulation with multiple probabilistic virtual guides,” in *2015 IEEE/RSJ international conference on intelligent robots and systems (IROS)*. IEEE, 2015, pp. 7–13.
- [140] H. Saeidi, F. McLane, B. Sadrfaidpour, E. Sand, S. Fu, J. Rodriguez, J. R. Wagner, and Y. Wang, “Trust-based mixed-initiative teleoperation of mobile robots,” in *2016 American Control Conference (ACC)*. IEEE, 2016, pp. 6177–6182.
- [141] D. Katzourakis, M. Alirezaei, J. C. de Winter, M. Corno, R. Happee, A. Ghaffari, and R. Kazemi, “Shared control for road departure prevention,” in *2011 IEEE International Conference on Systems, Man, and Cybernetics*. IEEE, 2011, pp. 1037–1043.
- [142] C. Ezech, P. Trautman, L. Devigne, V. Bureau, M. Babel, and T. Carlson, “Probabilistic vs linear blending approaches to shared control for wheelchair driving,” in *2017 International Conference on Rehabilitation Robotics (ICORR)*. IEEE, 2017, pp. 835–840.
- [143] A. D. Dragan and S. S. Srinivasa, “A policy-blending formalism for shared control,” *The Int. Journal of Robotics Research*, vol. 32, no. 7, pp. 790–805, 2013.

- [144] M. Mulder, D. A. Abbink, M. M. Van Paassen, and M. Mulder, “Design of a haptic gas pedal for active car-following support,” *IEEE Transactions on Intelligent Transportation Systems*, vol. 12, no. 1, pp. 268–279, 2010.
- [145] H. Yu, M. Spenko, and S. Dubowsky, “An adaptive shared control system for an intelligent mobility aid for the elderly,” *Autonomous Robots*, vol. 15, no. 1, pp. 53–66, 2003.
- [146] A. D. Dragan and S. S. Srinivasa, *Formalizing assistive teleoperation*. MIT Press, July, 2012.
- [147] S. Musić and S. Hirche, “Control sharing in human-robot team interaction,” *Annual Reviews in Control*, vol. 44, pp. 342–354, 2017.
- [148] H. Saeidi, J. D. Opfermann, M. Kam, S. Raghunathan, S. Léonard, and A. Krieger, “A confidence-based shared control strategy for the smart tissue autonomous robot (star),” in *2018 IEEE/RSJ International Conference on Intelligent Robots and Systems (IROS)*. IEEE, 2018, pp. 1268–1275.
- [149] R. Balachandran, H. Mishra, M. Cappelli, B. Weber, C. Secchi, C. Ott, and A. Albu-Schaeffer, “Adaptive authority allocation in shared control of robots using bayesian filters,” *Submitted to IEEE ICRA*, 2020.
- [150] V. Izadi, A. Bhardwaj, and A. H. Ghasemi, “Impedance modulation for negotiating control authority in a haptic shared control paradigm,” *arXiv preprint arXiv:2001.07779*, 2020.
- [151] H. M. Zwaan, S. M. Petermeijer, and D. A. Abbink, “Haptic shared steering control with an adaptive level of authority based on time-to-line crossing,” *IFAC-PapersOnLine*, vol. 52, no. 19, pp. 49–54, 2019.
- [152] S. James, P. Wohlhart, M. Kalakrishnan, D. Kalashnikov, A. Irpan, J. Ibarz, S. Levine, R. Hadsell, and K. Bousmalis, “Sim-to-real via sim-to-sim: Data-efficient robotic grasping via randomized-to-canonical adaptation networks,” in *Proceedings of the IEEE Conference on Computer Vision and Pattern Recognition*, 2019, pp. 12 627–12 637.
- [153] J. Tobin, L. Biewald, R. Duan, M. Andrychowicz, A. Handa, V. Kumar, B. McGrew, A. Ray, J. Schneider, P. Welinder *et al.*, “Domain randomization and generative models for robotic grasping,” in *2018 IEEE/RSJ International Conference on Intelligent Robots and Systems (IROS)*. IEEE, 2018, pp. 3482–3489.

-
- [154] S. Levine, P. Pastor, A. Krizhevsky, J. Ibarz, and D. Quillen, “Learning hand-eye coordination for robotic grasping with deep learning and large-scale data collection,” *The International Journal of Robotics Research*, vol. 37, no. 4-5, pp. 421–436, 2018.
- [155] M. Kopicki, R. Detry, M. Adjigble, R. Stolkin, A. Leonardis, and J. L. Wyatt, “One-shot learning and generation of dexterous grasps for novel objects,” *The International Journal of Robotics Research*, vol. 35, no. 8, pp. 959–976, 2016.
- [156] J. Varley, C. DeChant, A. Richardson, J. Ruales, and P. Allen, “Shape completion enabled robotic grasping,” in *2017 IEEE/RSJ International Conference on Intelligent Robots and Systems (IROS)*. IEEE, 2017, pp. 2442–2447.
- [157] L. Baronti, M. Alston, N. Mavrakis, E. Ghalamzan, M. Amir, M. Castellani *et al.*, “Primitive shape fitting in point clouds using the bees algorithm,” *Applied Sciences*, vol. 9, no. 23, p. 5198, 2019.
- [158] M. S. Kopicki, D. Belter, and J. L. Wyatt, “Learning better generative models for dexterous, single-view grasping of novel objects,” *The International Journal of Robotics Research*, vol. 38, no. 10-11, pp. 1246–1267, 2019.
- [159] T. Pardi, R. Stolkin *et al.*, “Choosing grasps to enable collision-free post-grasp manipulations,” in *2018 IEEE-RAS 18th International Conference on Humanoid Robots (Humanoids)*. IEEE, 2018, pp. 299–305.
- [160] A. Ghalazman-E and M. Ragaglia, “Robot learning from demonstrations: Emulation learning in environments with moving obstacles,” *Robotics and Autonomous Systems*, vol. 101, pp. 45–56, 2018.
- [161] N. Ratliff, M. Zucker, J. A. Bagnell, and S. Srinivasa, “Chomp: Gradient optimization techniques for efficient motion planning,” in *IEEE International Conference on Robotics and Automation*. IEEE, 2009, pp. 489–494.
- [162] A. M. Ghalamzan E., N. Mavrakis, M. Kopicki, R. Stolkin, A. Leonardis *et al.*, “Task-relevant grasp selection: A joint solution to planning grasps and manipulative motion trajectories,” in *IEEE/RSJ International Conference on Intelligent Robots and Systems*. IEEE, 2016, pp. 907–914.
- [163] M. Zucker, N. Ratliff, A. D. Dragan, M. Pivtoraiko, M. Klingensmith, C. M. Dellin, J. A. Bagnell, and S. S. Srinivasa, “Chomp: Covariant hamiltonian

- optimization for motion planning,” *The International Journal of Robotics Research*, vol. 32, no. 9-10, pp. 1164–1193, 2013.
- [164] J. Schulman, Y. Duan, J. Ho, A. Lee, I. Awwal, H. Bradlow, J. Pan, S. Patil, K. Goldberg, and P. Abbeel, “Motion planning with sequential convex optimization and convex collision checking,” *The International Journal of Robotics Research*, vol. 33, no. 9, pp. 1251–1270, 2014.
- [165] P. Abbeel, A. Coates, and A. Y. Ng, “Autonomous helicopter aerobatics through apprenticeship learning,” *The International Journal of Robotics Research*, vol. 29, no. 13, pp. 1608–1639, 2010.
- [166] R. Detry, J. Papon, and L. Matthies, “Task-oriented grasping with semantic and geometric scene understanding,” in *2017 IEEE/RSJ International Conference on Intelligent Robots and Systems (IROS)*. IEEE, 2017, pp. 3266–3273.
- [167] M. B. Horowitz and J. W. Burdick, “Combined grasp and manipulation planning as a trajectory optimization problem,” in *International Conference on Robotics and Automation*. IEEE, 2012, pp. 584–591.
- [168] N. Vahrenkamp, M. Przybylski, T. Asfour, and R. Dillmann, “Bimanual grasp planning,” in *IEEE-RAS International Conference on Humanoid Robots*, 2011, pp. 493–499.
- [169] N. Vahrenkamp, T. Asfour, G. Metta, G. Sandini, and R. Dillmann, “Manipulability analysis,” in *12th IEEE-RAS International Conference on Humanoid Robots*, 2012, pp. 568–573.
- [170] N. Mavrakis, A. M. Ghalamzan E., R. Stolkin, L. Baronti, M. Kopicki, M. Castellani *et al.*, “Analysis of the inertia and dynamics of grasped objects, for choosing optimal grasps to enable torque-efficient post-grasp manipulations,” in *IEEE-RAS International Conference on Humanoid Robots (Humanoids)*. IEEE, 2016, pp. 171–178.
- [171] N. Mavrakis, A. M. Ghalamzan E., and R. Stolkin, “Safe robotic grasping: Minimum impact-force grasp selection,” in *IEEE/RSJ International Conference on Intelligent Robots and Systems*. IEEE, 2017, pp. –.
- [172] Y. Zhou, W. Wang, W. Guan, Y. Wu, H. Lai, T. Lu, and M. Cai, “Visual robotic object grasping through combining rgb-d data and 3d meshes,” in

-
- International Conference on Multimedia Modeling*. Springer, 2017, pp. 404–415.
- [173] M. Achibet, M. Marchal, F. Argelaguet, and A. Lécuyer, “The virtual mitten: A novel interaction paradigm for visuo-haptic manipulation of objects using grip force,” in *IEEE Symposium on 3D User Interfaces (3DUI)*, 2014, pp. 59–66.
- [174] C. Cipriani, F. Zaccone, S. Micera, and M. C. Carrozza, “On the shared control of an emg-controlled prosthetic hand: Analysis of user prosthesis interaction,” *IEEE Transactions on Robotics*, vol. 24, no. 1, pp. 170–184, 2008.
- [175] H. Boessenkool, D. A. Abbink, C. J. M. Heemskerk, F. C. T. van der Helm, and J. G. W. Wildenbeest, “A task-specific analysis of the benefit of haptic shared control during telemanipulation,” *Transactions on Haptics*, vol. 6, no. 1, pp. 2–12, First 2013.
- [176] B. Nelson, J. Morrow, and P. Khosla, “Robotic manipulation using high bandwidth force and vision feedback,” *Mathematical and Computer Modelling*, vol. 24, no. 5, pp. 11 – 29, 1996.
- [177] C. Masone, P. Robuffo Giordano, H. H. Bühlhoff, and A. Franchi, “Semi-autonomous Trajectory Generation for Mobile Robots with Integral Haptic Shared Control,” in *International Conference on Robotics and Automation*, 2014, pp. 6468–6475.
- [178] A. T. Miller and P. K. Allen, “Graspit! a versatile simulator for robotic grasping,” *IEEE Robotics & Automation Magazine*, vol. 11, no. 4, pp. 110–122, 2004.
- [179] A. M. Zanchettin and P. Rocco, “A general user-oriented framework for holonomic redundancy resolution in robotic manipulators using task augmentation,” *IEEE Transactions on Robotics*, vol. 28, no. 2, pp. 514–521, 2011.
- [180] R. M. Murray, Z. Li, S. S. Sastry, and S. S. Sastry, *A mathematical introduction to robotic manipulation*. CRC press, 1994.
- [181] M. Maisto, C. Pacchierotti, F. Chinello, G. Salvietti, A. De Luca, and D. Prattichizzo, “Evaluation of wearable haptic systems for the fingers in

- augmented reality applications,” *IEEE Trans. Haptics*, vol. 10, no. 4, pp. 511–522, 2017.
- [182] L. Meli, C. Pacchierotti, G. Salvietti, F. Chinello, M. Maisto, A. De Luca, and D. Prattichizzo, “Combining wearable finger haptics and augmented reality: User evaluation using an external camera and the microsoft hololens,” *IEEE Robotics and Automation Letters*, vol. 3, no. 4, pp. 4297–4304, 2018.
- [183] F. Pearce. (2015) Shocking state of world’s riskiest nuclear waste site.
- [184] N. Mavrakis, A. M. G. E., and R. Stolkin, “Estimating an object’s inertial parameters by robotic pushing: A data-driven approach,” pp. 1–9, 2020.
- [185] L. McAtamney and E. N. Corlett, “Rula: a survey method for the investigation of work-related upper limb disorders,” *Applied ergonomics*, vol. 24, no. 2, pp. 91–99, 1993.
- [186] F. Chinello, C. Pacchierotti, J. Bimbo, N. G. Tsagarakis, and D. Prattichizzo, “Design and evaluation of a wearable skin stretch device for haptic guidance,” *IEEE Robotics and Automation Letters*, vol. 3, no. 1, pp. 524–531, 2018.
- [187] Y. Li, V. Patoglu, and M. K. O’Malley, “Negative efficacy of fixed gain error reducing shared control for training in virtual environments,” *ACM Trans. Applied Perception*, vol. 6, no. 1, pp. 3:1–3:21, 2009.
- [188] B. Busch, G. Maeda, Y. Mollard, M. Demangeat, and M. Lopes, “Postural optimization for an ergonomic human-robot interaction,” in *Proc. IEEE/RSJ Intl. Conf. Intelligent Robots and Systems*, 2017, pp. 2778–2785.
- [189] A. G. Marin, M. S. Shourijeh, P. E. Galibarov, M. Damsgaard, L. Fritzsche, and F. Stulp, “Optimizing contextual ergonomics models in human-robot interaction,” in *Proc. IEEE/RSJ Intl. Conf. Intelligent Robots and Systems*, 2018, pp. 1–9.
- [190] L. Chen, L. F. Figueredo, and M. R. Dogar, “Planning for muscular and peripersonal-space comfort during human-robot forceful collaboration,” in *Proc. IEEE Intl. Conf. Humanoid Robots*, 2018, pp. 1–8.
- [191] L. Peternel, W. Kim, J. Babi, and A. Ajoudani, “Towards ergonomic control of human-robot co-manipulation and handover,” in *Proc. IEEE-RAS Intl. Conf. Humanoid Robotics*, 2017, pp. 55–60.

-
- [192] F. Chaumette and S. Hutchinson, “Visual servo control, Part I: Basic approaches,” *IEEE Robotics and Automation Magazine*, vol. 13, no. 4, pp. 82–90, 2006.
- [193] M. Shimizu, W.-K. Yoon, and K. Kitagaki, “A practical redundancy resolution for 7 dof redundant manipulators with joint limits,” in *Proc. IEEE Intl. Conf. Robotics and Automation*, 2007, pp. 4510–4516.
- [194] H. Seraji, “Configuration control of redundant manipulators: Theory and implementation,” *IEEE Trans. Robotics and Automation*, vol. 5, no. 4, pp. 472–490, 1989.
- [195] M. Kang, H. Shin, D. Kim, and S.-E. Yoon, “Torm: Collision-free trajectory optimization of redundant manipulator given an end-effector path,” *arXiv preprint arXiv:1909.12517*, 2019.
- [196] C. Pacchierotti, D. Prattichizzo, and K. J. Kuchenbecker, “Displaying sensed tactile cues with a fingertip haptic device,” *IEEE Trans. Haptics*, vol. 8, no. 4, pp. 384–396, 2015.
- [197] S. G. Hart and L. E. Staveland, “Development of nasa-tlx (task load index): Results of empirical and theoretical research,” in *Advances in psychology*. Elsevier, 1988, vol. 52, pp. 139–183.
- [198] D. Michel, A. Qammaz, and A. A. Argyros, “Markerless 3d human pose estimation and tracking based on rgbd cameras: an experimental evaluation,” in *Proc. International Conference on Pervasive Technologies Related to Assistive Environments*, 2017, pp. 115–122.
- [199] H. Su, N. Enayati, L. Vantadori, A. Spinoglio, G. Ferrigno, and E. De Momi, “Online human-like redundancy optimization for tele-operated anthropomorphic manipulators,” *International Journal of Advanced Robotic Systems*, vol. 15, no. 6, p. 1729881418814695, 2018.
- [200] E. Biryukova, A. Roby-Brami, A. Frolov, and M. Mokhtari, “Kinematics of human arm reconstructed from spatial tracking system recordings,” *Journal of biomechanics*, vol. 33, no. 8, pp. 985–995, 2000.
- [201] A. M. Zanchettin, P. Rocco, L. Bascetta, I. Symeonidis, and S. Peldschus, “Kinematic analysis and synthesis of the human arm motion during a manipulation task,” in *2011 IEEE International Conference on Robotics and Automation*. IEEE, 2011, pp. 2692–2697.

- [202] V. Patnaik, R. K. Singla, and V. Bansal, “Surgical incisions—their anatomical basis part iv-abdomen,” *Journal of the Anat. Soc. India*, vol. 50, no. 2, pp. 170–8, 2001.
- [203] M. DeDonato et al., “Human-in-the-loop control of a humanoid robot for disaster response: A report from the darpa robotics challenge trials,” *J. Field Robotics*, vol. 32, no. 2, pp. 275–292, 2015.
- [204] F. Abi-Farraj, B. Henze, A. Werner, M. Panzirsch, C. Ott, and M. A. Roa, “Humanoid teleoperation using task-relevant haptic feedback,” in *IEEE/RSJ Intl. Conf. Intell. Robots and Systems*, 2018, pp. 5010–5017.
- [205] G. Campion, B. d’Andrea Novel, and G. Bastin, “Controllability and state feedback stabilizability of non holonomic mechanical systems,” in *Advanced Robot Control*, C. Canudas de Wit, Ed., 1991, pp. 106–124.
- [206] A. M. Bloch, M. Reyhanoglu, and N. H. McClamroch, “Control and stabilization of nonholonomic dynamic systems,” *IEEE Trans. Automatic Control*, vol. 37, no. 11, pp. 1746–1757, 1992.
- [207] H. McClamroch, M. Reyhanoglu, and M. Rehan, “Knife-edge motion on a surface as a nonholonomic control problem,” *IEEE Control Systems Letters*, vol. 1, no. 1, pp. 26–31, 2017.
- [208] R. Prada and S. Payandeh, “A study on design and analysis of virtual fixtures for cutting in training environments,” in *Proc. World Haptics Conference*, March 2005, pp. 375–380.
- [209] R. B. Gillespie, J. E. Colgate, and M. A. Peshkin, “A general framework for cobot control,” *IEEE Trans. Robotics and Automation*, vol. 17, no. 4, pp. 391–401, 2001.
- [210] C. A. Moore, M. A. Peshkin, and J. E. Colgate, “Cobot implementation of virtual paths and 3d virtual surfaces,” *IEEE Trans. Robotics and Automation*, vol. 19, no. 2, pp. 347–351, 2003.
- [211] H. Arai, T. Takubo, Y. Hayashibara, and K. Tanie, “Human-robot cooperative manipulation using a virtual nonholonomic constraint,” in *Proc. IEEE Intl. Conf. Robotics and Automation*, vol. 4, 2000, pp. 4063–4069 vol.4.
- [212] X. Li and P. Kazanzides, “Task frame estimation during model-based teleoperation for satellite servicing,” in *Proc. IEEE Intl. Conf. Robotics and Automation*, 2016, pp. 2834–2839.

-
- [213] S. Vozar, Z. Chen, P. Kazanzides, and L. L. Whitcomb, “Preliminary study of virtual nonholonomic constraints for time-delayed teleoperation,” in *Proc. IEEE/RSJ Intl. Conf. Intell. Robots and Systems*, 2015, pp. 4244–4250.
- [214] N. Marturi, A. Rastegarpanah, C. Takahashi, M. Adjigble, R. Stolkin, S. Zurek, M. Kopicki, M. Talha, J. A. Kuo, and Y. Bekiroglu, “Towards advanced robotic manipulation for nuclear decommissioning: A pilot study on tele-operation and autonomy,” in *Proc. Int. Conf. Robotics and Automation for Humanitarian Applications*, 2016, pp. 1–8.
- [215] E. Gadelmawla, M. Koura, T. Maksoud, I. Elewa, and H. Soliman, “Roughness parameters,” *Journal of Mat. Process. Tech.*, vol. 123, no. 1, pp. 133–145, 2002.
- [216] D. Lee and K. Huang, “Passive-set-position-modulation framework for interactive robotic systems,” *IEEE Trans. on Robotics*, vol. 2, no. 26, pp. 354–369, 2010.
- [217] “SoMa: Soft-bodied intelligence for Manipulation,” https://cordis.europa.eu/project/rcn/194335_en.html, 2018, [Online; accessed 23-July-2018].
- [218] S. Soper and A. Sherma, “Amazon robots poised to revamp how whole foods runs warehouses,” <https://goo.gl/15tjvY>, 2017, [Online; accessed 23-July-2018].
- [219] A. Saxena, J. Driemeyer, and A. Y. Ng, “Robotic grasping of novel objects using vision,” *The International Journal of Robotics Research*, vol. 27, no. 2, pp. 157–173, 2008.
- [220] H. Zhang, X. Zhou, X. Lan, J. Li, Z. Tian, and N. Zheng, “A real-time robotic grasping approach with oriented anchor box,” *IEEE Transactions on Systems, Man, and Cybernetics: Systems*, 2019.
- [221] C. Liu, B. Fang, F. Sun, X. Li, and W. Huang, “Learning to grasp familiar objects based on experience and objects’ shape affordance,” *IEEE Transactions on Systems, Man, and Cybernetics: Systems*, vol. 49, no. 12, pp. 2710–2723, 2019.
- [222] E. L. Sauser, B. D. Argall, G. Metta, and A. G. Billard, “Iterative learning of grasp adaptation through human corrections,” *Robotics and Autonomous Systems*, vol. 60, no. 1, pp. 55–71, 2012.

- [223] A. Namiki and M. Ishikawa, "Optimal grasping using visual and tactile feedback," in *Multisensor Fusion and Integration for Intelligent Systems, 1996. IEEE/SICE/RSJ International Conference on*, 1996, pp. 589–596.
- [224] C. E. Smith and N. P. Papanikolopoulos, "Vision-guided robotic grasping: Issues and experiments," in *Robotics and Automation, 1996. Proceedings., 1996 IEEE International Conference on*, vol. 4, 1996, pp. 3203–3208.
- [225] R. Johansson and G. Westling, "Roles of glabrous skin receptors and sensorimotor memory in automatic control of precision grip when lifting rougher or more slippery objects," *Experimental Brain Research*, vol. 56, no. 3, pp. 550–564, 1984.
- [226] G. Westling and R. Johansson, "Factors influencing the force control during precision grip," *Experimental Brain Research*, vol. 53, no. 2, pp. 277–284, 1984.
- [227] A. Bolopion and S. Régnier, "A review of haptic feedback teleoperation systems for micromanipulation and microassembly," *IEEE Transactions on automation science and engineering*, vol. 10, no. 3, pp. 496–502, 2013.
- [228] C. Pacchierotti, S. Scheggi, D. Prattichizzo, and S. Misra, "Haptic feedback for microrobotics applications: a review," *Frontiers in Robotics and AI*, vol. 3, no. 53, 2016.
- [229] C. Pacchierotti, F. Ongaro, F. Van den Brink, C. Yoon, D. Prattichizzo, D. H. Gracias, and S. Misra, "Steering and control of miniaturized untethered soft magnetic grippers with haptic assistance," *IEEE Trans. Automation Science and Engineering*, vol. 15, no. 1, pp. 290–306, 2018.
- [230] S. E. Salcudean, S. Ku, and G. Bell, "Performance measurement in scaled teleoperation for microsurgery," in *Proc. First Joint Conference on Computer Vision, Virtual Reality and Robotics in Medicine and Medial Robotics and Computer-Assisted Surgery*, 1997, pp. 789–798.
- [231] L. Moody, C. Baber, and T. N. Arvanitis, "Objective surgical performance evaluation based on haptic feedback," *Studies in health technology and informatics*, pp. 304–310, 2002.
- [232] C. Pacchierotti, D. Prattichizzo, and K. J. Kuchenbecker, "Cutaneous feedback of fingertip deformation and vibration for palpation in robotic surgery,"

-
- IEEE Transactions on Biomedical Engineering*, vol. 63, no. 2, pp. 278–287, 2016.
- [233] A. G. Billard, S. Calinon, and R. Dillmann, “Learning from humans,” in *Springer handbook of robotics*, 2016, pp. 1995–2014.
- [234] E. Misimi, A. Olofsson, A. Eilertsen, E. R. Øye, and J. R. Mathiassen, “Robotic handling of compliant food objects by robust learning from demonstration,” in *Proc. IEEE/RSJ International Conference on Intelligent Robots and Systems*, vol. 1, 2018.
- [235] P. Kormushev, S. Calinon, and D. G. Caldwell, “Imitation learning of positional and force skills demonstrated via kinesthetic teaching and haptic input,” *Advanced Robotics*, vol. 25, no. 5, pp. 581–603, 2011.
- [236] K. Kukliński, K. Fischer, I. Marhenke, F. Kirstein, V. Maria, D. Sølvason, N. Krüger, and T. R. Savarimuthu, “Teleoperation for learning by demonstration: Data glove versus object manipulation for intuitive robot control,” in *Proc. International Congress on Ultra Modern Telecommunications and Control Systems and Workshops*, 2014, pp. 346–351.
- [237] P. Evrard, E. Gribovskaya, S. Calinon, A. Billard, and A. Kheddar, “Teaching physical collaborative tasks: object-lifting case study with a humanoid,” in *Proc. IEEE-RAS International Conference on Humanoid Robots*, 2009, pp. 399–404.
- [238] Y. Lin, S. Ren, M. Clevenger, and Y. Sun, “Learning grasping force from demonstration,” in *Proc. IEEE International Conference on Robotics and Automation*, 2012, pp. 1526–1531.
- [239] P. Kormushev, D. N. Nenchev, S. Calinon, and D. G. Caldwell, “Upper-body kinesthetic teaching of a free-standing humanoid robot,” in *Robotics and Automation (ICRA), 2011 IEEE International Conference on*, 2011, pp. 3970–3975.
- [240] C. Schou, J. S. Damgaard, S. Bogh, and O. Madsen, “Human-robot interface for instructing industrial tasks using kinesthetic teaching,” in *Proc. International Symposium on Robotics*, 2013, pp. 1–6.
- [241] E. Knoop, M. Bächer, V. Wall, R. Deimel, O. Brock, and P. Beardsley, “Handshakiness: Benchmarking for human-robot hand interactions,” in *Intelligent Robots and Systems (IROS), 2017 IEEE/RSJ International Conference on*. IEEE, 2017, pp. 4982–4989.

- [242] E. Hyttinen, D. Kragic, and R. Detry, “Learning the tactile signatures of prototypical object parts for robust part-based grasping of novel objects,” in *Robotics and Automation (ICRA), 2015 IEEE International Conference on*. IEEE, 2015, pp. 4927–4932.
- [243] S. Luo, J. Bimbo, R. Dahiya, and H. Liu, “Robotic tactile perception of object properties: A review,” *Mechatronics*, vol. 48, pp. 54–67, 2017.
- [244] M. Stachowsky, T. Hummel, M. Moussa, and H. A. Abdullah, “A slip detection and correction strategy for precision robot grasping,” *IEEE/ASME Transactions on Mechatronics*, vol. 21, no. 5, pp. 2214–2226, 2016.
- [245] M. C. Gemici and A. Saxena, “Learning haptic representation for manipulating deformable food objects,” in *Intelligent Robots and Systems (IROS 2014), 2014 IEEE/RSJ International Conference on*. IEEE, 2014, pp. 638–645.
- [246] N. Kamakura, M. Matsuo, H. Ishii, F. Mitsuboshi, and Y. Miura, “Patterns of static prehension in normal hands,” *American Journal of Occupational Therapy*, vol. 34, no. 7, pp. 437–445, 1980.
- [247] P. Menesatti, C. Angelini, F. Pallottino, F. Antonucci, J. Aguzzi, and C. Costa, “Rgb color calibration for quantitative image analysis: the “3d thin-plate spline” warping approach,” *Sensors*, vol. 12, no. 6, pp. 7063–7079, 2012.
- [248] Q. Yuan, C.-Y. Weng, F. Suárez-Ruiz, and I.-M. Chen, “Flexible telemanipulation based handy robot teaching on tape masking with complex geometry,” *Robotics and Computer-Integrated Manufacturing*, vol. 66, p. 101990, 2020.
- [249] J. R. Napier, “The prehensile movements of the human hand,” *The Journal of bone and joint surgery. British volume*, vol. 38, no. 4, pp. 902–913, 1956.
- [250] A. Pettersson, T. Ohlsson, S. Davis, J. Gray, and T. Dodd, “A hygienically designed force gripper for flexible handling of variable and easily damaged natural food products,” *Innovative Food Science & Emerging Technologies*, vol. 12, no. 3, pp. 344–351, 2011.
- [251] D. M. Barrett, J. C. Beaulieu, and R. Shewfelt, “Color, flavor, texture, and nutritional quality of fresh-cut fruits and vegetables: desirable levels,

-
- instrumental and sensory measurement, and the effects of processing,” *Critical reviews in food science and nutrition*, vol. 50, no. 5, pp. 369–389, 2010.
- [252] S. Schaal, “Learning from demonstration,” in *Advances in neural information processing systems*, 1997, pp. 1040–1046.
- [253] B. D. Argall, S. Chernova, M. Veloso, and B. Browning, “A survey of robot learning from demonstration,” *Robotics and autonomous systems*, vol. 57, no. 5, pp. 469–483, 2009.
- [254] V. Mnih, K. Kavukcuoglu, D. Silver, A. A. Rusu, J. Veness, M. G. Bellemare, A. Graves, M. Riedmiller, A. K. Fidjeland, G. Ostrovski *et al.*, “Human-level control through deep reinforcement learning,” *Nature*, vol. 518, no. 7540, p. 529, 2015.
- [255] H. Van Hoof, T. Hermans, G. Neumann, and J. Peters, “Learning robot in-hand manipulation with tactile features,” in *Humanoid Robots (Humanoids), 2015 IEEE-RAS 15th International Conference on*. IEEE, 2015, pp. 121–127.
- [256] K.-R. Müller, A. J. Smola, G. Rätsch, B. Schölkopf, J. Kohlmorgen, and V. Vapnik, “Predicting time series with support vector machines,” in *International Conference on Artificial Neural Networks*. Springer, 1997, pp. 999–1004.
- [257] E. Misimi, E. R. Øye, A. Eilertsen, J. R. Mathiassen, O. B. Asebø, T. Gjerstad, J. Buljo, and Ø. Skotheim, “Gribbot—robotic 3d vision-guided harvesting of chicken fillets,” *Computers and Electronics in Agriculture*, vol. 121, pp. 84–100, 2016.
- [258] V. Lippiello, B. Siciliano, and L. Villani, “Position-based visual servoing in industrial multirobot cells using a hybrid camera configuration,” *IEEE Transactions on Robotics*, vol. 23, no. 1, pp. 73–86, 2007.
- [259] S. Sundaram, P. Kellnhofer, Y. Li, J.-Y. Zhu, A. Torralba, and W. Matusik, “Learning the signatures of the human grasp using a scalable tactile glove,” *Nature*, vol. 569, no. 7758, pp. 698–702, 2019.

Titre : Contrôle Partagé et Répartition d'Autorité pour la Téléopération Robotique

Mots clés : Robotique, Contrôle Partagé, Téléopération, Interfaces Haptiques

Résumé : L'interaction homme-robot est au cœur des développements de la robotique au fil des ans. En effet, même si l'autonomie robotique a été mise au point dans des environnements structurés et prévisibles, le recours à l'homme est encore nécessaire dans des environnements variables. Le travail présenté s'inscrit dans le cadre du thème général de l'interaction homme-robot. Plus précisément, la thèse traite de l'interaction à distance sous forme de téléopération. Nous concevons de nouvelles architectures de contrôle partagé pour une téléopération robotique sûre et intuitive, avec divers types d'interaction (notamment des retours haptiques) et différents niveaux d'automatisation.

Nous concevons d'abord de nouvelles architectures de contrôle partagé pour la saisie et la manipulation robotique avec retours haptiques, ciblant à la fois les phases de préhension et de post-préhension. La première vise à minimiser l'effort du robot en phase de post-préhension, tandis que la seconde se concentre sur la réduction de la charge de travail humaine pendant l'exécution de la tâche. Nous ciblons également une application de découpe robotique, et élaborons une nouvelle technique de contrôle partagé imposant des contraintes non holonomes motivées par la tâche de découpe. Enfin, nous mettons en évidence le rôle de l'interaction haptique dans la conception d'algorithmes de saisie autonome, en utilisant l'expérience humaine et les retours haptiques pour apprendre au robot la saisie autonome d'objets déformables.

Title : Shared Control and Authority Distribution for Robotic Teleoperation

Keywords : Robotics, Shared Control, Teleoperation, Haptics

Abstract : Human robot interaction is at the core of the robotic developments over the years. In fact, while robotic autonomy has been perfected in structured and predictable environments, the human input is still needed in many cases, especially in a variable setting. This thesis falls under the general human robot interaction topic. More specifically, it deals with remote interaction under the form of teleoperation. We design novel shared control architectures for safe and intuitive robotic teleoperation, with various types of interaction and different levels of automation. We focus in this work on the use of haptics as a means of interaction, whether for providing contact forces as a feedback to the user, or as a means of guiding the user in the task execution.

Starting with a robotic grasping and manipulation application, we design new haptic shared control targeting both the pre-grasp and the post-grasp phases. One shared control architecture aims to minimize the robot torques in a post-grasp phase, while the other focuses on minimizing the human workload during task execution. We also target a robotic cutting application, and design a novel haptic shared control technique for robotic cutting imposing non-holonomic constraints motivated by the cutting task. We finally highlight the role of haptic interaction and human input in the design of autonomous grasping algorithms, using the human experience and haptic feedback to learn autonomous grasping policies for compliant objects.